

AL-TR-1992-0049

DTIC
ELECTE
SEP 3 1992
S C D

(2)



AD-A255 544



HYBRID II AND HYBRID III DUMMY NECK PROPERTIES FOR COMPUTER MODELING

Eric K. Spittle
Buford W. Shipley, Jr.
Ints Kaleps

VULNERABILITY ASSESSMENT BRANCH
BIODYNAMICS & BIOCOMMUNICATIONS DIVISION
CREW SYSTEMS DIRECTORATE
WRIGHT-PATTERSON AFB, OH 45433-6573

Donna Jo Miller

SYSTEMS RESEARCH LABORATORIES
2800 INDIAN RIPPLE ROAD
DAYTON, OH 45440

FEBRUARY 1992

42446

92-24301



13848

INTERIM REPORT FOR THE PERIOD JANUARY 1991 TO FEBRUARY 1992

Approved for public release; distribution is unlimited.

92 9 02 008

AIR FORCE SYSTEMS COMMAND
WRIGHT-PATTERSON AIR FORCE BASE, OHIO 45433-6573

NOTICES

When US Government drawings, specifications, or other data are used for any purpose other than a definitely related Government procurement operation, the Government thereby incurs no responsibility nor any obligation whatsoever, and the fact that the Government may have formulated, furnished, or in any way supplied the said drawings, specifications, or other data, is not to be regarded by implication or otherwise, as in any manner, licensing the holder or any other person or corporation, or conveying any rights or permission to manufacture, use or sell any patented invention that may in any way be related thereto.

Please do not request copies of this report from the Armstrong Laboratory. Additional copies may be purchased from:

National Technical Information Service
5285 Port Royal Road
Springfield VA 22161

Federal Government agencies and their contractors registered with Defense Technical Information Center should direct requests for copies of this report to:

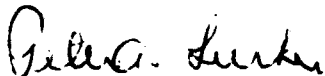
Defense Technical Information Center
Cameron Station
Alexandria VA 22314

TECHNICAL REVIEW AND APPROVAL

AL-TR-1992-0049

This report has been reviewed by the Office of Public Affairs (PA) and is releasable to the National Technical Information Service (NTIS). At NTIS, it will be available to the general public, including foreign nations.

This technical report has been reviewed and is approved for publication.



PETER A. LURKER, Lt Col, USAF, BSC
Acting Director
Biodynamics and Biocommunications Division
Armstrong Laboratory

REPORT DOCUMENTATION PAGEForm Approved
OMB No. 0704-0188

Public reporting burden for this collection of information is estimated to average 1 hour per response, including the time for reviewing instructions, searching existing data sources, gathering and maintaining the data needed, and completing and reviewing the collection of information. Send comments regarding this burden estimate or any other aspect of this collection of information, including suggestions for reducing this burden, to Washington Headquarters Services, Directorate for Information Operations and Reports, 1215 Jefferson Davis Highway, Suite 1204, Arlington, VA 22202-4302, and to the Office of Management and Budget, Paperwork Reduction Project (0704-0188), Washington, DC 20503.

1. AGENCY USE ONLY (Leave blank)		2. REPORT DATE February, 1992	3. REPORT TYPE AND DATES COVERED Interim Jan 91 - Feb 92
4. TITLE AND SUBTITLE Hybrid II and Hybrid III Dummy Neck Properties for Computer Modeling			5. FUNDING NUMBERS PE 62202F PR 7231 TA 36 and 23 WU 02 and 01
6. AUTHOR(S) Eric K. Spittle, 1st Lt, USAF Donna Jo Miller, SRL Buford W. Shipley, Jr., Capt, USAF Ints Kaleps			
7. PERFORMING ORGANIZATION NAME(S) AND ADDRESS(ES) Vulnerability Assessment Branch Biodynamics and Biocommunications Division Crew Systems Directorate Armstrong Laboratory Wright-Patterson AFB OH 45433-6573			8. PERFORMING ORGANIZATION REPORT NUMBER AL-TR-1992-0049
9. SPONSORING/MONITORING AGENCY NAME(S) AND ADDRESS(ES)			10. SPONSORING/MONITORING AGENCY REPORT NUMBER
11. SUPPLEMENTARY NOTES			
12a. DISTRIBUTION/AVAILABILITY STATEMENT Approved for Public Release, distribution is unlimited.			12b. DISTRIBUTION CODE A
13. ABSTRACT (Maximum 200 words) <p>Existing rigid body dynamics and finite element computer codes do not have adequate databases for manikin neck structures to properly model head/neck system dynamics occurring in crash or ejection testing. This report describes measured static stiffness and dynamic damping and stiffness characteristics of the Hybrid II and Hybrid III manikin necks and uses these data to improve the current manikin neck data sets of the Articulated Total Body (ATB) model and the Head Spine Model (HSM). The Hybrid II and Hybrid III manikin necks are used extensively throughout the automotive industry, the Department of Transportation, and the Department of Defense for safety testing.</p> <p>Static stiffness characteristics were determined from loading and unloading the necks in flexion, extension, and lateral bending. Dynamic damping and stiffness characteristics were determined from abrupt deceleration tests in the 'X' and 'Y' directions. Current computer data sets for the Hybrid II and Hybrid III necks were compared to the experimental dynamic results to determine inconsistencies. The data sets were then revised using the results obtained experimentally. Finally, the new data sets</p>			
14. SUBJECT TERMS Hybrid II, Hybrid III, Dummy Neck, Mechanical Properties, Static, Dynamic, Hysteresis, Computer Modeling, ATB, HSM			15. NUMBER OF PAGES 138
			16. PRICE CODE
17. SECURITY CLASSIFICATION OF REPORT Unclassified	18. SECURITY CLASSIFICATION OF THIS PAGE Unclassified	19. SECURITY CLASSIFICATION OF ABSTRACT Unclassified	20. LIMITATION OF ABSTRACT Unlimited

ABSTRACT (Continued)

were compared to the experimental dynamic results to show improvements.

The conclusion reached was that the dynamic response of the necks was highly complex. Simplifying assumptions and approximations were made to reduce the experimental data into acceptable form for the computer model data sets.

PREFACE

The investigations described in this report were conducted by the Vulnerability Assessment Branch, Biodynamics and Biocommunications Division, Crew Systems Directorate, Armstrong Laboratory (AL/CFBV) and supported by Systems Research Laboratories, Inc. (SRL), 2800 Indian Ripple Road, Dayton, Ohio. The tests were conducted in the Manikin Testing Laboratory (MTL), Building 824, Area B, WPAFB, OH. The computer modeling analysis was performed in Building 441, Area B, WPAFB, OH.

Lt Eric K. Spittle served as the principal investigator. Capt Buford Shipley performed the Head Spine Model (HSM) analysis and Donna Jo Miller (SRL) performed the Articulated Total Body (ATB) analysis. Greg Thompson (SRL) provided test support throughout the test program.

Special thanks are given to Buford, Donna, and Greg for their outstanding efforts throughout this project. Special thanks are also given to Dr Ints Kaleps for his help in this work.

Accession For

	✓
	□
	□
	□

Acquisition Codes
Serial and/or
Part Serial

A-1

TABLE OF CONTENTS

BACKGROUND	1
INTRODUCTION	3
HYBRID II AND HYBRID III HEAD/NECK STRUCTURES	6
STATIC TESTS	14
Static Neck Tester	14
Description of Static Tests	15
Test Data	16
Stiffness Characteristics	26
Hybrid II Necks	26
Hybrid III Necks	33
DYNAMIC TESTS	50
Head/Neck Pendulum	50
Description of Dynamic Tests	53
Test Data	58
Stiffness and Damping Characteristics	62
Hybrid II Necks	62
Hybrid III Necks	67
ATB MODEL	80
Model Description	80
Current Data Set	81
New Data Set	81
Modeling Results	83
Hybrid II	83
Hybrid III	86
HSM MODEL	102
Model Description	102
Current Data Set	102
New Data Set	103
Modeling Results	103
Hybrid II	103
Hybrid III	105

CONCLUSIONS	108
Static Tests	108
Dynamic Tests	108
ATB Model	109
HSM Model	110
RECOMMENDATIONS	111
BIBLIOGRAPHY	112
LIST OF SYMBOLS	116
APPENDICES	120
Appendix A: New ATB Model Input Deck	120
Appendix B: New HSM Model Input Deck	125

LIST OF FIGURES

Figure	page
1 Anatomical Coordinate System	7
2 Lateral View of Anatomical Axis System	7
3 Head Free Body Diagram	8
4 Neck Free Body Diagram	9
5 Hybrid II Head	9
6 Hybrid II Neck	10
7 Hybrid III Head	10
8 Hybrid III Neck	10
9 Hybrid II Head/Neck Interface	12
10 Hybrid III Neck with End Cap	12
11 Denton Inc. Head/Neck Load Cell	12
12 Hybrid III Head/Neck Interface	13
13 Side View of the SNT	14
14 End View of the SNT Under Load	15
15 First Order Regression Fit to Flexion Loading Data	18
16 Second Order Regression Fit to Flexion Loading Data	19
17 Third Order Regression Fit to Flexion Loading Data	20
18 Third Order Regression Fit to Flexion Unloading Data	22
19 First Order Regression Fit to Flexion Unloading Data	23

20	Second Order Regression Fit to Flexion Unloading Data	24
21	Neck Compression During Loading	27
22	Flexion Loading Hybrid II Neck 1	28
23	Flexion Loading Hybrid II Neck 2	29
24	Average Flexion Loading Hybrid II Necks	30
25	Extension Loading Hybrid II Neck 1	31
26	Flexion Unloading Hybrid II Neck 1	32
27	Loading and Unloading Curves Hybrid II	34
28	Flexion Loading Hybrid III Neck 2	35
29	Flexion Loading Hybrid III Both Necks	36
30	Flexion Loading to 40° Hybrid III Both Necks	37
31	Flexion Unloading Hybrid III Neck 2	38
32	Average Flexion Loading and Unloading Hybrid III	39
33	Extension Loading Hybrid III Neck 2	41
34	Extension Unloading Hybrid III Neck 2	42
35	Lateral Loading Hybrid III Neck 2	45
36	Lateral Unloading Hybrid III Neck 2	46
37	Side View of the HNP	50
38	End View of the HNP	51
39	Hybrid II Head and Neck on HNP	51
40	Hybrid III Head and Neck on HNP	52
41	Hybrid III Neck Flexion Certification Total Moment	54
42	Hybrid III Neck Flexion Certification Total Rotation	55
43	Hybrid II Neck Flexion Certification Total Rotation	56

44	Hybrid II Neck Flexion Certification Chordal Displacement	57
45	Hybrid III Rotational Damping All Angles	59
46	Hybrid III Total Moment Vs. Neck Rotation	60
47	Hybrid III Total Moment Vs. Neck Rotation All Angles	61
48	Hybrid II Neck 1 Rotation 90° Flexion	63
49	Hybrid II Neck 1 Rotation 90° Extension	64
50	Hybrid II Neck 1 Chordal Displacement 90° Flexion	65
51	Hybrid II Neck 1 Chordal Displacement 90° Extension	66
52	Hybrid III Neck Rotation Comparison 120°	68
53	Hybrid III Neck Rotation Comparison 90°	69
54	Hybrid III Neck Rotation Comparison 65°	70
55	Hybrid III Neck Rotation Comparison 40°	71
56	Hybrid III Neck Rotation Comparison 20°	72
57	Hybrid III Neck Moment Vs. Rotation Comparison 120°	73
58	Hybrid III Neck Moment Vs. Rotation Comparison 90°	74
59	Hybrid III Neck Moment Vs. Rotation Comparison 65°	75
60	Hybrid III Neck Moment Vs. Rotation Comparison 40°	76
61	Hybrid III Neck Moment Vs. Rotation Comparison 20°	77
62	Hybrid III Neck Moment Vs. Rotation Static Overlay	78
63	ATB Model Representation of a Human Body	80
64	Hybrid II Flexion Neck Rotation ATB Simulation	84
65	Hybrid II Flexion Head Rotation ATB Simulation	85
66	Hybrid III Flexion Neck Rotation ATB Simulation	87
67	Hybrid III Flexion O.C. Rotation ATB Simulation	88
68	Hybrid III Extension Neck Rotation ATB Simulation	89

69	Hybrid III Extension O.C. Rotation ATB Simulation	90
70	Hybrid III Lateral Neck Rotation ATB Simulation	91
71	Hybrid III Lateral O.C. Rotation ATB Simulation	92
72	Hybrid III Neck Stiffness Coefficient Simulation	93
73	Hybrid III O.C. Stiffness Coefficient Simulation	94
74	Graphical Comparison for Flexion Test	96-97
75	Graphical Comparison for Extension Test	98-99
76	Graphical Comparison for Lateral Test	100-101
77	HSM Hybrid II Flexion Simulation	104
78	HSM Hybrid III Flexion Simulation	106
79	HSM Hybrid III Extension Simulation	107

LIST OF TABLES

Table		page
1	Static Neck Tester Test Matrix For Hybrid II and Hybrid III Necks	17
2	Static Flexion Tests Hybrid III S/N 569 Resistive Torque During Loading	21
3	Static Flexion Tests Hybrid III S/N 569 Resistive Torque During Unloading	25
4	Static Hysteresis Data Hybrid II	33
5	Static Hysteresis Data Hybrid III	40
6	Static Extension Tests Hybrid III S/N 569 Resistive Torque During Loading	43
7	Static Extension Tests Hybrid III S/N 569 Resistive Torque During Unloading	44
8	Static Lateral Tests Hybrid III S/N 569 Resistive Torque During Loading	47
9	Static Lateral Tests Hybrid III S/N 569 Resistive Torque During Unloading	48
10	Head/Neck Pendulum Test Matrix For Hybrid II and Hybrid III Necks	53
11	Damping Ratios For Hybrid II Necks	62
12	Damping Ratios For Hybrid III Necks	67

BACKGROUND

The Department of Defense (DOD) has long been interested in the development and use of crash dummies to improve safety for air crew members. The Navy began their development of a crash dummy, or manikin, in the early 1960's with the Grumman Alderson Research Dummy (GARD). The Air Force became involved in manikin development with the advent of the "Golden Shells" program. Golden Shells developed a set of exterior flesh molds for several anthropometric sized manikins. The largest of these molds was used by the Air Force in the development of the Dynamic Analog Anthropomorphic Dummy¹, often referred to by its nickname "Dynamic Dan". Dynamic Dan was designed with an emphasis on vertical impacts and to replicate human ranges of motion.

In the 1980's the Air Force developed the Advanced Dynamic Anthropomorphic Manikin (ADAM)^{2,3}. ADAM, which was also designed with an emphasis on vertical impact response, is a highly instrumented manikin that is being used in the design and evaluation of present and future ejection seats.

The Department of Transportation (DOT) and the automotive industry have developed crash dummies to improve automobile safety. The Department of Transportation sponsored the development of the Vehicle Impact Protection (VIP) manikin in the early 1970's. Following the VIP manikin, General Motors (GM) developed several automotive safety dummies, the first of which was called the Hybrid II^{4,5}. GM also developed the Anthropomorphic Test Dummy (ATD)^{6,7} and its final version the Hybrid III⁸ in the mid seventies. The Hybrid II and Hybrid III dummies are widely used by the automotive industry, the Department of Transportation, and the Department of Defense for use in crash tests to determine occupant safety.

Until the completion of ADAM, Hybrid II and Hybrid III manikins had replaced most of the DOD developed manikins. Now a transition from the Hybrid II and Hybrid III dummies to ADAM, as the Air Force test manikin, is taking place.

Although ADAM is designed differently from the Hybrid II and Hybrid III dummies, it still retains several of their features, namely ADAM's head and neck. ADAM has a Hybrid II

head, which has been modified to accept a Denton Inc. head/neck six axis load cell, and a Hybrid III neck. Instrumentation is required to quantify the loads experienced by the manikin during a test. Accelerometers in the manikin's head and chest, as well as force and moment instrumentation at the top of the neck and bottom of the spine, provide some of the most critical data concerning injury potential. Low impact manikin test data are compared to equivalent human test data. Manikins are then tested at higher levels, which could be injurious to humans. The manikin data then provide a basis from which to extrapolate equivalent human load data. Instrumented manikin testing is a proven and valuable method of collecting high level impact load data.

INTRODUCTION

The head and neck are the most vulnerable parts of the human body during impact exposures. Because of this, numerous papers and models have been developed to predict the motion and injury of the head/neck system for various impacts. Several of the leading authors on this subject include Mertz^{9,10}, Wismans^{11,12}, Phillips^{13,14}, Ewing^{15,16}, Huston^{17,18}, Spenny^{19,20}, and Melvin^{21,22}.

Another approach to predicting occupant motion during simulated crashes is the use of computer models. Some of these models include the Mathematical Dynamic Model (MADYMO)²³, Crash Victim Simulator (CVS)²⁴, the Air Force derivative of the CVS - the Articulated Total Body (ATB) model^{25,26,27}, Isohuman Simulation Model (ISM)²⁸, and the Head Spine Model (HSM)^{29,30}. One of the more recent areas of computer modeling deals with modeling manikins to validate already conducted crash tests and to predict responses for other crash situations.

The mechanical properties of the Hybrid II and Hybrid III necks have been measured previously and simulation data bases prepared^{31,32,33}. These neck properties, however, have not been measured over the full range of static and dynamic loads that the necks experience in impact tests. Therefore, the existing databases are not adequate for modeling neck responses over the full range of anticipated use. Correct neck properties are critical, because of the subtle differences in neck response that must be resolved to determine whether a certain situation is hazardous or not.

This report describes the steps taken to measure the static stiffness and dynamic damping and stiffness characteristics of the Hybrid II and Hybrid III necks in flexion, extension, and lateral bending. Two Hybrid II and two Hybrid III necks were tested. The mechanical properties of the necks were then incorporated into already established computer data sets for the ATB model and HSM model to illustrate improvements in the dynamic response of these necks at various impact levels.

Static neck tests were performed on the Static Neck Tester (SNT)³⁴. The SNT is a device that applies a pure bending moment to the top of the neck, while the base of the neck is

held rigidly. Potentiometers measure the angle of rotation and a torque sensor measures the resistive torque of the neck, while a linear variable differential transformer (LVDT) measures the linear distance between the base and the top of the neck during rotation. Loading and unloading tests were conducted up to 80° rotation, and data were collected approximately every 5°.

Dynamic tests were performed on the Head/Neck Pendulum (HNP)³⁵. The HNP is a dynamic neck tester built to SAE J211 Part 572 Specifications³⁶. A head and neck are securely mounted to the end of a rigid pendulum arm. The arm is raised to a range of pre-determined heights that result in impact speeds between 5ft/sec and 23ft/sec. The arm is then released and free falls until it strikes a block of aluminum honeycomb. The honeycomb material provides a near square wave deceleration pulse for the pendulum arm. This rapid deceleration of the pendulum arm causes the head and neck to flex about the end of the pendulum arm. Accelerometers on the pendulum arm and in the head measure the deceleration of the system. A potentiometer device mounted between the base of the neck and the head measures the rotation of the head and neck. Finally, a Denton six axis load cell measures the forces and moments at the head/neck interface. Flexion (forward), extension (backward), and lateral (sideways) tests were performed at impact speeds between 5ft/sec and 23ft/sec.

Data collected from the SNT were reduced using regression techniques to determine the torque versus rotation slopes and hysteresis effects of both necks in flexion, extension, and lateral static tests. Dynamic data collected from the HNP were reduced to torque versus rotation curves and overlaid with the static data and the computer model data for analysis. Neck rotation versus time curves provided data to calculate the damping characteristics of the neck. Several tests were also photographed by high speed cameras to provide position data to correlate to computer model graphical output.

The ATB rigid body dynamics model was one of two computer codes used to model the head and neck responses of HNP tests. Pendulum arm deceleration data were used with existing data sets for the Hybrid III neck. No current data set existed for the Hybrid II neck. ATB tabular and graphical output were compared to actual test data for accuracy. The data sets were then revised using the new stiffness, damping, and energy loss properties measured in this study. The models were rerun and the output compared to the actual test data. Improvements in response with the new data were observed.

The HSM finite element code was the second computer model used in these tests. Similar runs, comparisons, and changes were

made to this model. Again, the new data compared better to the actual test data than the previous data sets.

This study has shown that the data measured on the SNT and HNP have resulted in improved neck property data than that measured from previous test fixtures³¹. These neck data once reduced can be easily incorporated into existing computer model data sets such as the ATB and HSM. Improvements to such computer model data sets considerably enhance the utility of these models for predictive simulation of manikin head/neck structure dynamics. Such improvements allow effective modeling of the head and neck with encumbering equipment such as helmets, night vision goggles, and helmet mounted display systems for likelihood of injury potential and safety of flight certification.

HYBRID II AND HYBRID III HEAD/NECK STRUCTURES

In order to understand the approach and tests described in this report, a discussion defining the generic concepts and theory motivating this subject must first be addressed. The scope of this report will be limited to the head and neck structures. The design of most manikin head and neck structures are based on human impact response data described by Mertz (et al)⁹. These data were derived from human experiments to determine the mechanical properties of human head and necks during various impacts. The Hybrid II head and neck were designed before these specifications were written and therefore do not exhibit the same biofidelity (humanlike response) as the Hybrid III head and neck, which were based on the Mertz data.

Manikin head structures are rigid to idealize the structural integrity of the skull. The weight and center of mass correspond to a human head of the same anthropometric size. An anatomical coordinate system defines a reference to the human head center of mass. Figure 1 illustrates a generic manikin head structure with an anatomical coordinate system.

The anatomical coordinate system follows the right hand rule. The 'Y' axis is defined as the line passing through the left and right tragions, positive to the left. The 'X' axis intersects and is perpendicular to the 'Y' axis passing through the right infraorbital, positive out of the face. The 'Z' axis is the cross-product of the 'X' and 'Y' axes as shown in equation (1).

$$\vec{Z} = \vec{X} \times \vec{Y} \quad (1)$$

The origin of the anatomical axis system is the intersection of the 'Y' axis and a line drawn perpendicular to the 'Y' axis passing through the sellion.

Figure 2 shows a lateral view of a generic head with the anatomical coordinate system. In the X-Z plane, the head center of gravity (c.g.) is above and forward of the axis system origin and the occipital condyle (o.c.), which is the joint between the head and neck. Figure 3 illustrates an isometric view of the head free body diagram.

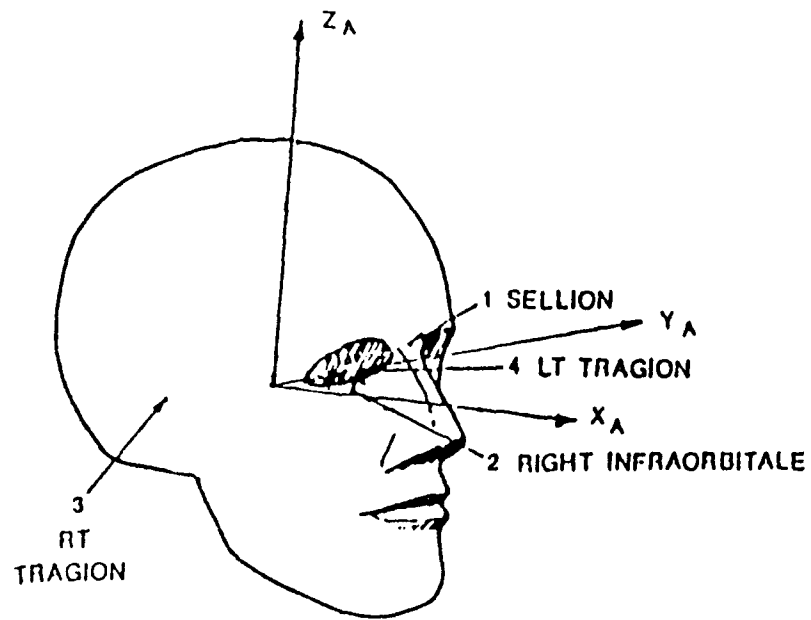


Figure 1. Anatomical Coordinate System

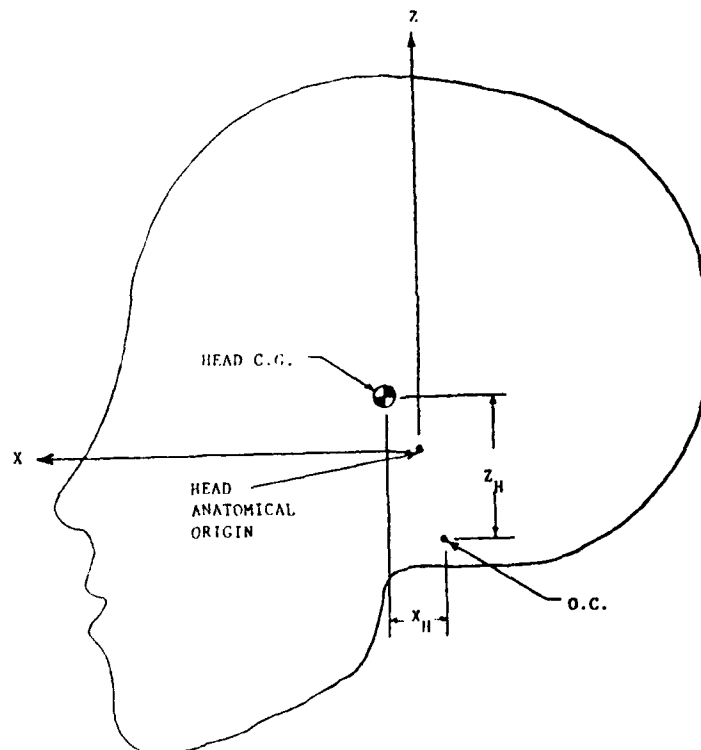


Figure 2. Lateral View of Anatomical Axis System

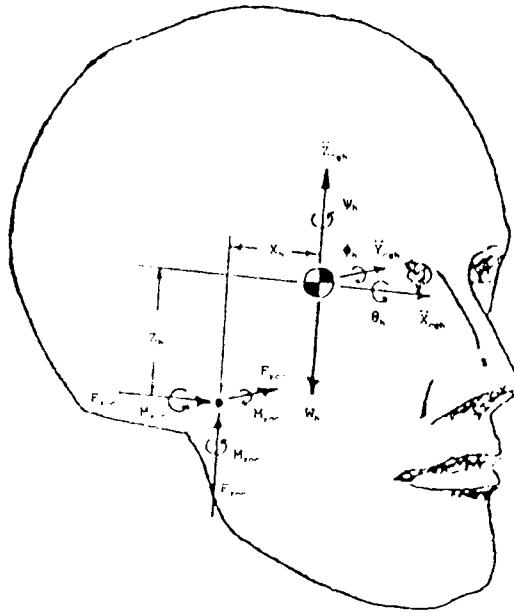


Figure 3. Head Free Body Diagram

The free body diagram allows large deflections in any direction and large roll, pitch, and yaw angles. The head rotates about the o.c. Head translation occurs due to bending of the neck.

A neck structure's design requirements are slightly more complicated. Unlike the head, the neck is not a rigid body. The neck is a deformable body that exhibits axial and rotational stiffness and damping properties during various impacts. The neck also does not exhibit the same response in each direction. For example, the neck when rotated into extension (backward) has a lower stiffness than when rotated into flexion (forward). The length and the location of the joints must match those of an equivalent human neck for obtaining the correct head and neck rotation angles. The end joints of the neck are taken to be the occipital condyle at the top of the neck and T1 at the base of the neck (refer to figure 2). Figure 4 illustrates the free body diagram of the neck.

The free body diagram allows large deflections in any direction and large roll, pitch, and yaw rotations. Additionally, the neck can experience large deformations in any direction. The neck structures are usually made of viscoelastic materials, which closely match the observed nonlinear characteristics of the human neck.

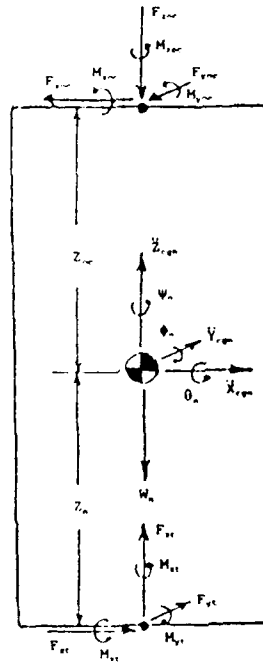


Figure 4. Neck Free Body Diagram

The test articles used for this study include a Hybrid II head, two Hybrid II necks, a Hybrid III head, and two Hybrid III necks. Figure 5 illustrates a Hybrid II head and figure 6 shows a Hybrid II neck.

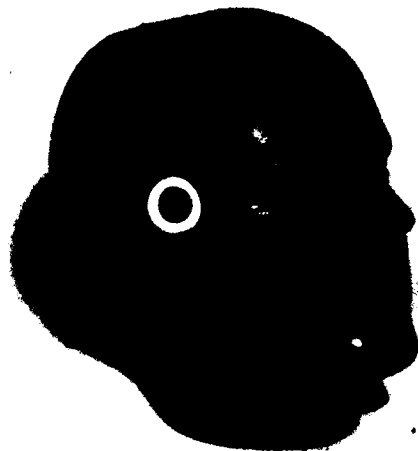


Figure 5. Hybrid II Head

Figure 7 illustrates a Hybrid III head and figure 8 shows a Hybrid III neck.

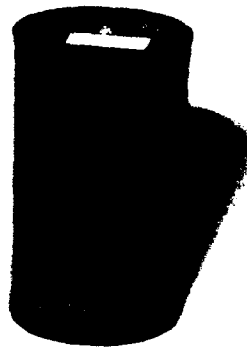


Figure 6. Hybrid II Neck

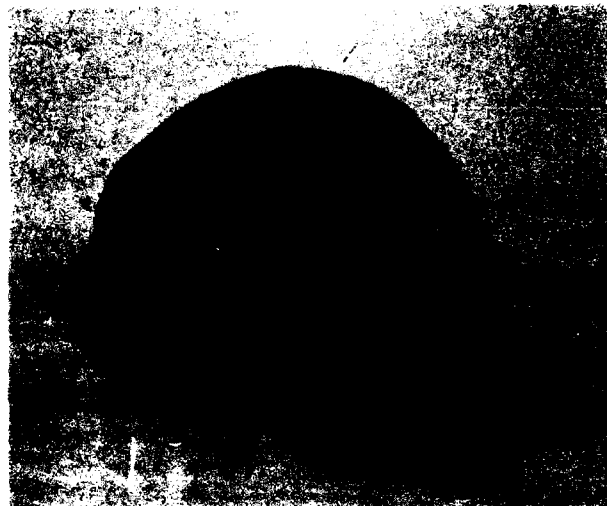


Figure 7. Hybrid III Head



Figure 8. Hybrid III Neck

The Hybrid II and Hybrid III are very different looking head/neck structures. The Hybrid II head looks more like a human head than the Hybrid III head, where the chin area of the Hybrid III was removed to allow the head to rotate farther in flexion similar to a human head. Both heads are aluminum cast shells with a vinyl covering^{4,8}.

The Hybrid II neck is a symmetric cylindrical butyl rubber mold with steel end plates. A 0.5in hole runs the length of this otherwise solid rubber cylinder. Except for the asymmetric inertial properties of the Hybrid II head, the symmetric Hybrid II neck would be expected to give the same dynamic response for any impact angle⁴.

The Hybrid III neck was designed with an emphasis on frontal impacts, which results only in flexion and extension rotations. The Hybrid III neck, like the Hybrid II, is made of butyl rubber with steel end plates, but the similarities end here. There is less butyl rubber in the Hybrid III neck than the Hybrid II neck, because the Hybrid II neck is too stiff, so the Hybrid III neck has three interior steel plates to provide the correct mass. These plates also contribute inertial effects during impacts, which tend to cause the neck to translate as it rotates, similar to a human neck. The Hybrid III neck also has a steel cable that runs through its center. Torqued to the specified 12in-lb, it only acts to limit the rotation of the neck at large angles and does not contribute significantly to the stiffness characteristics of the neck. The Hybrid III neck also incorporates asymmetric flexion/extension stiffness corresponding to that observed in the human, by distributing the rubber material asymmetrically, and by making a horizontal cut through the rubber along the front of the neck between each of the steel disks⁸ (refer to figure 8).

Both the Hybrid II and Hybrid III necks are bolted to the Hybrid II and Hybrid III upper torso respectively, so the interface acts as a fixed joint. The Hybrid II neck is also bolted to the Hybrid II head, as shown in figure 9. This interface also acts as a fixed joint.

A steel end cap is mounted to the top of a Hybrid III neck before it can be mounted to the Hybrid III head, as shown in figure 10. This end cap allows the use of the Denton Inc. Head/Neck load cell, as shown in figure 11.

The Denton load cell is a six axis balance that measures three orthogonal forces and their corresponding moments about the top of the neck. The neck cap and load cell are connected by a condyle pin, which runs parallel to the 'Y' axis at the o.c. as shown in figure 12. This interface acts as a pin joint.



Figure 9. Hybrid II Head/Neck Interface



Figure 10. Hybrid III Neck with End Cap

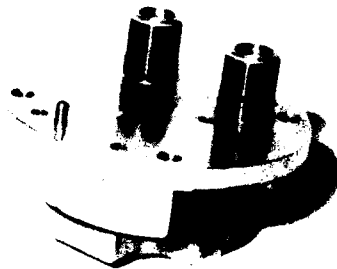


Figure 11. Denton Inc. Head/Neck Load Cell



Figure 12. Hybrid III Head/Neck Interface

Since the head is now free to pivot about the condyle pin, two butyl rubber blocks called nodding blocks are mounted into the end cap of the neck to provide the appropriate stiffness for head rotation alone (refer to figure 12).

For static and dynamic tests, two Hybrid II and two Hybrid III necks were tested to provide two data sets for each test. The Hybrid II and Hybrid III heads were only used for the dynamic tests.

STATIC TESTS

Static Neck Tester

Static tests of the Hybrid II and Hybrid III necks were conducted using a Static Neck Tester (SNT)³⁴. The SNT is a test fixture that quasi-statically loads and unloads a neck in flexion, extension, or lateral bending. Figure 13 shows a side view of the SNT. When pressurized, the cylinder pulls the cable which is connected to the large aluminum disks, causing them to rotate.

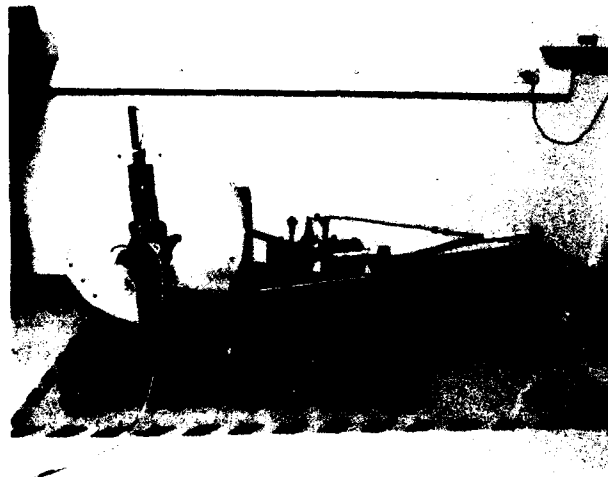


Figure 13. Side View of the SNT

Figure 14 shows an end view of the fixture with a Hybrid III neck under load. The neck is mounted upright in the fixture with the base of the neck rigidly secured to the frame. A mounting plate is attached to the top of the neck and a steel bar passes through it and slots in the large disks. Bearings are secured to the end of the bar, and the two tracks on both disks allow the bar to freely slide along the track as the disks rotate (refer to figures 13 and 14). With this design,

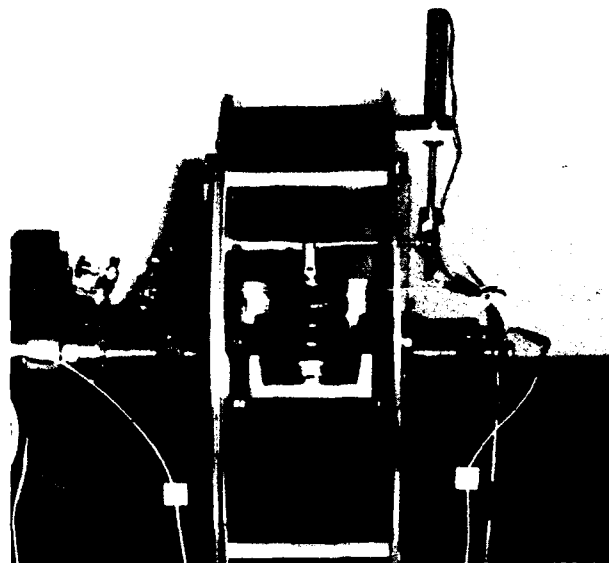


Figure 14. End View of the SNT Under Load

the fixture is able to apply a pure bending moment to the top of the neck throughout the rotation of the disks. Orienting the neck at 0° , 90° , or 180° allows flexion, lateral bending, and extension testing of the necks.

Instrumentation on the SNT includes a torque sensor mounted at the base of the neck to measure the resistive torque of the neck to the applied bending moment, two rotational potentiometers to measure the angular displacement of the neck during rotation, and a linear variable differential transformer (LVDT) to measure the linear compression of the neck between the end plates during rotation. Data were collected on all of these sensors at 5° rotation intervals.

Description of Static Tests

A loading test was performed as a sequence of incremental load applications over a specified range of motion. Loading tests began with the neck at 0° rotation and baseline data were collected. The disks were rotated 5° and data were collected. The disks were rotated another 5° and data were again collected. This procedure was repeated until the final disk rotation angle was reached. After all test data had been collected, the accumulators were depressurized and the neck was returned back to its original position. There was a 60 minute recovery period between tests.

An unloading test was performed as an incremental release of a full-scale load. Unloading tests began with the neck at 0° rotation. The disks were then rotated to the maximum rotation angle for the tests. Data were collected and the pressure reduced until the neck rotated back 5°, where data were again collected. This procedure was repeated until the neck had returned to 0°. Again, there was a 60 minute recovery period between tests. Table 1 lists the loading and unloading tests performed on each of the four necks.

Test Data

Static stiffness was determined by plotting resistive torque versus rotation angle and using regression techniques to determine the loading and unloading slopes. A plot of all of the flexion loading tests, listed in table 1, performed on a Hybrid III neck, is shown in figure 15. This plot is a first order least squares fit of each test's data. The plot shows how repeatable the stiffnesses were as each test's data overlays the previous test's results. The data were very linear through the first 40° but a stiffening of the neck was evident beyond 40°. A first order regression did not fit the data well over the full rotation. Figure 16 illustrates a second order fit of the same data. The results were better, but still did not match the large rotation angle test data well. Figure 17 illustrates a third order fit of all of the data points. The third order regression did match the data well over the full range, but was not as linear over the first 40°. Table 2 lists the regression coefficients and the accuracy of fit to the flexion loading data for first, second, and third order regressions for this neck.

Unloading test data resulted in different looking plots, as figure 18 illustrates. The large drop in resistive torque between the first two data points collected for each test was the hysteresis, or the energy lost before the neck began to rotate back to its original position. Figure 18 illustrated the third order regression fit to the data, because as figures 19 and 20 illustrate, first and second order regression fits were poor. Each unloading test exhibited this characteristic. Table 3 lists the regression coefficients and their accuracy of fit to the flexion unloading data for first, second, and third order regressions for this neck.

Rotational neck compression was measured to determine the repeatability of the neck rotation curve throughout the testing. Rotational neck compression was measured by an LVDT. One end of the LVDT was fixed to the frame, and the other end was fixed to the bar that attached to the top of the neck. As

**TABLE 1. STATIC NECK TESTER TEST MATRIX
FOR HYBRID II AND HYBRID III NECKS**

Loading Characteristic	Flexion Angle of Rotation	Extension Angle of Rotation	Lateral Angle of Rotation
Load	0-10	0-10	0-10
Load	0-20	0-20	0-20
Load	0-30	0-30	0-30
Load	0-40	0-40	0-40
Load	0-50	0-50	0-50
Load	0-60	0-60	0-60
Load	0-70	0-70	0-70
Load	0-80	-	-
Unload	80-0	-	-
Unload	70-0	70-0	70-0
Unload	60-0	60-0	60-0
Unload	50-0	50-0	50-0
Unload	40-0	40-0	40-0
Unload	30-0	30-0	30-0
Unload	20-0	20-0	20-0
Unload	10-0	10-0	10-0

STATIC FLEXION TESTS HYBRID III S/N 569
 FIRST ORDER REGRESSION
 RESISTIVE TORQUE DURING LOADING

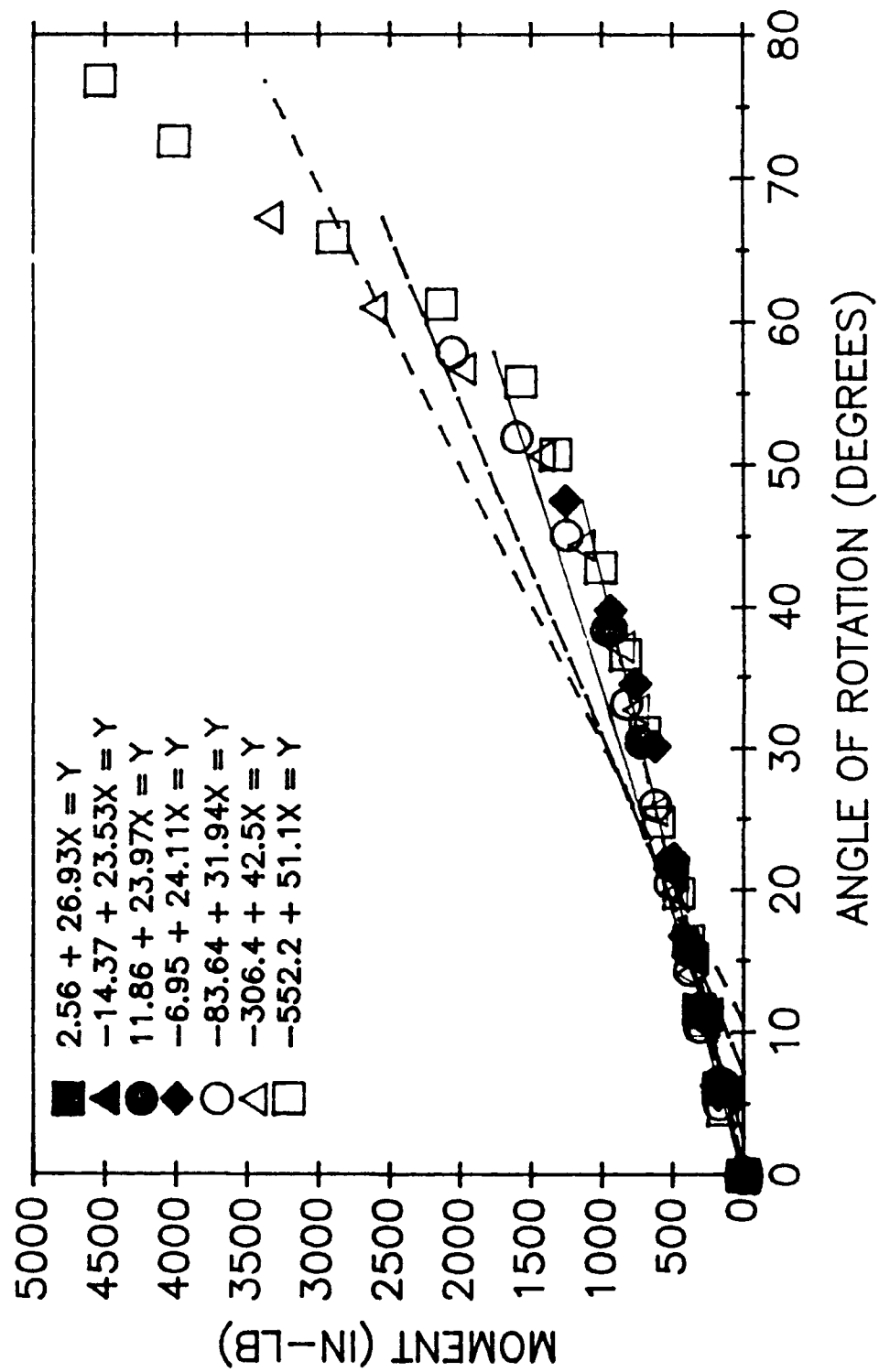


Figure 15 - First Order Regression Fit to Flexion Loading Data

STATIC FLEXION TESTS HYBRID III S/N 569
SECOND ORDER REGRESSION
RESISTIVE TORQUE DURING LOADING

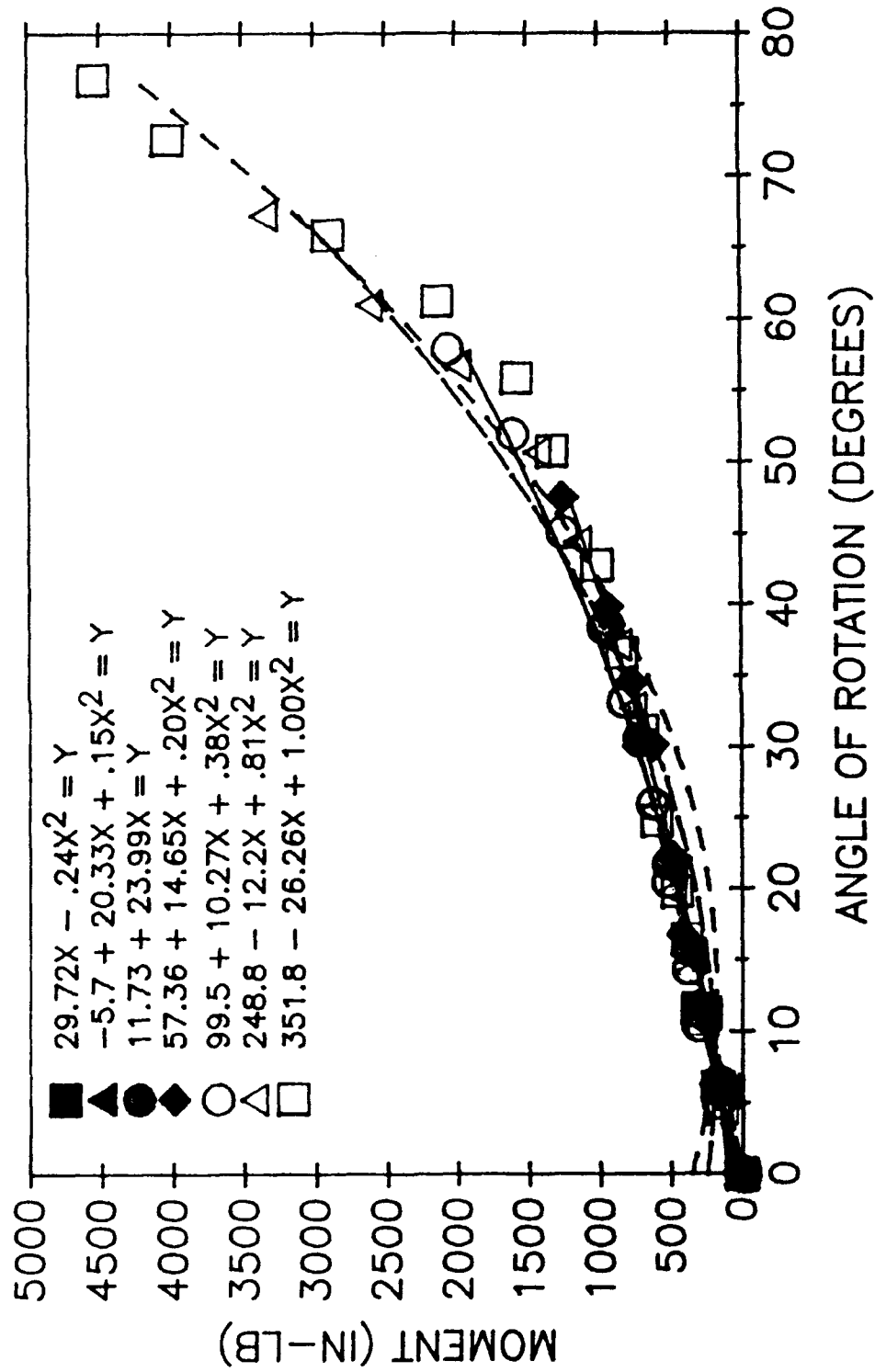


Figure 16 - Second Order Regression Fit to Flexion Loading Data

STATIC FLEXION TESTS HYBRID III S/N 569
THIRD ORDER REGRESSION
RESISTIVE TORQUE DURING LOADING

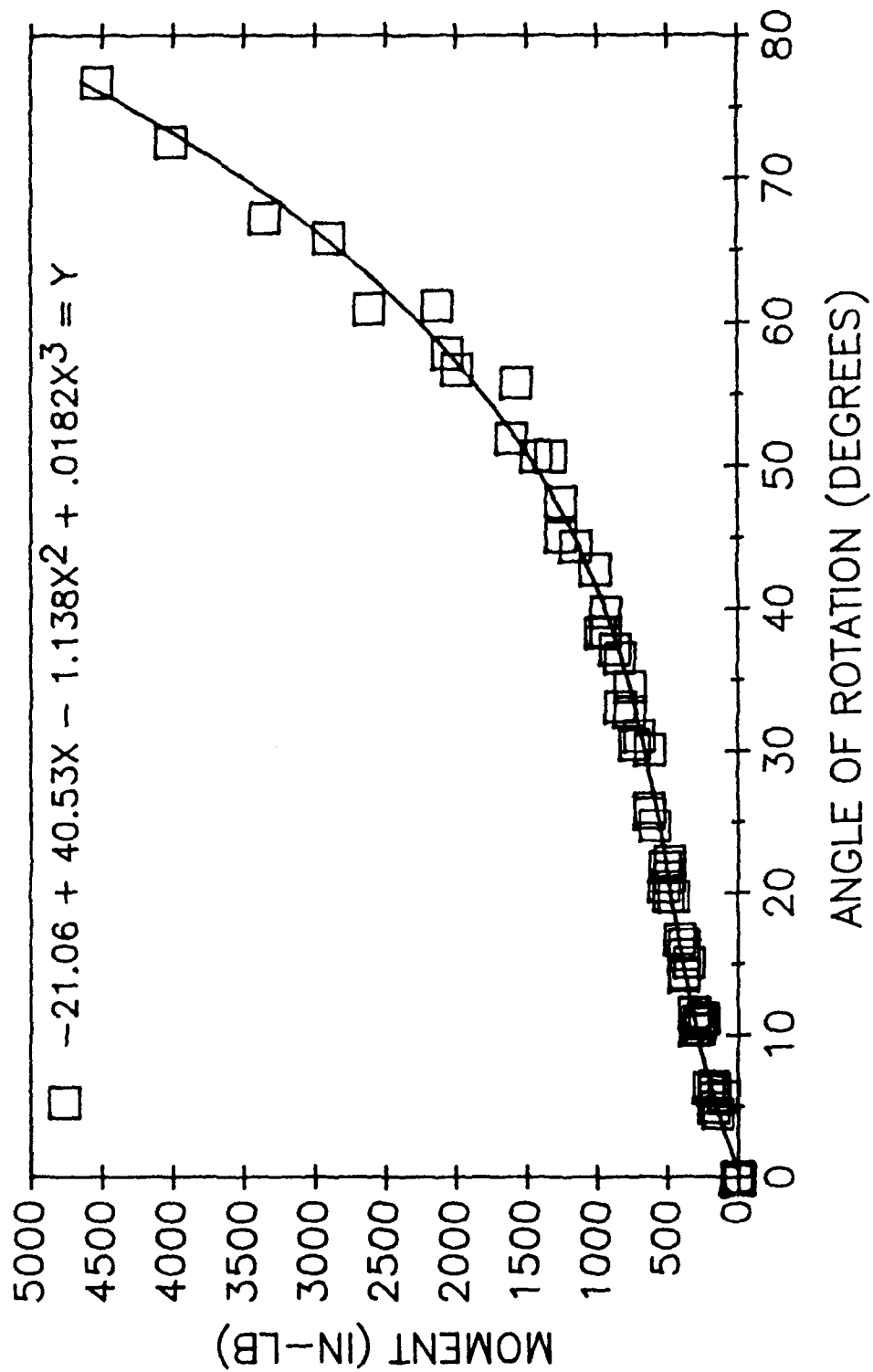


Figure 17 - Third Order Regression Fit to Flexion Loading Data

**TABLE 2. STATIC FLEXION TESTS HYBRID III S/N 569
RESISTIVE TORQUE DURING LOADING**

FIRST ORDER REGRESSION ANALYSIS

Test Rotation Angle	x^0	x^1	RVAL
0-11.7	2.56	26.93	.99955
0-21.2	-14.37	23.53	.99789
0-38.4	11.86	23.97	.99910
0-47.6	-6.95	24.11	.98729
0-58.0	-83.64	31.94	.97743
0-67.3	-306.4	42.50	.93272
0-76.9	-552.2	51.10	.91179
All Test Data	-270.4	41.38	.91514

SECOND ORDER REGRESSION ANALYSIS

Test Rotation Angle	x^0	x^1	x^2	RVAL
0-11.7	0.00	29.72	-.241	1.00000
0-21.2	-5.70	20.33	.152	.99880
0-38.4	11.73	23.99	-.001	.99910
0-47.6	57.36	14.65	.202	.99344
0-58.0	99.49	10.27	.376	.99455
0-67.3	248.8	-12.20	.811	.98540
0-76.9	351.8	-26.26	1.001	.98283
All test data	205.3	-9.73	.774	.98079

THIRD ORDER REGRESSION ANALYSIS

Test Angle	x^0	x^1	x^2	x^3	RVAL
All test data	-21.06	40.53	-1.138	.018	.99638

STATIC FLEXION TESTS HYBRID III S/N 569
THIRD ORDER REGRESSION
RESISTIVE TORQUE DURING UNLOADING

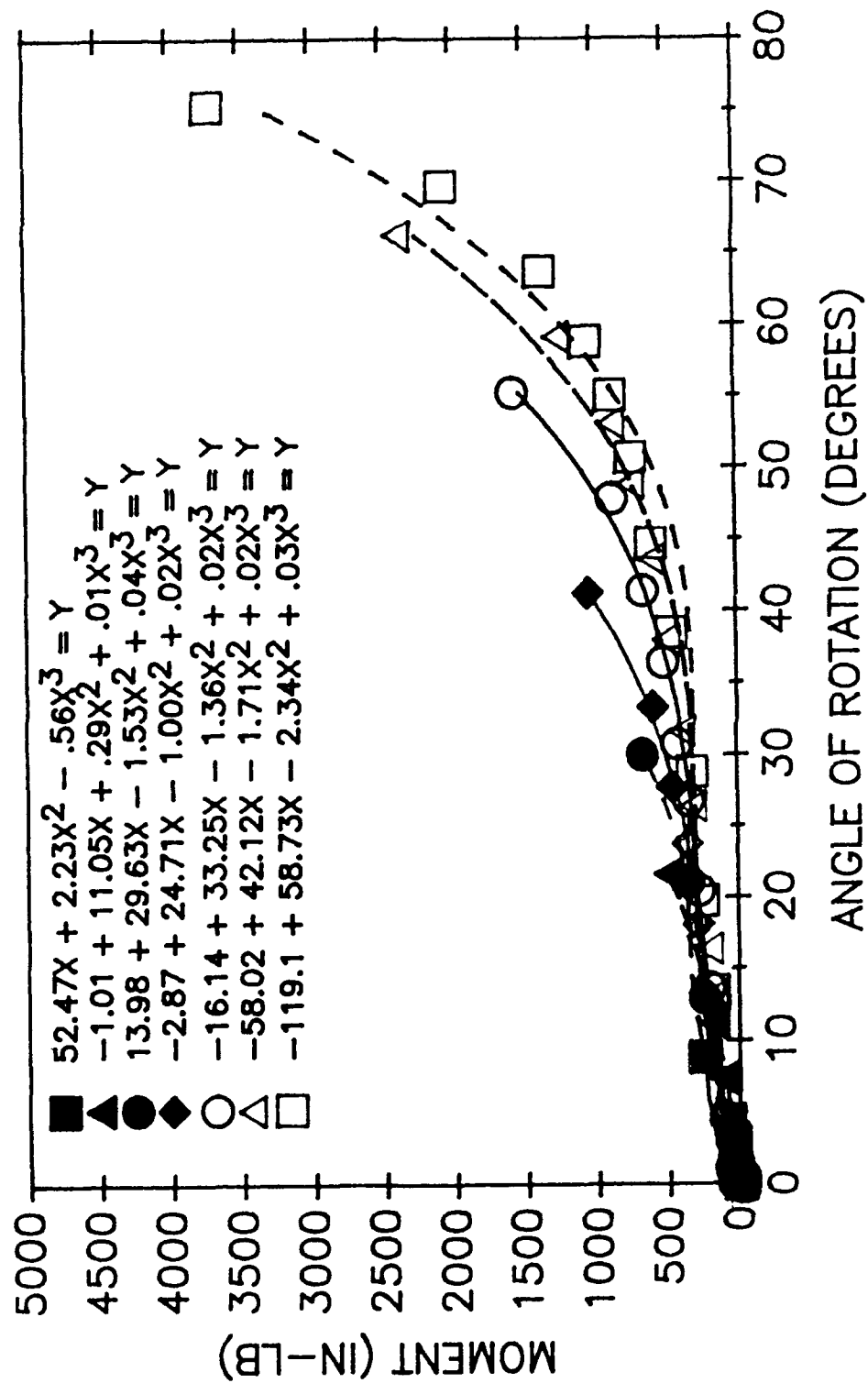


Figure 18 - Third Order Regression Fit to Flexion Unloading Data

STATIC FLEXION TESTS HYBRID III S/N 569
 FIRST ORDER REGRESSION
 RESISTIVE TORQUE DURING UNLOADING

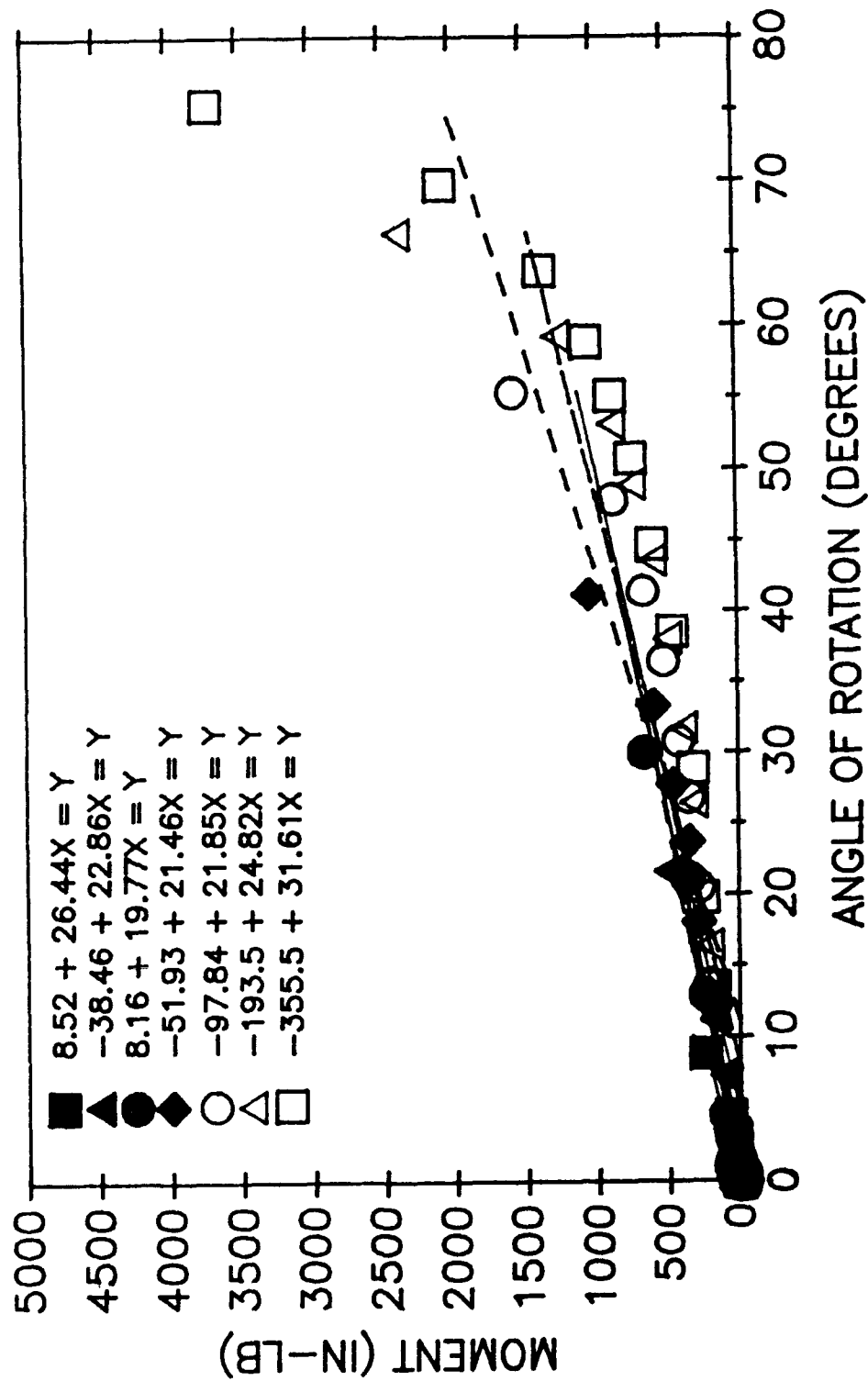


Figure 19 - First Order Regression Fit to Flexion Unloading Data

STATIC FLEXION TESTS HYBRID III S/N 569
SECOND ORDER REGRESSION
RESISTIVE TORQUE DURING UNLOADING

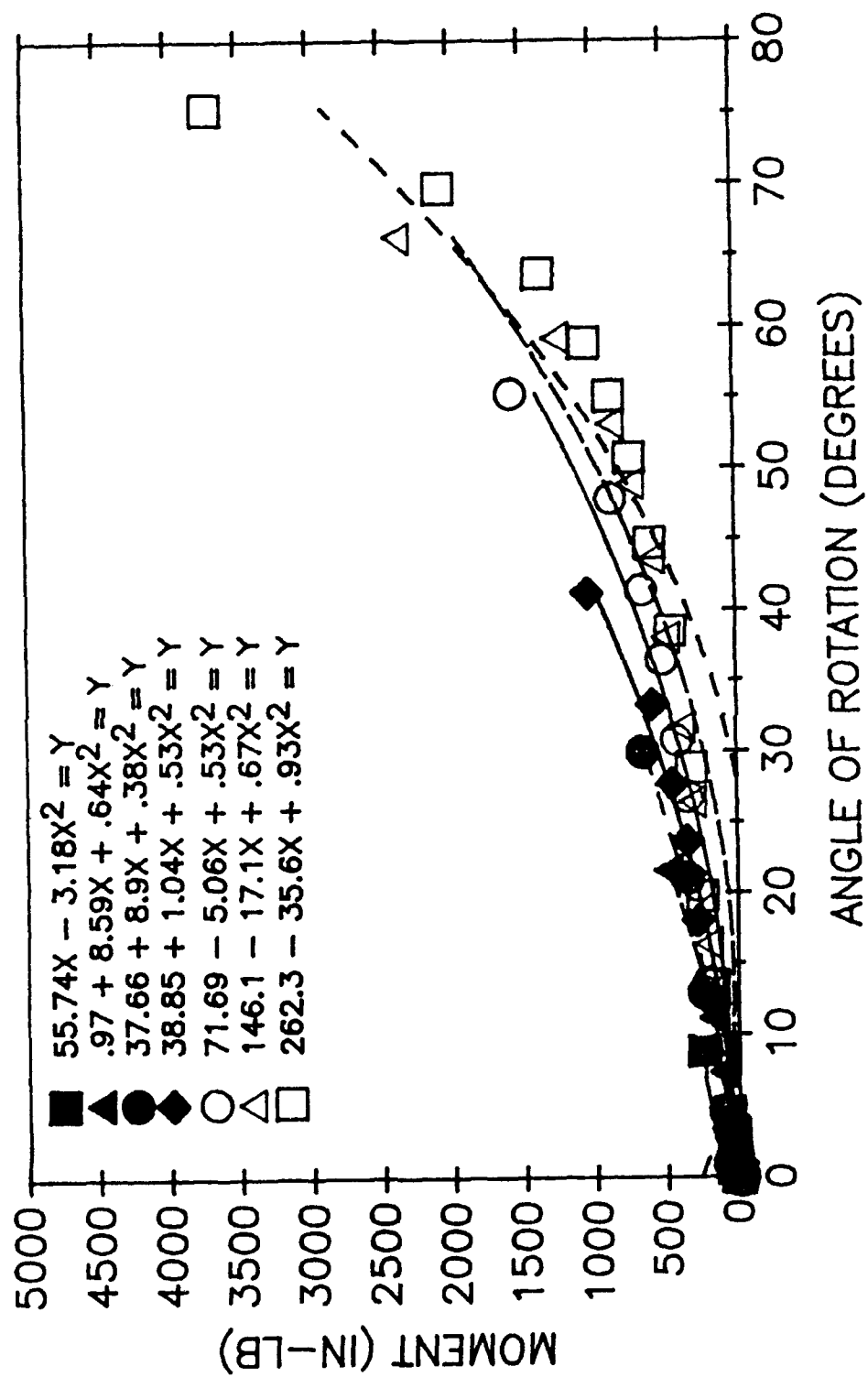


Figure 20 - Second Order Regression Fit to Flexion Unloading Data

**TABLE 3. STATIC FLEXION TESTS HYBRID III S/N 569
RESISTIVE TORQUE DURING UNLOADING**

FIRST ORDER REGRESSION ANALYSIS

Test Rotation Angle	x^0	x^1	RVAL
0-8.9	8.52	26.44	.99774
0-21.7	-38.46	22.86	.98299
0-30.0	8.16	19.77	.97263
0-41.3	-51.93	21.46	.95220
0-55.3	-97.84	21.85	.91381
0-66.4	-193.5	24.82	.86158
0-75.4	-355.5	31.6	.81617

SECOND ORDER REGRESSION ANALYSIS

Test Rotation Angle	x^0	x^1	x^2	RVAL
0-8.9	0.00	55.74	-3.18	1.00000
0-21.7	.97	8.59	.64	.99985
0-30.0	37.66	8.90	.38	.99092
0-41.3	38.85	1.04	.53	.99125
0-55.3	71.69	-5.06	.53	.97671
0-66.4	146.1	-17.1	.67	.95634
0-75.4	262.3	-35.6	.93	.94196

THIRD ORDER REGRESSION ANALYSIS

Test Angle	x^0	x^1	x^2	x^3	RVAL
0-8.9	0.0	52.47	2.23	-.56	1.00000
0-21.7	-1.01	11.05	.29	.01	.99992
0-30.0	13.98	29.63	-1.53	.04	.99774
0-41.3	-2.87	24.71	-1.00	.02	.99906
0-55.3	-16.14	33.25	-1.36	.02	.99663
0-66.4	-58.02	42.12	-1.71	.02	.99093
0-75.4	-119.1	58.73	-2.34	.03	.98522

the neck was rotated, the LVDT measured the linear distance between the top and bottom of the neck. Figure 21 illustrates the repeatability of the rotational neck compression between tests. It can be concluded from this plot that the neck was rotated through the same arc for each test. Similar results were found for every neck in flexion, extension, and lateral testing.

Stiffness Characteristics

Two Hybrid II and two Hybrid III necks were tested with the SNT. Loading and unloading flexion, extension, and lateral bending tests were conducted on each of the necks as listed in table 1.

Hybrid II Necks

Figure 22 illustrates the linear stiffness of the first Hybrid II neck during flexion loading. The second Hybrid II neck also exhibited linear stiffness throughout the testing range, but the slopes were slightly less as the fit equations in figure 23 illustrate. Figure 24 illustrates a comparison between slopes of all of the data for both necks.

Since the Hybrid II neck is symmetric in geometry and material, identical stiffness results would be expected for flexion, extension, and lateral bending tests. Figure 25 illustrates the almost identical loading stiffness for an extension test. Similar loading results were found with both Hybrid II necks in flexion, extension, and lateral bending. Therefore, a single bending stiffness can define the loading stiffness of the neck at any orientation. This bending stiffness was taken as the average of the two Hybrid II necks, as shown in figure 24.

The Hybrid II necks did not show the same degree of hysteresis as shown in the previous section for a Hybrid III neck. Figure 26 illustrates an unloading test of a Hybrid II neck. Similar results were found with both Hybrid II necks.

Internal hysteresis was defined as the energy lost between loading and unloading a specimen. Equation (2) illustrates the method used in the SAE Part 572 Specifications for calculating internal hysteresis³⁶.

$$\frac{\text{area between curves}}{\text{area under loading curve}} \times 100\% = \text{Hysteresis} \quad (2)$$

STATIC FLEXION TESTS HYBRID III S/N 569
SECOND ORDER REGRESSION
NECK COMPRESSION DURING LOADING

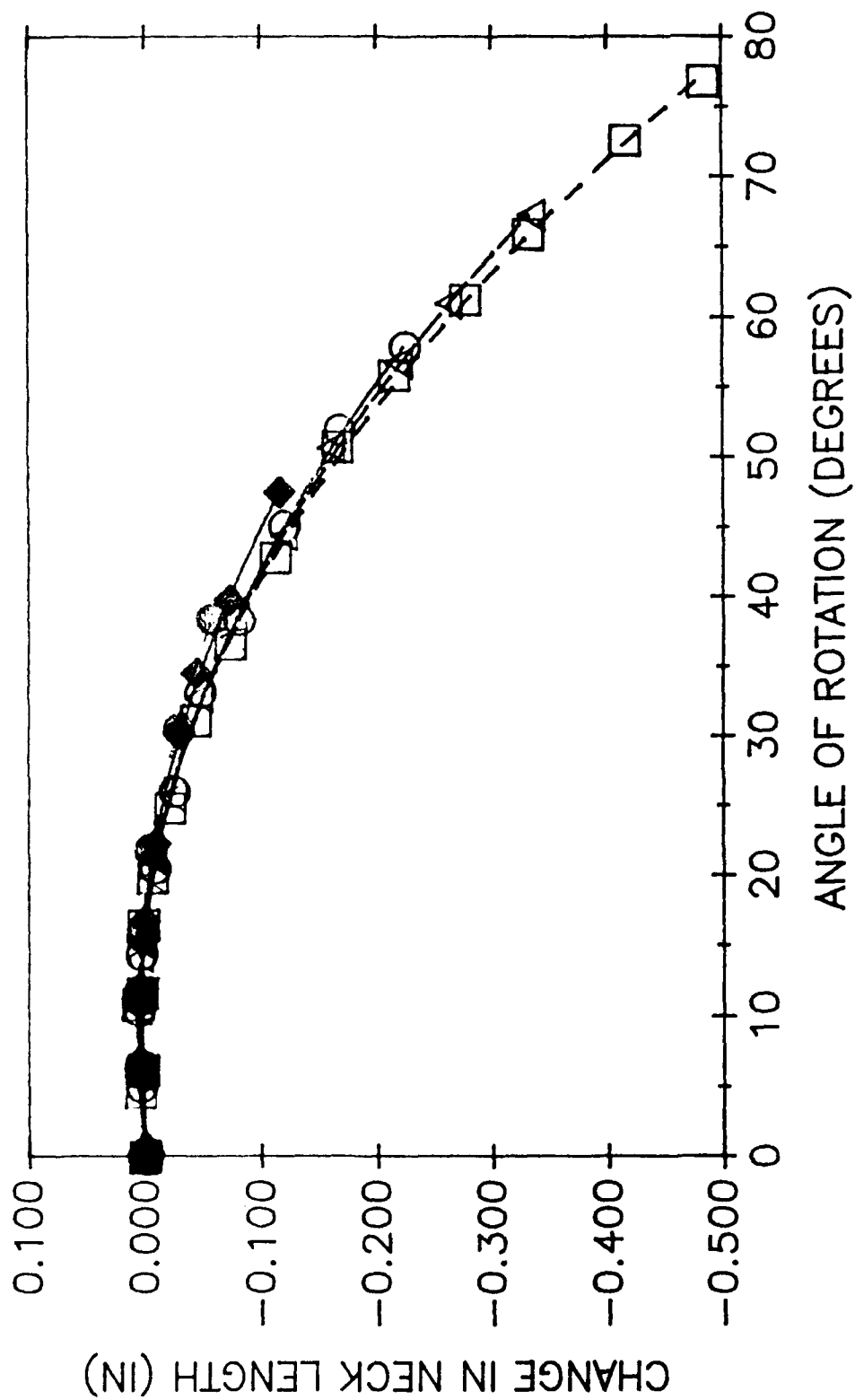


Figure 21 - Neck Compression During Loading

STATIC FLEXION TESTS HYBRID II S/N 3232
FIRST ORDER REGRESSION
RESISTIVE TORQUE DURING LOADING

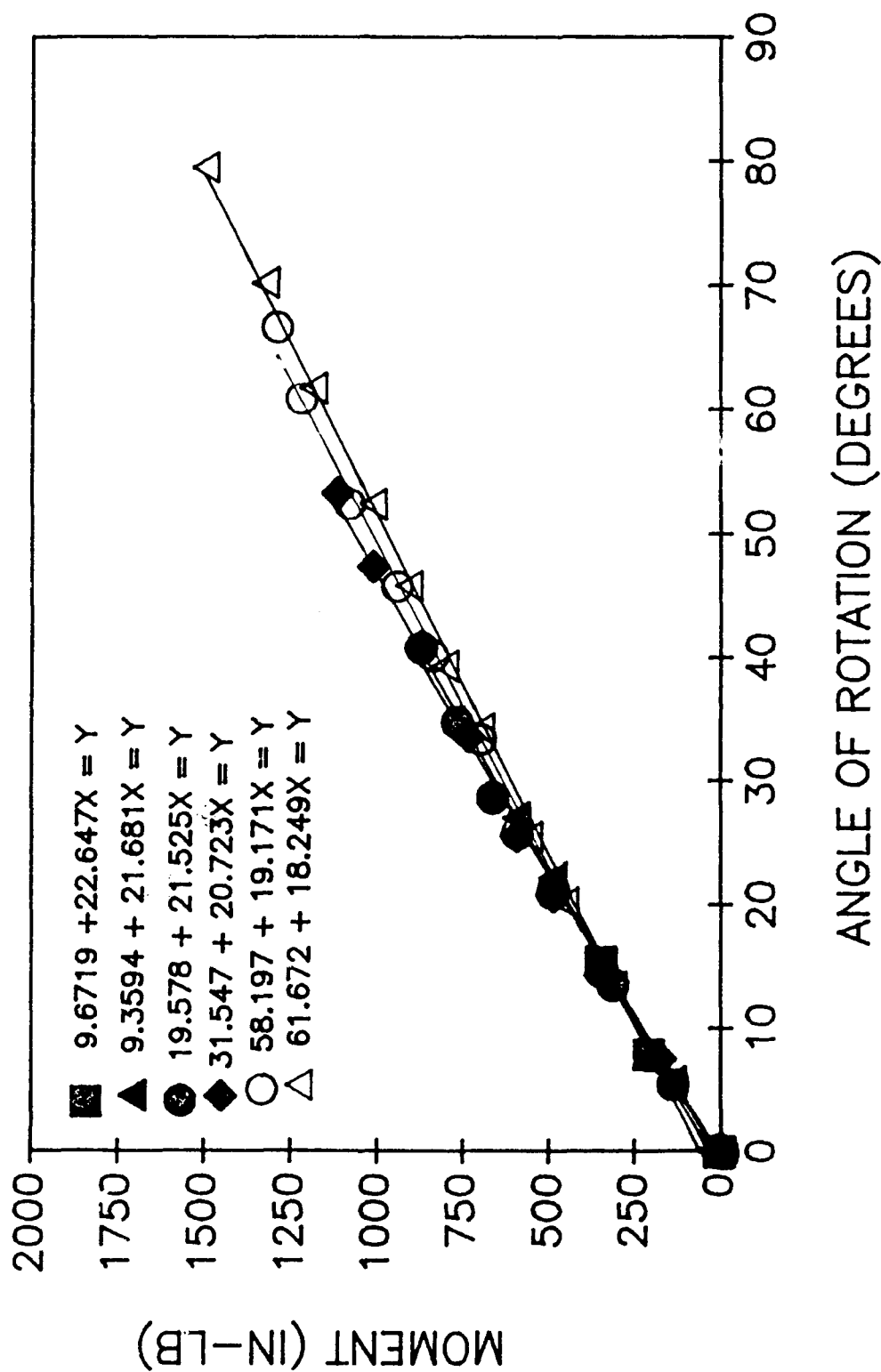


Figure 22 - Flexion Loading Hybrid II Neck 1

STATIC FLEXION TESTS HYBRID II S/N 0262P
 FIRST ORDER REGRESSION
 RESISTIVE TORQUE DURING LOADING

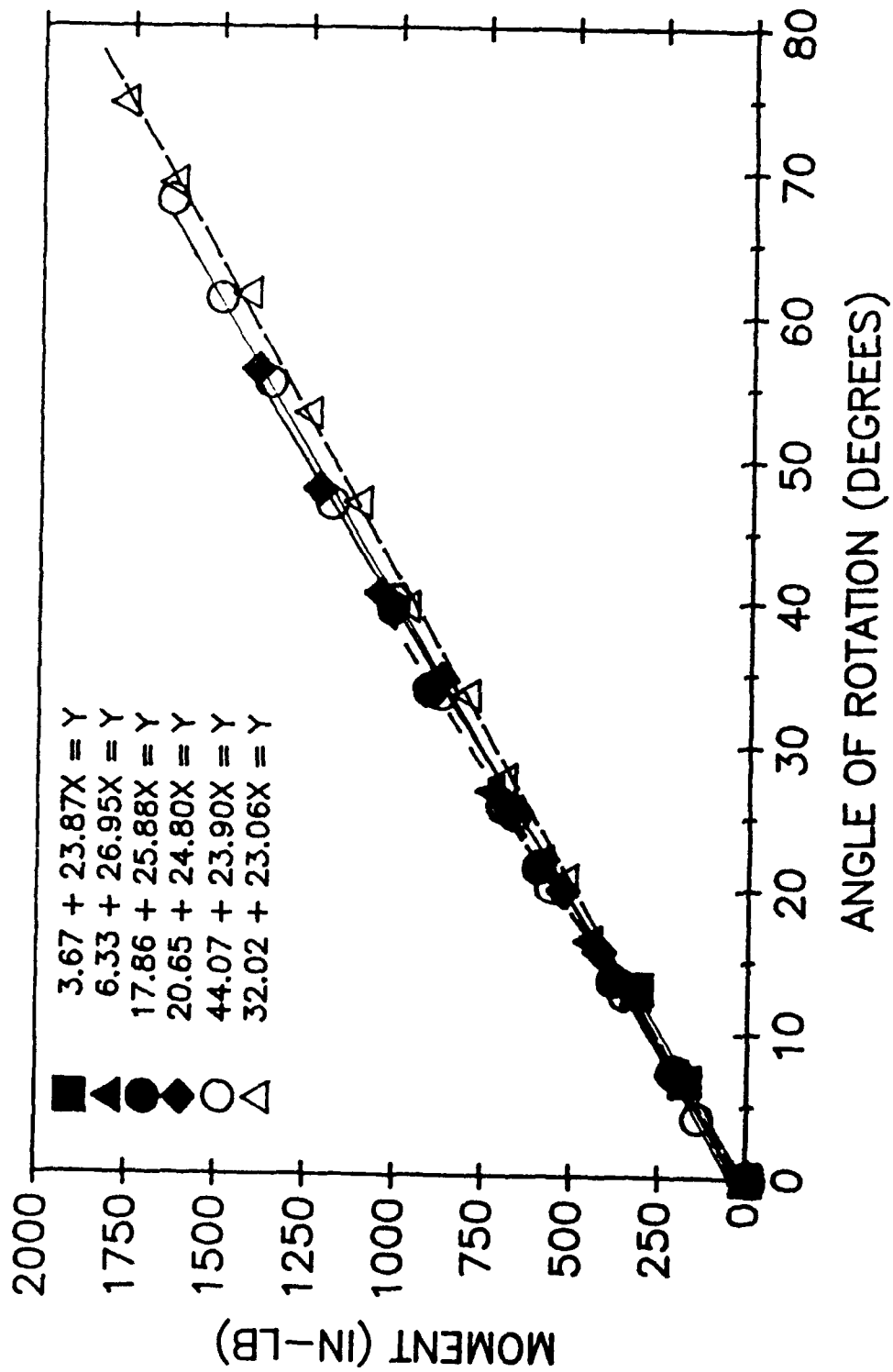


Figure 23 - Flexion Loading Hybrid II Neck 2

STATIC FLEXION TESTS HYBRID II
FIRST ORDER REGRESSION
RESISTIVE TORQUE DURING LOADING

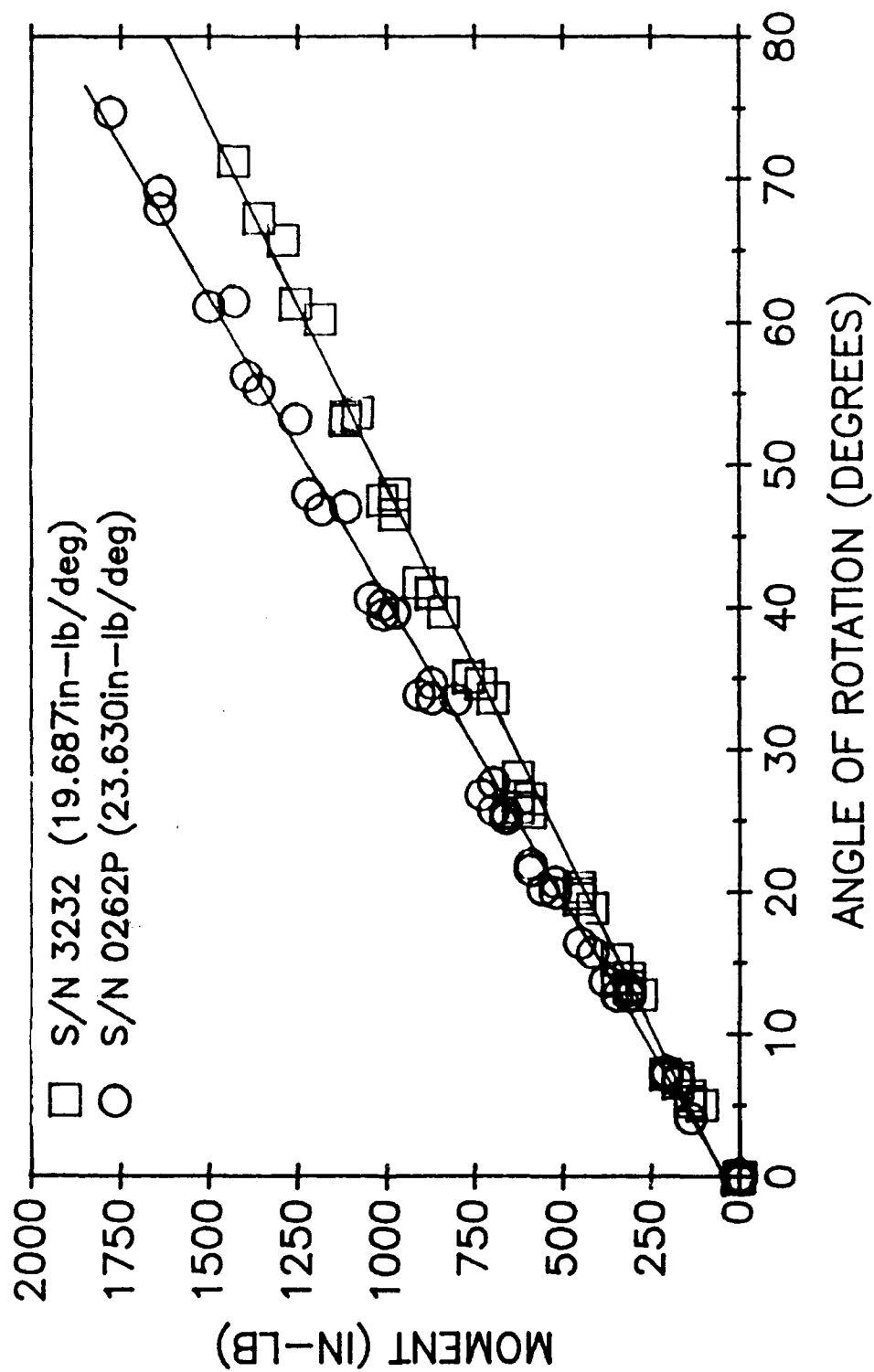


Figure 24 - Average Flexion Loading Hybrid II Necks

STATIC EXTENSION TESTS HYBRID II S/N 3232
 FIRST ORDER REGRESSION
 RESISTIVE TORQUE DURING LOADING

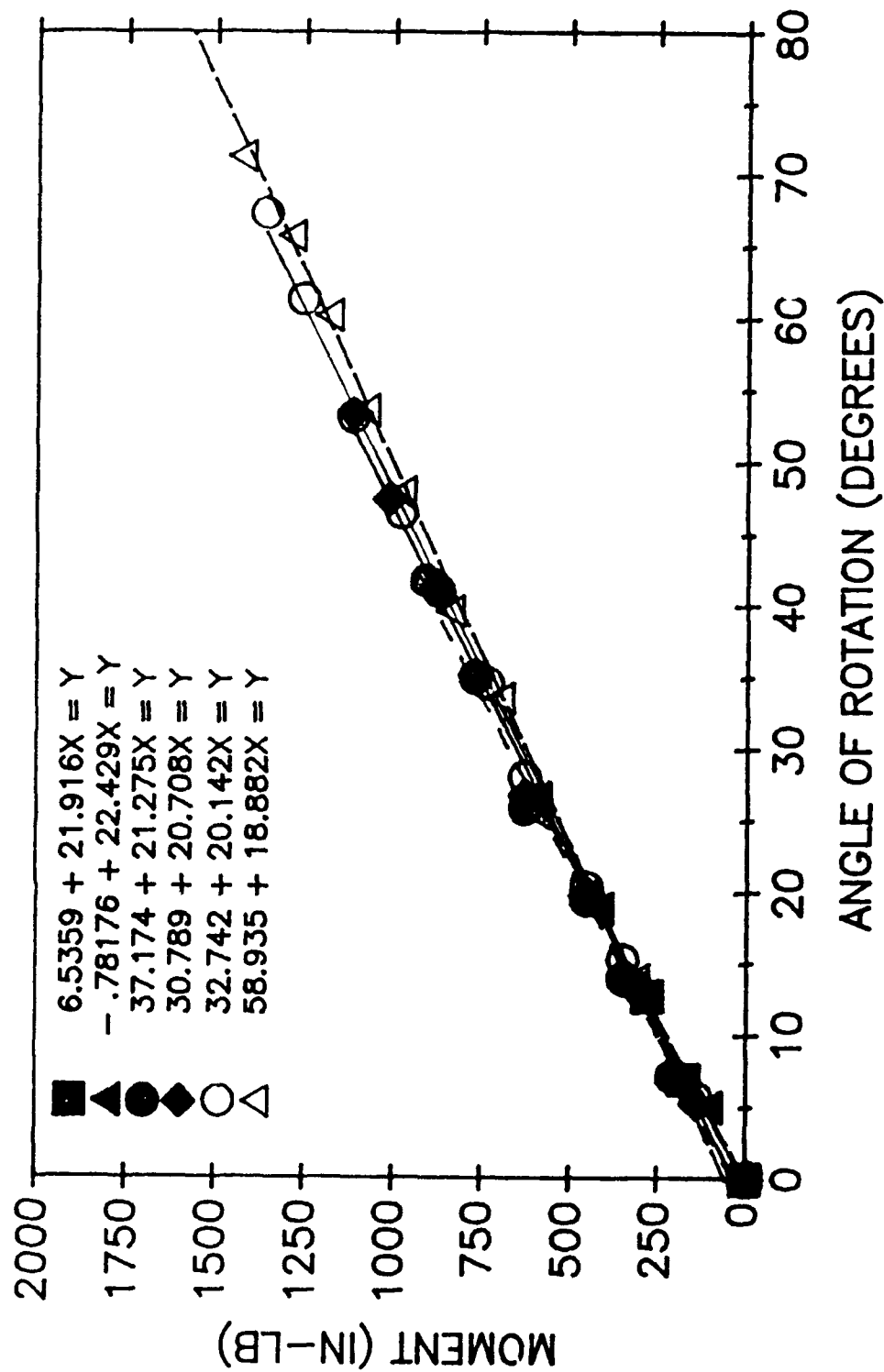


Figure 25 - Extension Loading Hybrid II Neck 1

STATIC FLEXION TESTS HYBRID II S/N 3232
THIRD ORDER REGRESSION
RESISTIVE TORQUE DURING UNLOADING

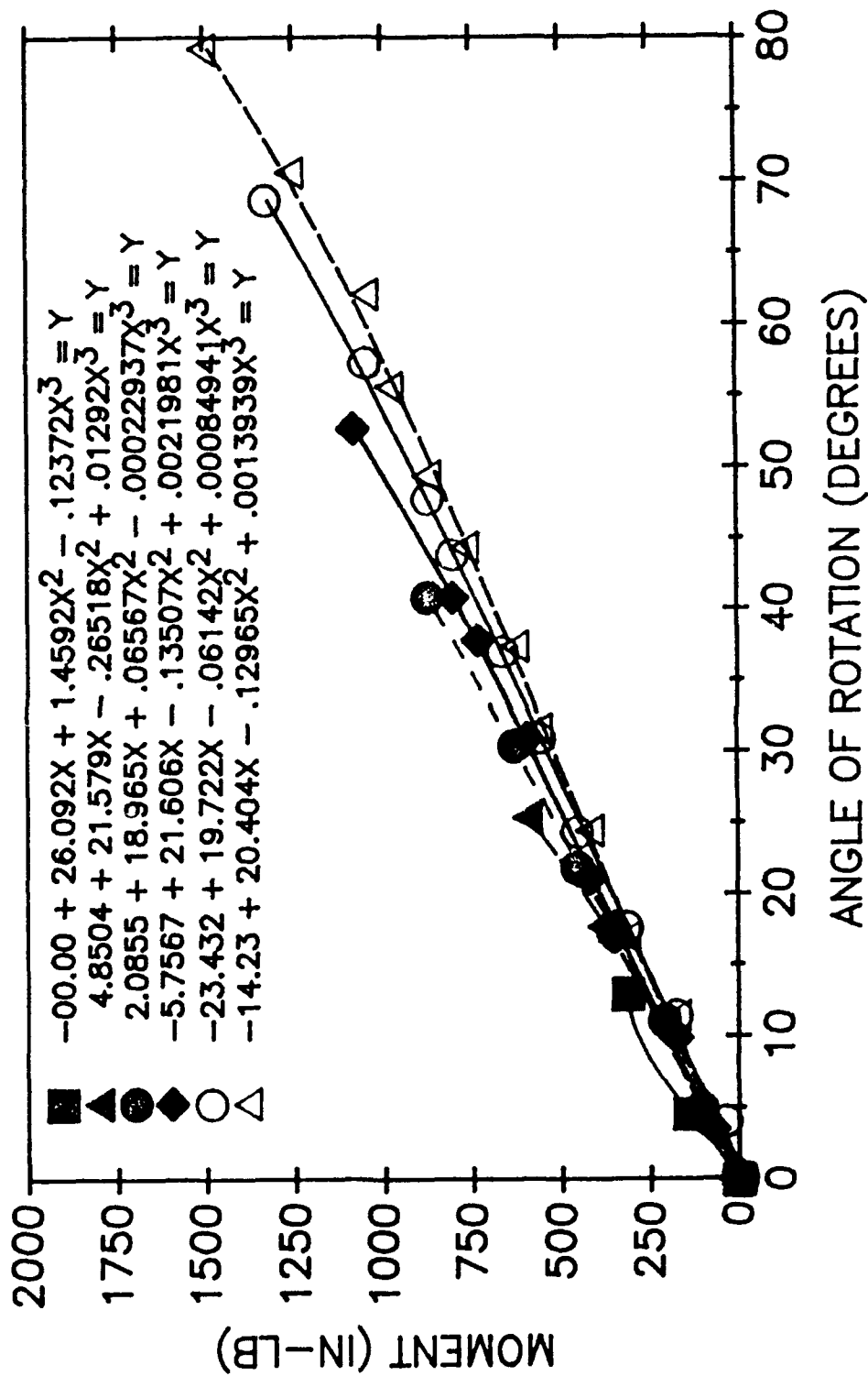


Figure 26 - Flexion Unloading Hybrid II Neck 1

Figure 27 illustrates loading and unloading curves for a Hybrid II neck. To calculate the percent of hysteresis, the coefficients of the regression fit were used to form two polynomials: one loading curve polynomial, and one unloading curve polynomial. The two equations were integrated from zero to their intersection point. Then equation (2) was used to calculate the percent of internal hysteresis. This calculation was performed using the loading curve and each of the unloading curves. Since the percent of hysteresis was relatively low for the Hybrid II necks, an average hysteresis was calculated for each Hybrid II neck and for both necks, as shown in table 4. Note that the first average unloading curve was not used because its average was higher than the average loading curve. This occurred because the neck data was averaged and the small rotation angle of the neck.

TABLE 4. STATIC HYSTERESIS DATA HYBRID II

	S/N 3232 (%)	S/N 0262P (%)	Average (%)
Bending	9.5	8.7	9.1

Hybrid III Necks

As would be expected from its asymmetric geometry, Hybrid III neck stiffness is sensitive to orientation. Figures 15-22 illustrated the stiffness characteristics of one of the two Hybrid III necks in flexion. Figure 28 illustrates the flexion loading curves for the second Hybrid III neck. Although similar in shape, the exact curve was not replicated. Figure 29 illustrates the flexion loading curves of both Hybrid III necks overlaid. The data for the first 40° appears very similar. Figure 30 illustrates a first order fit to both plots for the first 40° rotation. The slopes differ by 2.89in-lb/deg. The average stiffness is a fair representation of both data sets.

Unloading data for the second Hybrid III neck was also similar, but not an exact match. Figure 31 illustrates the flexion unloading data for the second Hybrid III neck. When the flexion unloading curves were averaged, just as the flexion loading curves were, both were plotted to determine internal hysteresis. Figure 32 illustrates the average flexion loading and unloading curves for the Hybrid III necks. Internal hysteresis was calculated similarly to that for the Hybrid II necks, by using the coefficients of the regression fits. Table 5 lists the internal hysteresis

STATIC FLEXION TESTS HYBRID II RESISTIVE TORQUE DURING LOADING AND UNLOADING

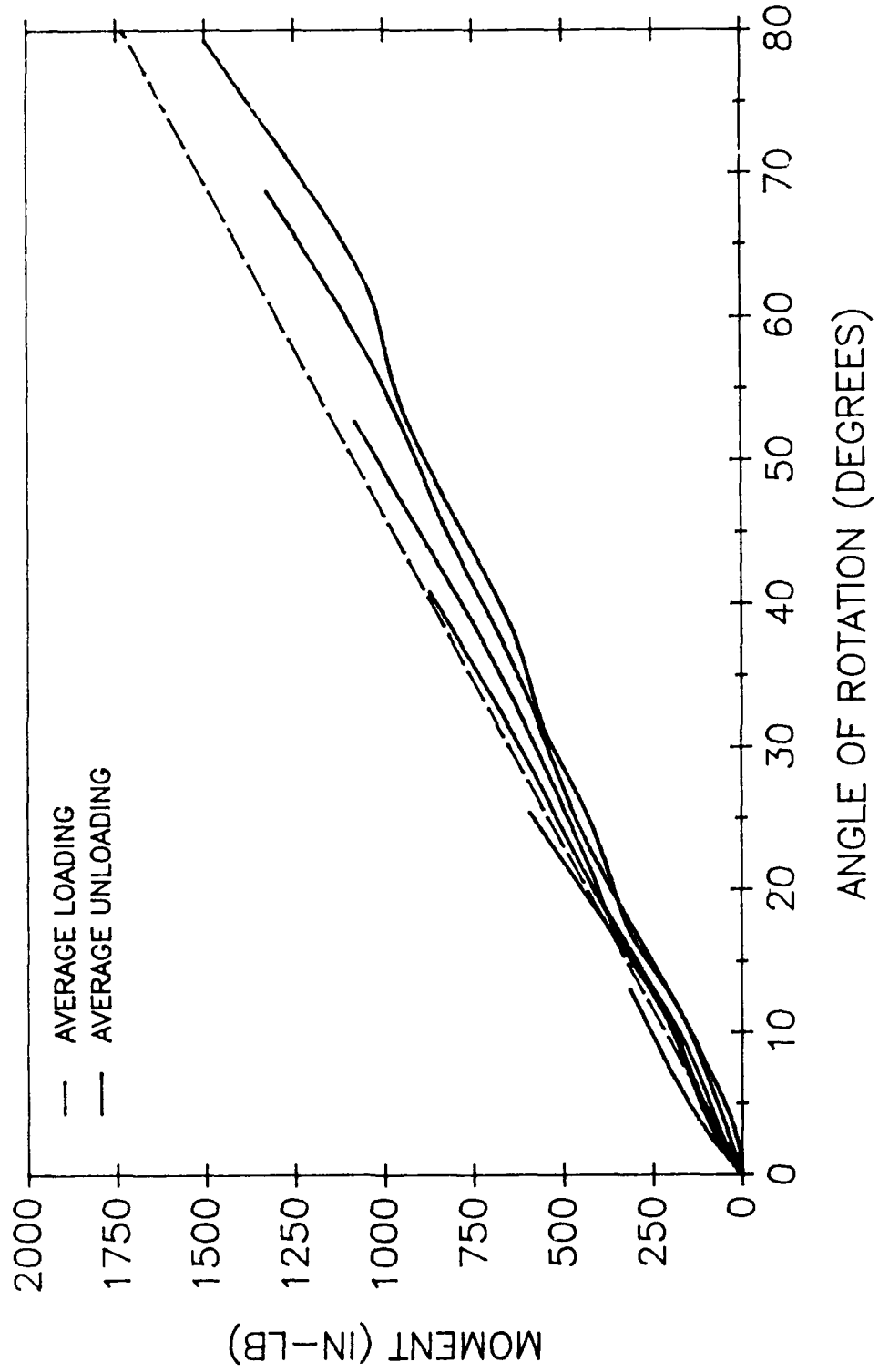


Figure 27 - Loading and Unloading Curves Hybrid II

STATIC FLEXION TESTS HYBRID III S/N 1201
SECOND ORDER REGRESSION
RESISTIVE TORQUE DURING LOADING

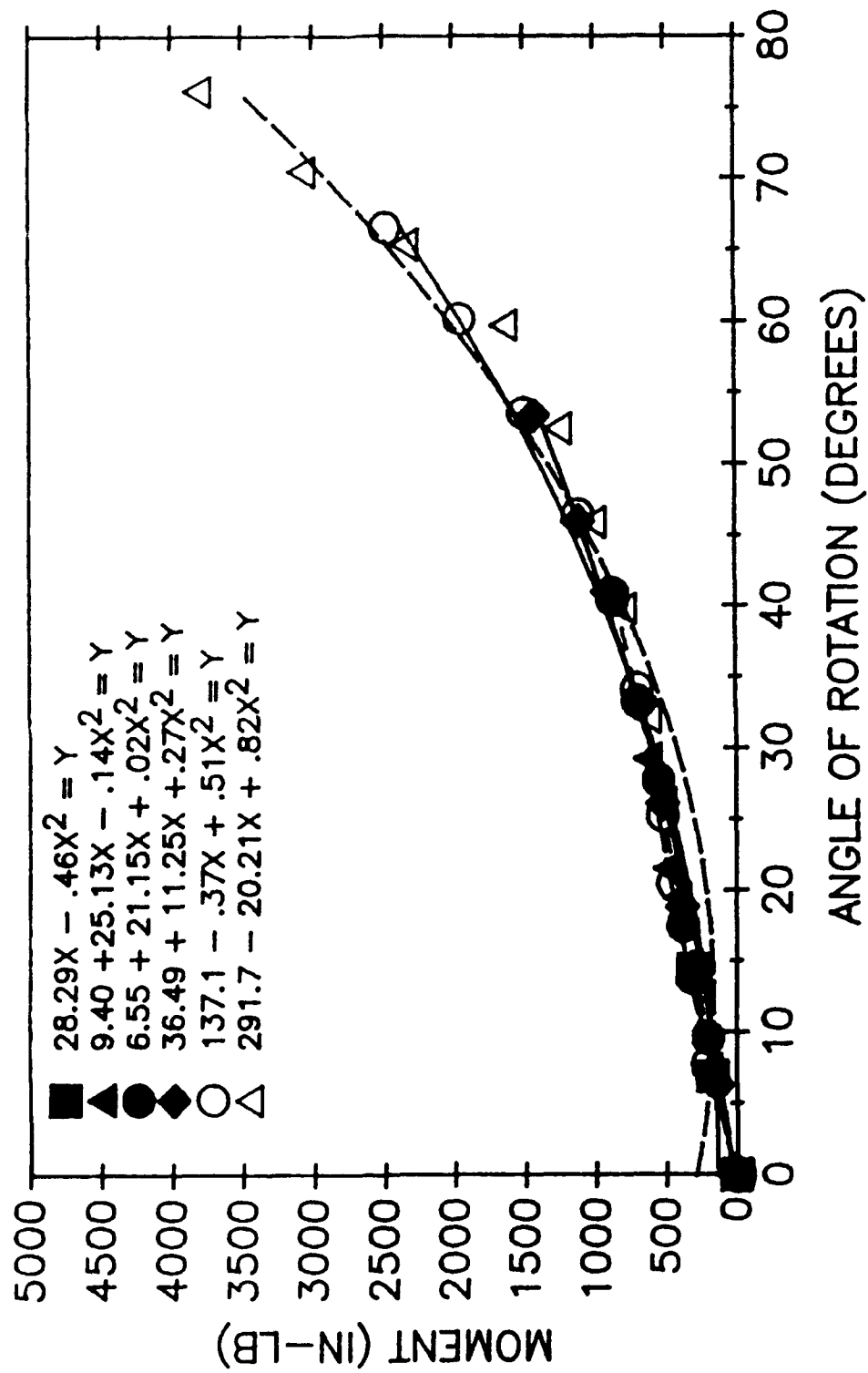


Figure 28 - Flexion Loading Hybrid III Neck 2

STATIC FLEXION TESTS HYBRID III
THIRD ORDER REGRESSION
RESISTIVE TORQUE DURING LOADING

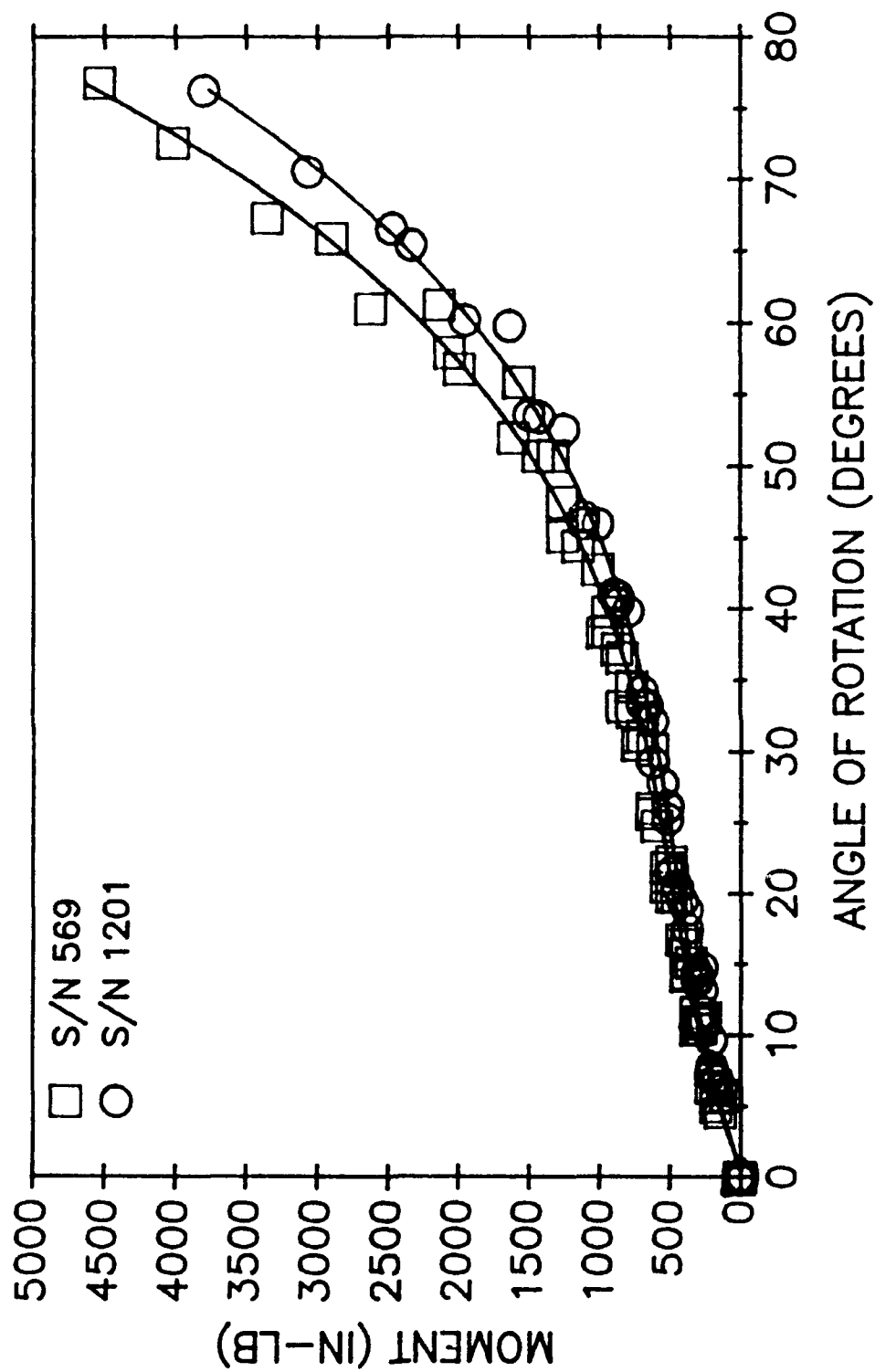


Figure 29 - Flexion Loading Hybrid III Both Necks

STATIC FLEXION TESTS HYBRID III
FIRST ORDER REGRESSION
RESISTIVE TORQUE DURING LOADING

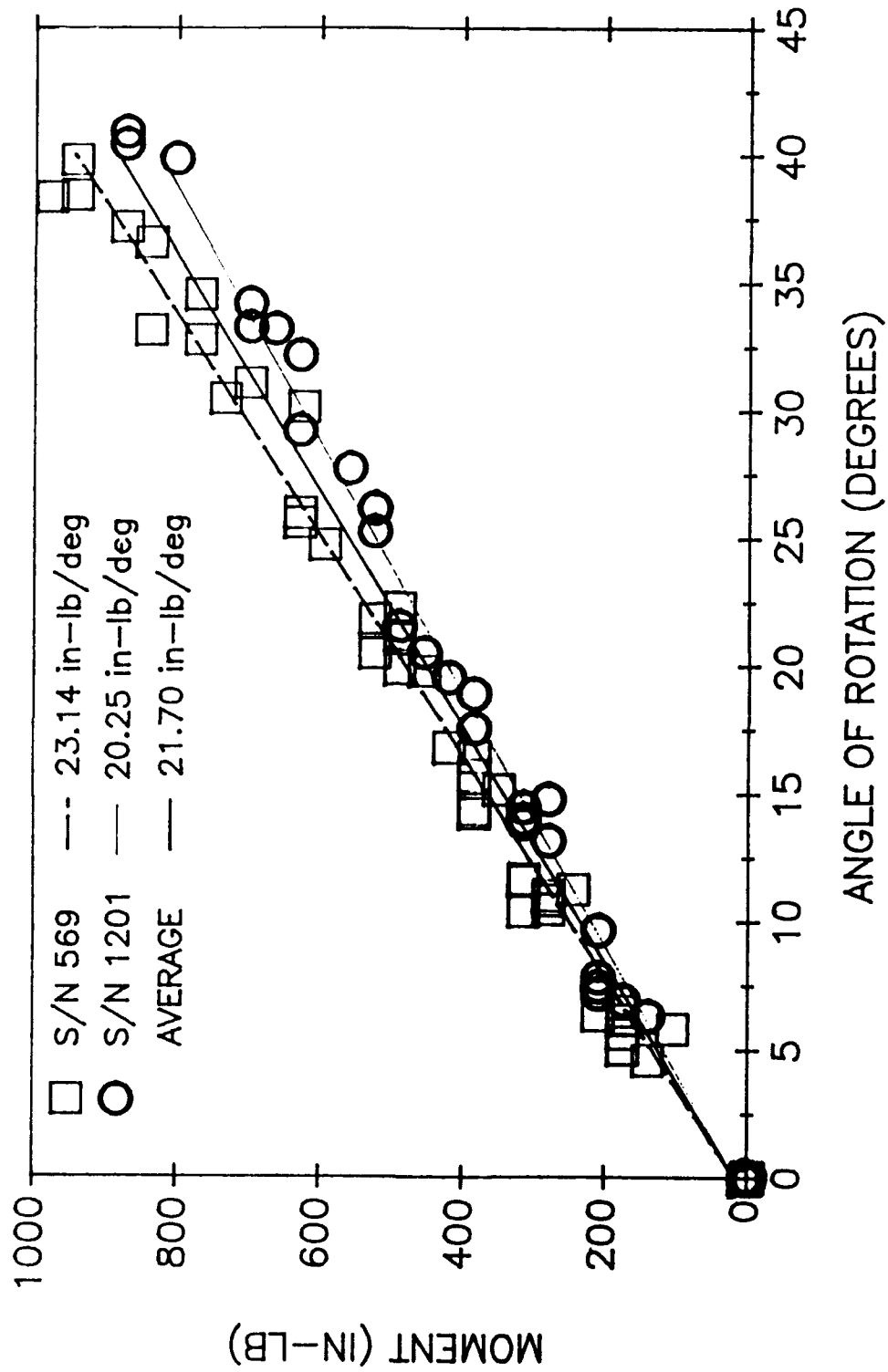


Figure 30 - Flexion Loading to 40° Hybrid III Both Necks

STATIC FLEXION TESTS HYBRID III S/N 1201
THIRD ORDER REGRESSION
RESISTIVE TORQUE DURING UNLOADING

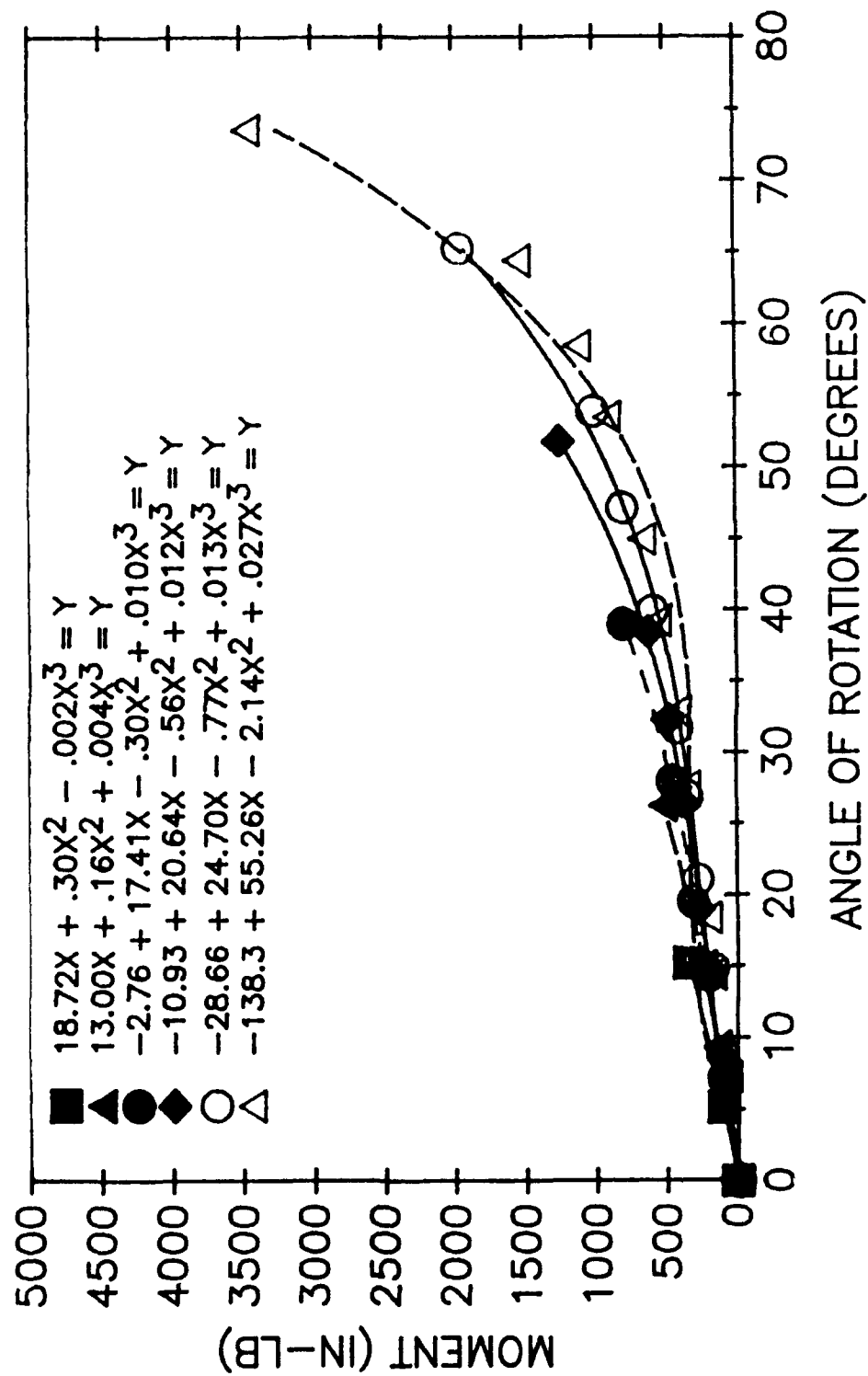


Figure 31 - Flexion Unloading Hybrid III Neck 2

STATIC FLEXION TESTS HYBRID III RESISTIVE TORQUE DURING LOADING AND UNLOADING

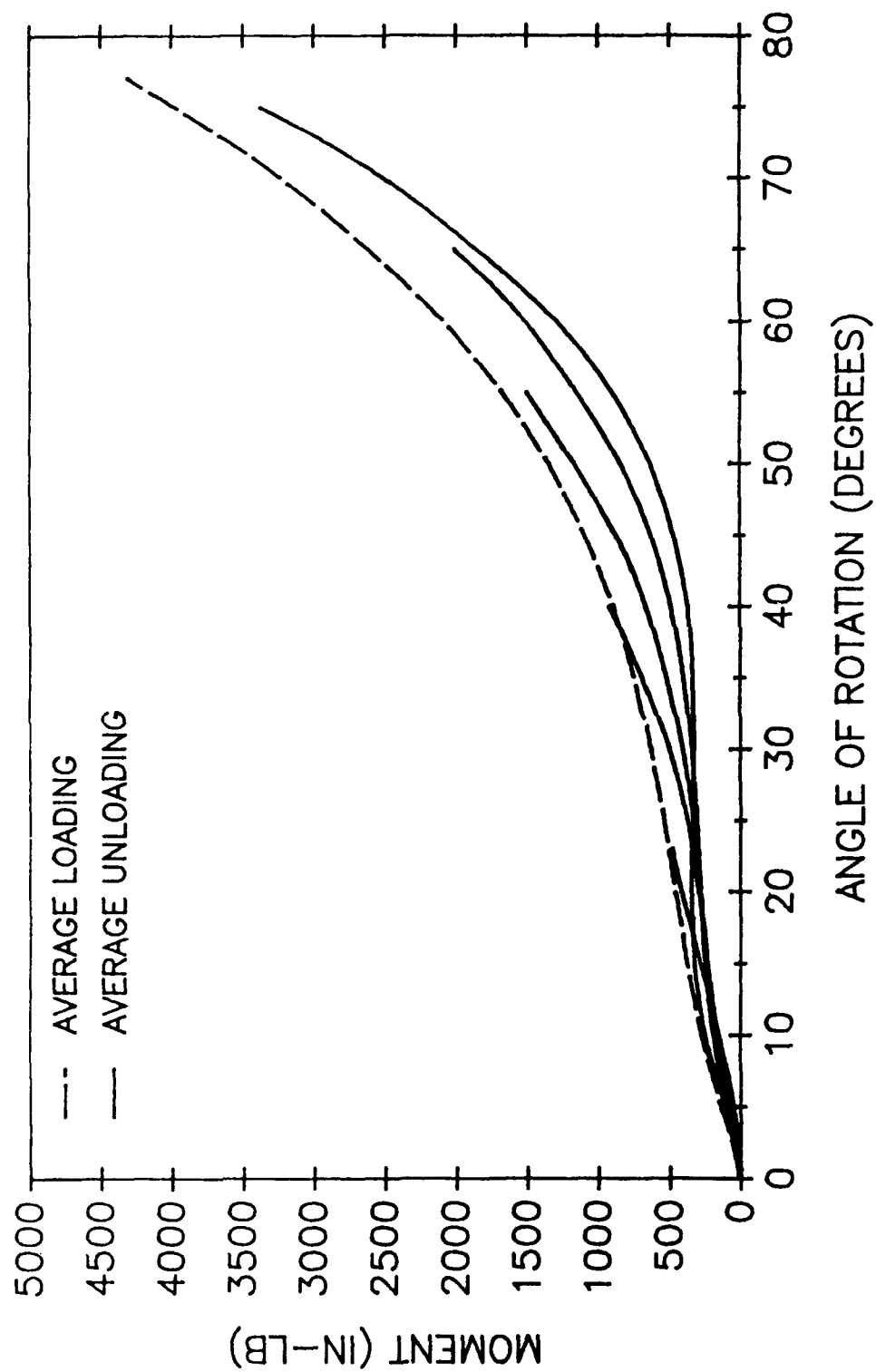


Figure 32 - Average Flexion Loading and Unloading Hybrid III

percentage for each of the Hybrid III necks and their average.

TABLE 5. STATIC HYSTERESIS DATA HYBRID III

	S/N 569 (%)	S/N 1201 (%)	Average (%)
Flexion	32.9	21.8	27.4
Extension	31.2	33.3	32.2
Lateral	29.9	30.2	30.1

Just as the different columns in table 5 indicate, there were different stiffness and hysteresis properties for the Hybrid III necks in flexion, extension, and lateral bending. Figures 33-34 illustrate a Hybrid III neck in extension loading and unloading respectively. Note the change in scale along the vertical axis. The Hybrid III neck is substantially less stiff in extension than flexion. The slots cut into the front of the Hybrid III neck (refer to figure 8) allow the material to separate along this cut during extension, thereby significantly reducing the actual material being elongated. Tables 6-7 list the coefficients for the curve fits for the extension tests for one of the Hybrid III necks. The coefficients are significantly less than for those in tables 2-3.

Lateral testing provided a third bending stiffness. Figure 35 illustrates a Hybrid III neck during lateral loading. The stiffness in this orientation falls between that for flexion and extension. Figure 36 illustrates a Hybrid III neck during lateral unloading. Again the stiffnesses are between that for flexion and extension, but the large drop between the first two points indicates significant internal hysteresis. Tables 8-9 list the coefficients for the curve fits for the lateral tests for one of the Hybrid III necks. The coefficients for the lateral tests generally fall between those for flexion and extension.

It is significant to note that the SAF Part 572 Specifications do not have a requirement for lateral impact response. The author is part of an SAE subcommittee that is dealing with this issue. The current objective is to determine lateral impact calibration corridors for the current Hybrid III neck. Future design changes may be forthcoming. The significance of lateral tests is the increasing emphasis being placed on side impact car crash

STATIC EXTENSION TESTS HYBRID III S/N 1201
THIRD ORDER REGRESSION
RESISTIVE TORQUE DURING LOADING

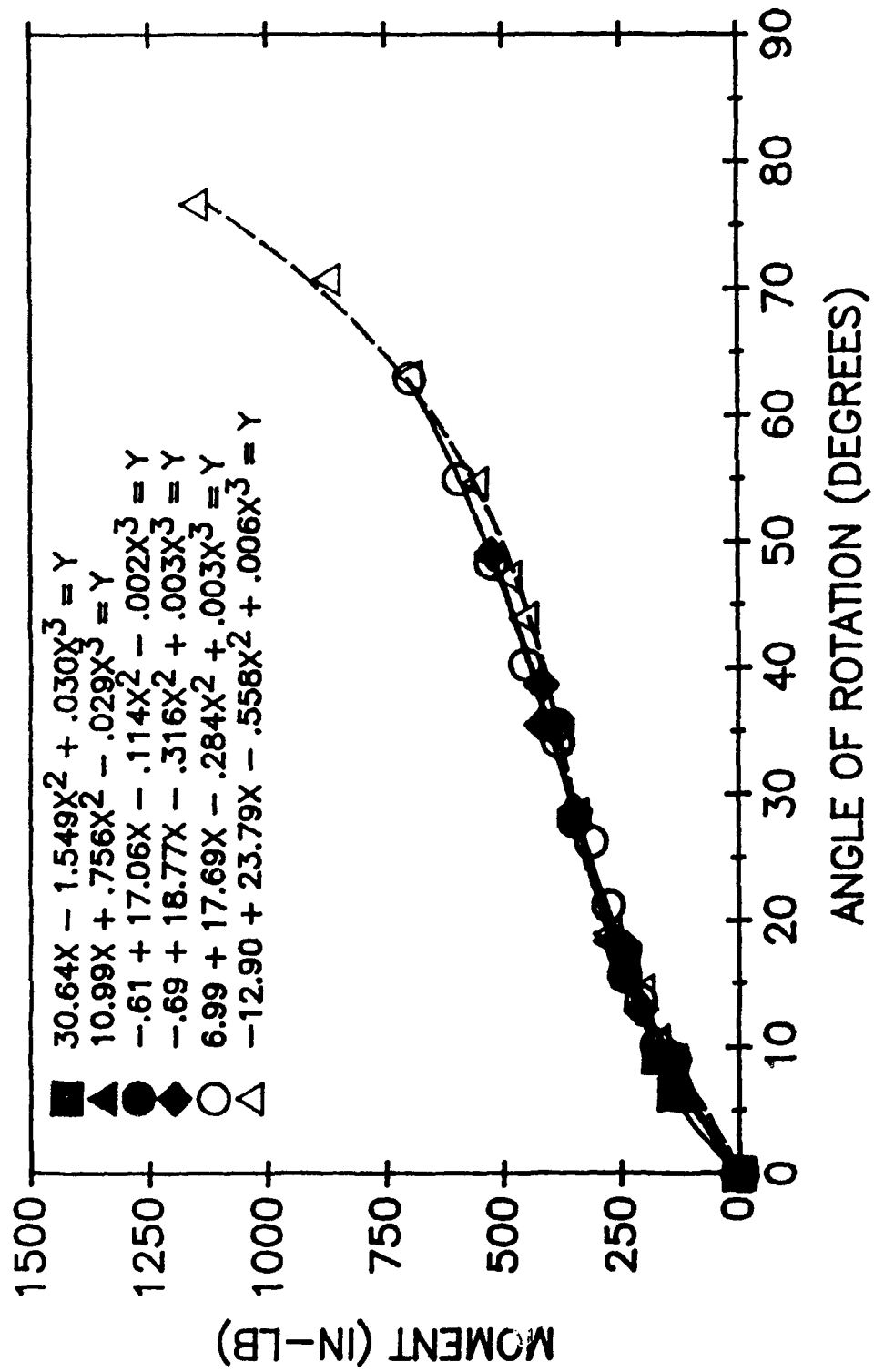


Figure 33 - Extension Loading Hybrid III Neck 2

STATIC EXTENSION TESTS HYBRID III S/N 1201
THIRD ORDER REGRESSION
RESISTIVE TORQUE DURING UNLOADING

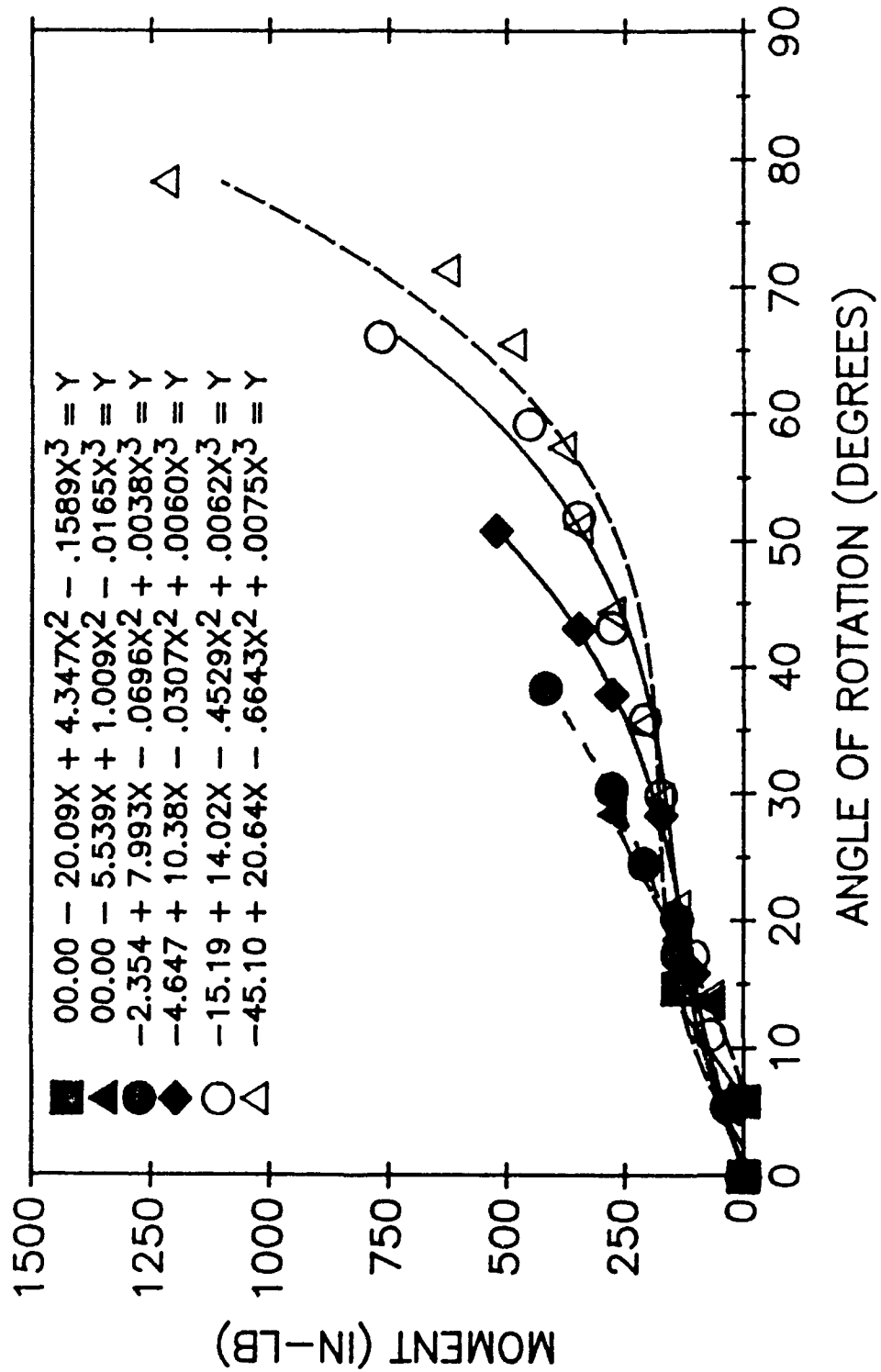


Figure 34 - Extension Unloading Hybrid III Neck 2

**TABLE 6. STATIC EXTENSION TESTS HYBRID III S/N 569
RESISTIVE TORQUE DURING LOADING**

FIRST ORDER REGRESSION ANALYSIS

Test Rotation Angle	X⁰	X¹	RVAL
0-13.3	11.26	12.93	.98075
0-27.0	14.70	10.13	.99397
0-43.9	30.71	9.00	.99176
0-57.8	25.14	9.31	.99680
0-74.0	-13.96	10.21	.98443
0-86.7	-73.14	12.70	.94954
All Test Data	-14.16	11.00	.96245

SECOND ORDER REGRESSION ANALYSIS

Test Rotation Angle	X⁰	X¹	X²	RVAL
0-13.3	0.00	22.29	-.69	1.00000
0-27.0	3.38	13.68	-.13	.99862
0-43.9	11.31	12.16	-.07	.99687
0-57.8	15.42	10.40	-.02	.99736
0-74.0	44.13	4.77	.07	.99543
0-86.7	91.00	.30	.14	.98408
All test data	57.71	4.12	.09	.98221

THIRD ORDER REGRESSION ANALYSIS

Test Angle	X⁰	X¹	X²	X³	RVAL
All test data	-.64	16.27	-.32	.003	.99720

**TABLE 7. STATIC EXTENSION TESTS HYBRID III S/N 569
RESISTIVE TORQUE DURING UNLOADING**

FIRST ORDER REGRESSION ANALYSIS

Test Rotation Angle	x^0	x^1	RVAL
0-16.6	-16.78	10.97	.97993
0-30.9	-6.57	9.95	.99380
0-45.6	-27.78	9.30	.97643
0-62.4	-37.76	8.50	.98263
0-75.1	-69.97	9.45	.94480
0-87.3	-130.0	11.60	.84077

SECOND ORDER REGRESSION ANALYSIS

Test Rotation Angle	x^0	x^1	x^2	RVAL
0-16.6	-2.19	1.88	.53	.99953
0-30.9	1.22	7.04	.10	.99732
0-45.6	2.59	2.98	.14	.99497
0-62.4	-2.23	3.85	.08	.99513
0-75.1	22.21	-.37	.14	.98867
0-87.3	85.58	-7.76	.23	.93441

THIRD ORDER REGRESSION ANALYSIS

Test Angle	x^0	x^1	x^2	x^3	RVAL
0-16.6	0.0	-2.76	1.49	-.040	1.00000
0-30.9	-1.42	9.37	-.11	.004	.99753
0-45.6	-10.96	9.46	-.24	.006	.99807
0-62.4	-15.92	7.66	-.08	.002	.99676
0-75.1	-19.22	9.12	-.19	.003	.99638
0-87.3	-58.59	23.22	-.74	.008	.98350

STATIC LATERAL TESTS HYBRID III S/N 1201
THIRD ORDER REGRESSION
RESISTIVE TORQUE DURING LOADING

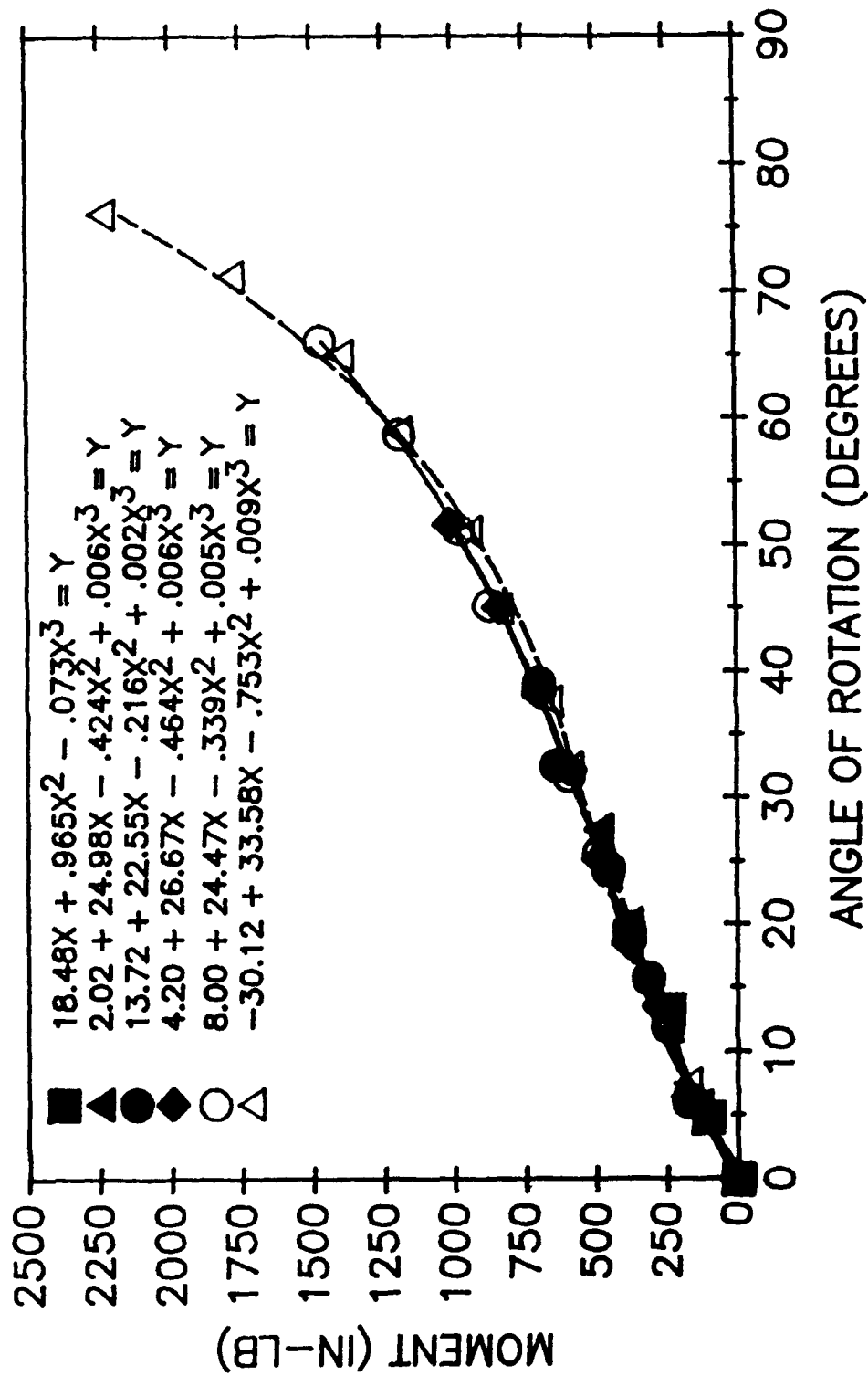


Figure 35 - Lateral Loading Hybrid III Neck 2

STATIC LATERAL TESTS HYBRID III S/N 1201
THIRD ORDER REGRESSION
RESISTIVE TORQUE DURING UNLOADING

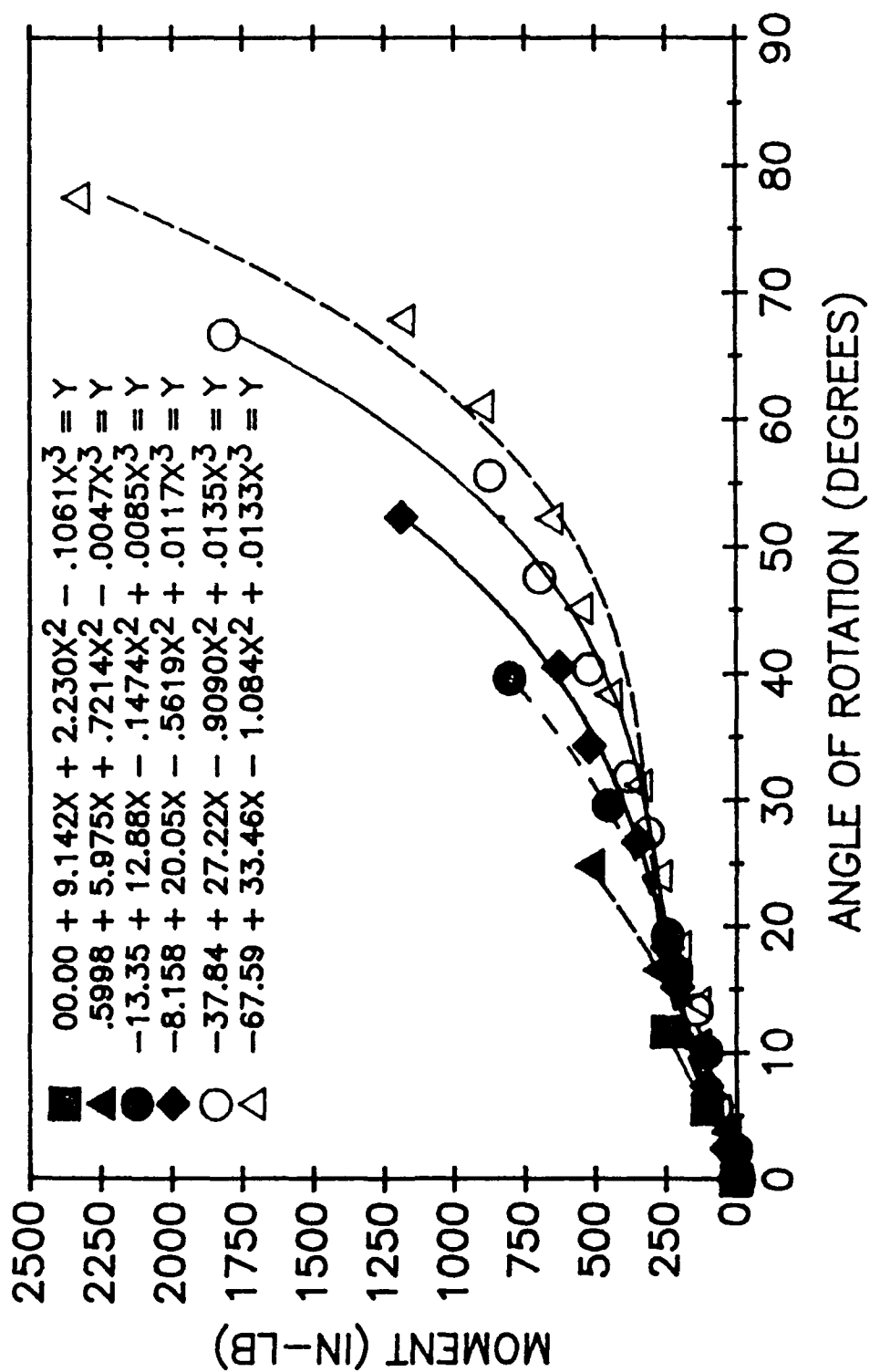


Figure 36 - Lateral Unloading Hybrid III Neck 2

**TABLE 8. STATIC LATERAL TESTS HYBRID III S/N 569
RESISTIVE TORQUE DURING LOADING**

FIRST ORDER REGRESSION ANALYSIS

Test Rotation Angle	x^0	x^1	RVAL
0-14.4	8.80	17.20	.98926
0-29.3	19.53	19.76	.99692
0-41.5	9.63	18.05	.99833
0-57.2	-20.92	21.23	.99355
0-69.4	-94.16	24.38	.97554
All Test Data	-44.94	22.42	.98073

SECOND ORDER REGRESSION ANALYSIS

Test Rotation Angle	x^0	x^1	x^2	RVAL
0-14.4	0.00	26.10	-.64	1.00000
0-29.3	7.67	22.82	-.10	.99812
0-41.5	9.61	18.05	0.00	.99833
0-57.2	36.33	14.55	.12	.99769
0-69.4	91.22	6.73	.25	.99524
All test data	54.08	11.08	.19	.99392

THIRD ORDER REGRESSION ANALYSIS

Test Angle	x^0	x^1	x^2	x^3	RVAL
All test data	3.35	24.31	-.37	.006	.99861

**TABLE 9. STATIC LATERAL TESTS HYBRID III S/N 569
RESISTIVE TORQUE DURING UNLOADING**

FIRST ORDER REGRESSION ANALYSIS

Test Rotation Angle	x^0	x^1	RVAL
0-15.8	-1.37	22.11	.99993
0-28.4	-12.70	17.82	.99124
0-43.8	-56.56	17.45	.97298
0-57.2	-77.54	17.23	.96118
0-70.8	-158.0	18.85	.92893

SECOND ORDER REGRESSION ANALYSIS

Test Rotation Angle	x^0	x^1	x^2	RVAL
0-15.8	0.00	21.16	.06	1.00000
0-28.4	7.47	10.20	.28	.99958
0-43.8	13.29	5.55	.27	.99358
0-57.2	46.52	2.11	.27	.99345
0-70.8	70.18	-3.68	.33	.98386

THIRD ORDER REGRESSION ANALYSIS

Test Angle	x^0	x^1	x^2	x^3	RVAL
0-15.8	0.0	40.26	-4.10	.186	1.00000
0-28.4	3.49	15.27	-.21	.011	.99986
0-43.8	-10.26	17.01	-.44	.011	.99759
0-57.2	-2.61	15.74	-.36	.007	.99964
0-70.8	-34.72	19.49	-.53	.008	.99660

tests. The BIOSID (Side Impact Dummy) was specifically designed for these types of crashes, yet uses a standard Hybrid III neck. The Hybrid III neck was only designed for frontal impacts. Therefore the stiffness results for lateral impacts is of particular concern.

DYNAMIC TESTS

Head/Neck Pendulum

Dynamic tests of the Hybrid II and Hybrid III necks were conducted using a Head/Neck Pendulum (HNP)³⁵. The HNP was built to meet SAE Part 572 Specifications for dummy neck certifications³⁶. The HNP is a fixture that dynamically tests the characteristics of a head and neck by attaching them to the end of a rigid pendulum arm and dropping it from a pre-determined height. The pendulum arm swings freely until the very bottom of its arc, when it strikes a block of aluminum honeycomb, which provides a near square wave deceleration pulse for the arm. During this abrupt deceleration, the head and neck flex forward and back. Figures 37-38 illustrate the HNP.

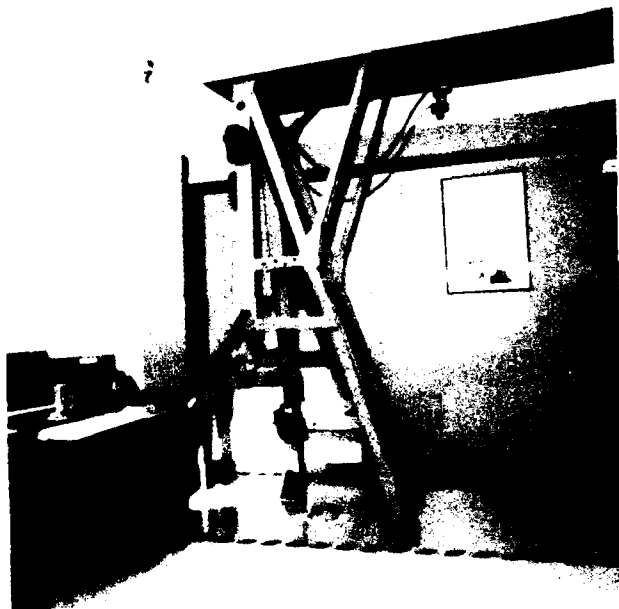


Figure 37. Side View of the HNP

The base of a Hybrid II neck is bolted directly to the end of the pendulum arm. The head is attached as previously described. A tri-axial accelerometer is mounted inside the head at the c.g. location. A three-potentiometer device is



Figure 38. End View of the HNP

mounted to the head c.g. and the frame as described in the specification³⁶. The three potentiometers provide data for the neck rotation, head rotation, and chordal displacement of the neck. Chordal displacement is defined as the linear distance the head c.g. translated during rotation from its location when the arm impacted the honeycomb material. Figure 39 illustrates a Hybrid II head and neck attached to the pendulum arm.

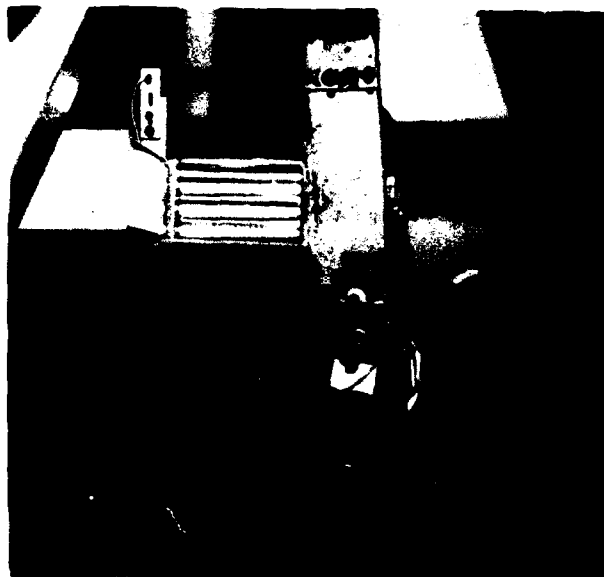


Figure 39. Hybrid II Head and Neck on HNP

The Hybrid III head and neck mounting procedures are slightly different. The base of the Hybrid III neck is bolted to an offset bracket that allows the neck cable to be torqued after the head and neck are mounted to the pendulum arm. The head is attached to the neck as previously described, but the condyle pin is replaced with the long pin of the two potentiometer device. The other end of the two potentiometer device is secured to the pendulum arm. The two potentiometers measure rotation about the neck base and rotation about the condyle pin. A tri-axial accelerometer can be mounted in the head at the c.g., but it is not required for the certification tests. A Denton Inc. six-channel load cell is used, and is installed in the head prior to securing the head and neck together. Figure 40 illustrates a Hybrid III head and neck attached to the pendulum arm.

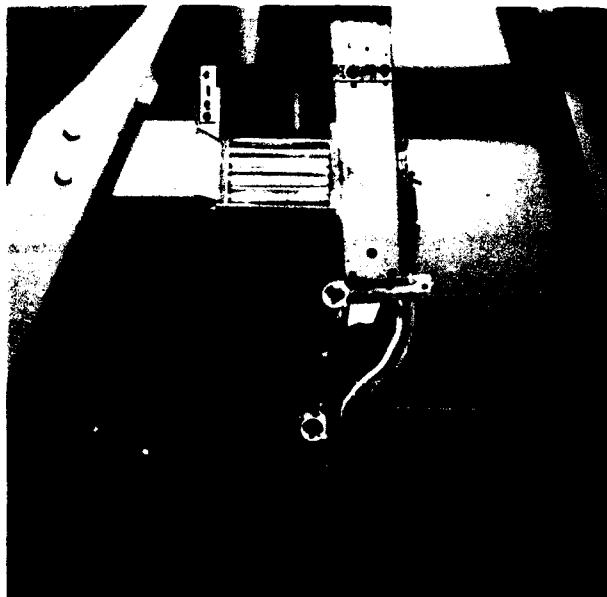


Figure 40. Hybrid III Head and Neck on HNP

Additional system instrumentation common to both neck tests are a tri-axial accelerometer mounted on the pendulum arm, a potentiometer mounted at the pendulum arm pivot to measure inclination, and a velocimeter to measure the pendulum velocity at impact. The pendulum reference angle is 0° , when the arm is at equilibrium (vertical down). Data were collected at 10KHz on each channel simultaneously, starting approximately 10msec before the pendulum arm struck the honeycomb (t_0). An impact event lasted 300-400msec.

Description of Dynamic Tests

Flexion, extension, and lateral tests were conducted on the HNP for all of the necks at impact velocities between 5ft/sec and 23ft/sec. Table 10. lists the dynamic tests that were conducted. Using the SAE Part 572 Specifications³⁶ drop angles were calculated to correspond to the desired impact velocities. 120° was the largest angle obtainable with the pendulum, which corresponded to a 23ft/sec impact velocity.

**TABLE 10. HEAD/NECK PENDULUM TEST MATRIX
FOR HYBRID II AND HYBRID III NECKS**

Flexion Impact Velocity (ft/sec)	Extension Impact Velocity (ft/sec)	Lateral Bending Impact Velocity (ft/sec)
5	5	5
9	9	9
14	14	14
20	20	20
23	23	23

Not only was the HNP used to collect dynamic data for the necks, it was used to certify them according to the Part 572 specifications prior to each series of static tests performed on the SNT. This continuous certification process assured that the necks were good and were retaining their integrity throughout the experiments. Figures 41-42 illustrate a Hybrid III neck meeting the Hybrid III certification corridors. Neither of the Hybrid II necks passed their certification tests. Note that the certification requirements were different for Hybrid II and Hybrid III necks in flexion and extension³⁶. Figures 43-44 illustrate the problem that occurred. The curves for both graphs appear to match the required amplitude and duration, but the response occurred too quickly to meet the certification corridors. Both necks had been certified within six months of the start of these tests, so the necks should have been good. The cell density of the honeycomb material that was impacted was changed, which helped a little, but the necks still did not meet certification requirements. Since the curves for the Hybrid II necks appeared to have the correct shape and they had recently been certified, Hybrid II tests proceeded, while the Hybrid

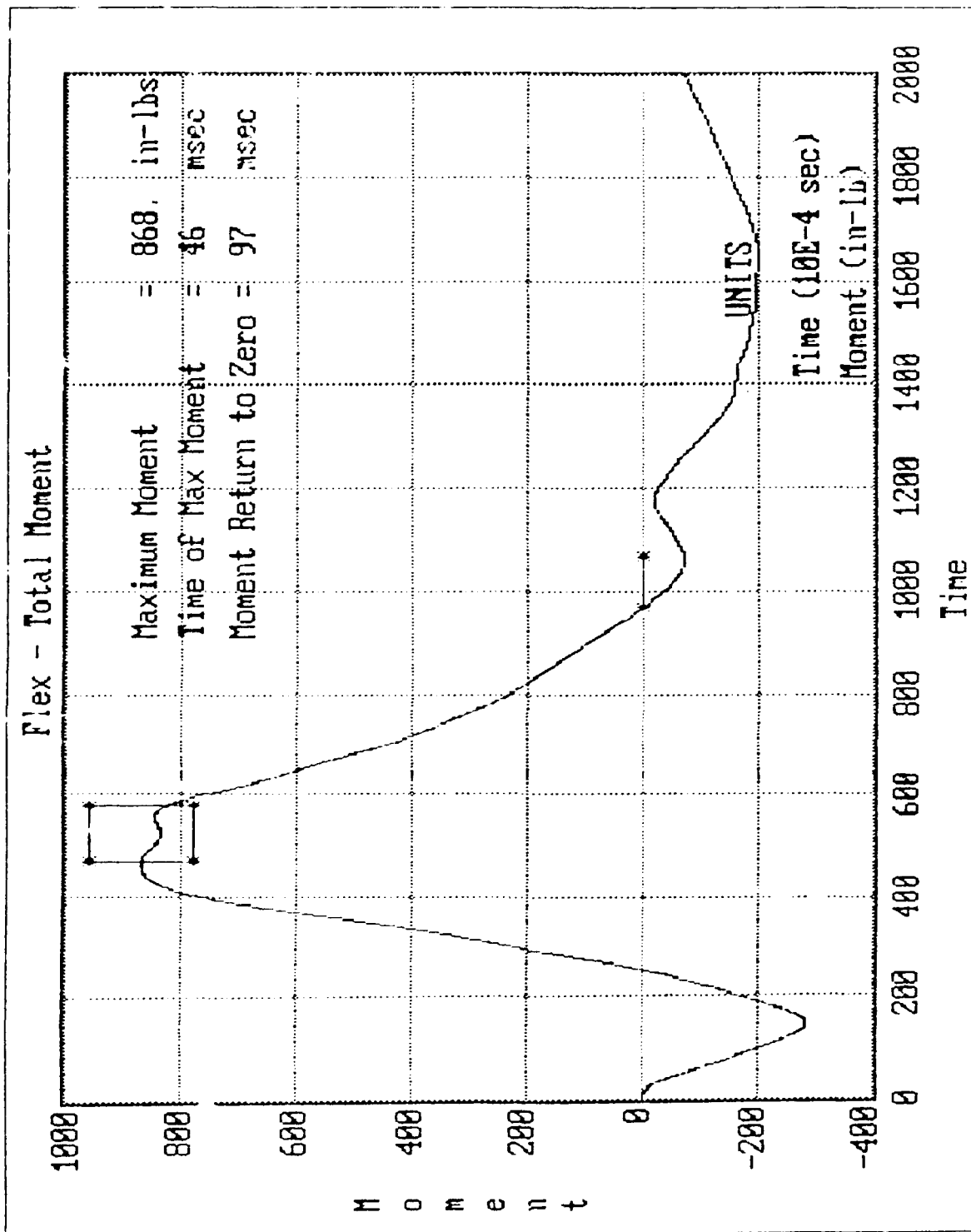


Figure 41. Hybrid III Neck Flexion Certification Total Moment

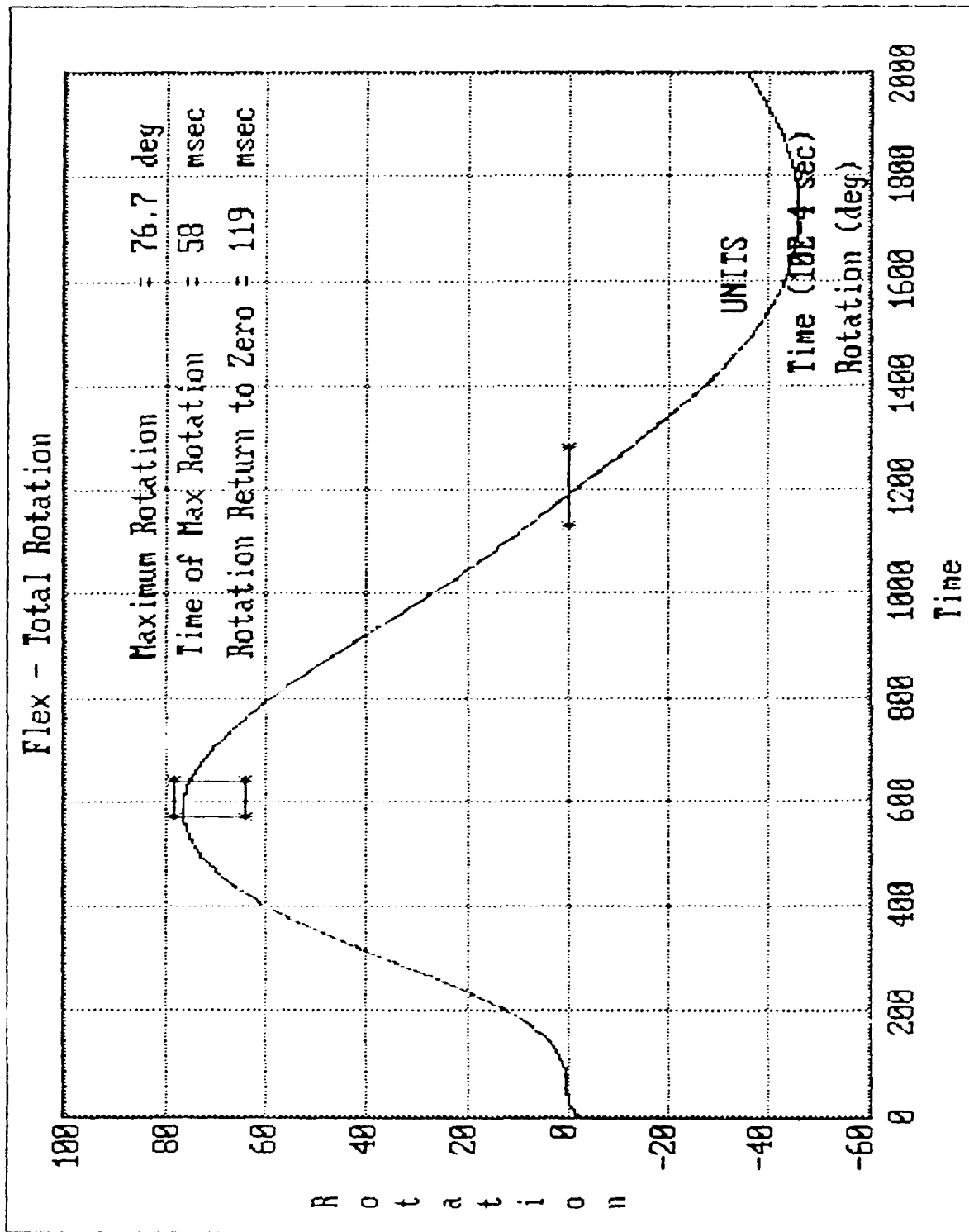


Figure 42. Hybrid III Neck Flexion Certification Total Rotation

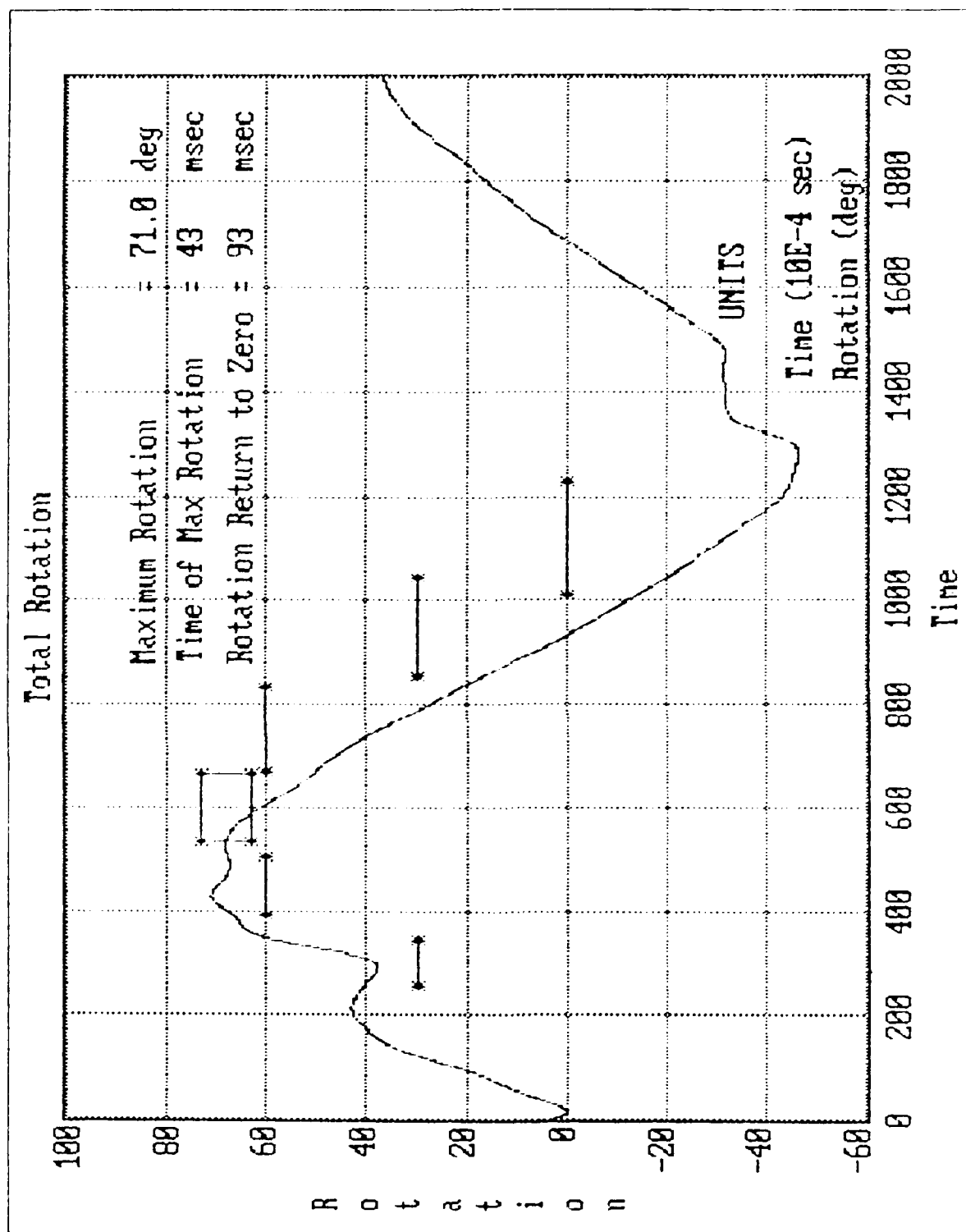


Figure 43. Hybrid II Neck Flexion Certification Total Rotation

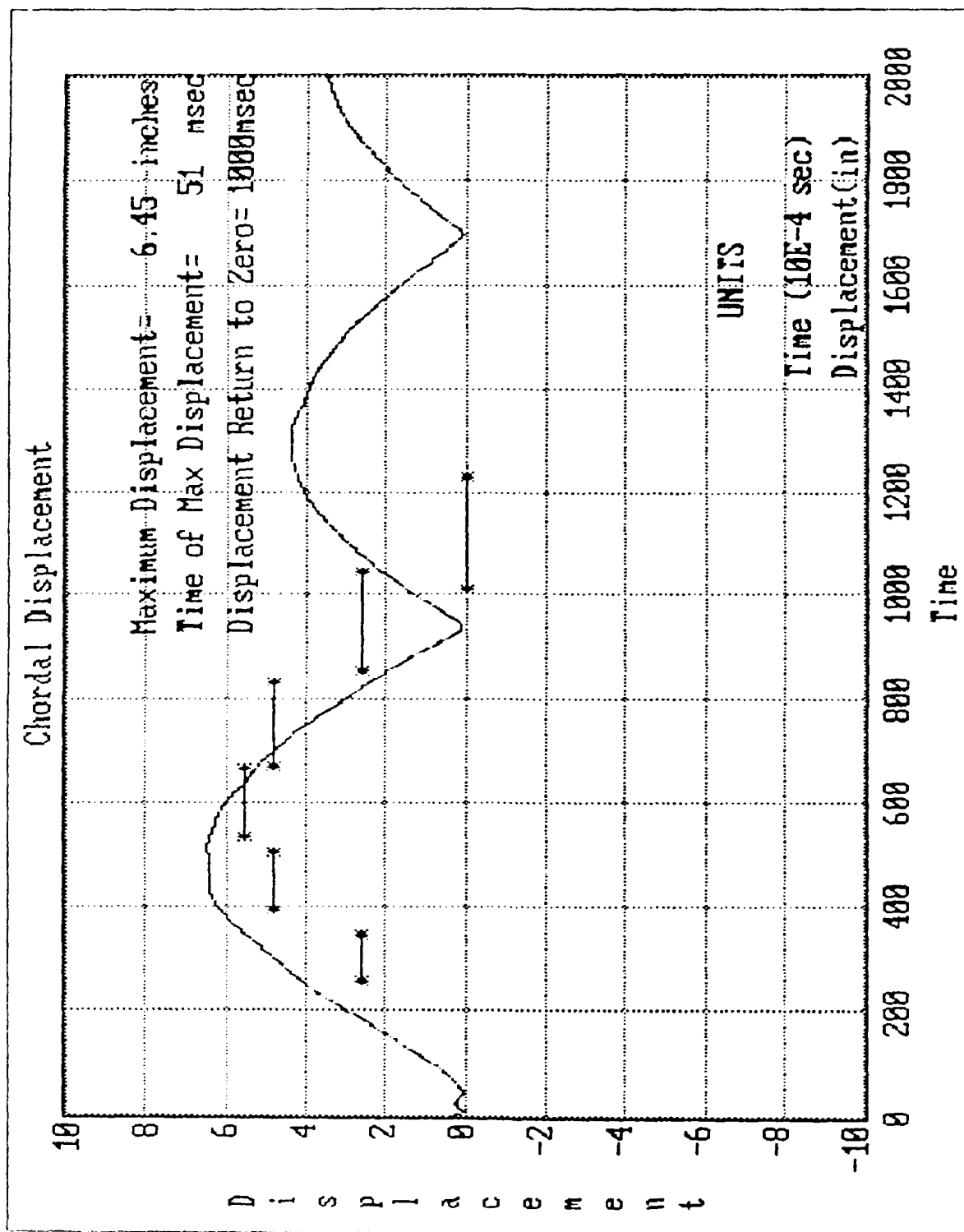


Figure 44. Hybrid II Neck Flexion Certification Chordal Displacement

II analysis software was scrutinized. There were no problems with the Hybrid III analysis software. The dynamic test data for the Hybrid II necks should be correct, but retesting with certified necks on the HNP is recommended.

Test Data

Rotational damping was determined by plotting neck rotation data versus time and finding two peaks. If 300msec of data were plotted, two rotation peaks were visible. Equation (3) was used to calculate the logarithmic decrement for the necks.

$$X_0/X_1 = e^{\Delta} \quad (3)$$

X_0 is the value of the first peak, and X_1 is the value of the second. The logarithmic decrement is a function of the damping ratio as shown in equation (4).

$$\Delta = 2\pi\delta/(1-\delta^2)^{1/2} \quad (4)$$

Equation (5) shows the solution for the damping ratio.

$$\delta = [1/(1+(4\pi^2/\Delta^2))]^{1/2} \quad (5)$$

Figure 45 illustrates the damping ratios for each test angle for a Hybrid III neck in flexion. Note that all of the ratios were fairly close despite the wide range of impact velocities.

Dynamic stiffness curves were generated by matching time lines for the total moment and neck rotation plots. The resulting plot of total moment versus neck rotation is illustrated in figure 46. The curve is quite dynamic, with a negative moment occurring initially before the moment reverses positive.

The negative moment characteristic is thought to occur from the shock wave at impact transmitted through the deformable neck to the head. The head therefore rotates ahead of the neck deformation and the load cell measures a moment pushing the head forward, which is the negative dip in the curve. The neck deformation quickly catches up to the head rotation and then resists the forward motion of the head, which causes the positive moment that resists the head and neck rotation. Figure 47 illustrates the moment versus rotation curves for all angles in flexion.

The curves become progressively smaller as the impact velocity decreases, but the slope of the initial loading becomes steeper. The small spike in the unloading curve that is most apparent for the 20°, 40°, and 65° drops may have been caused

HYBRID III ALL ANGLES FLEXION

ROTATION ABOUT NECK BASE

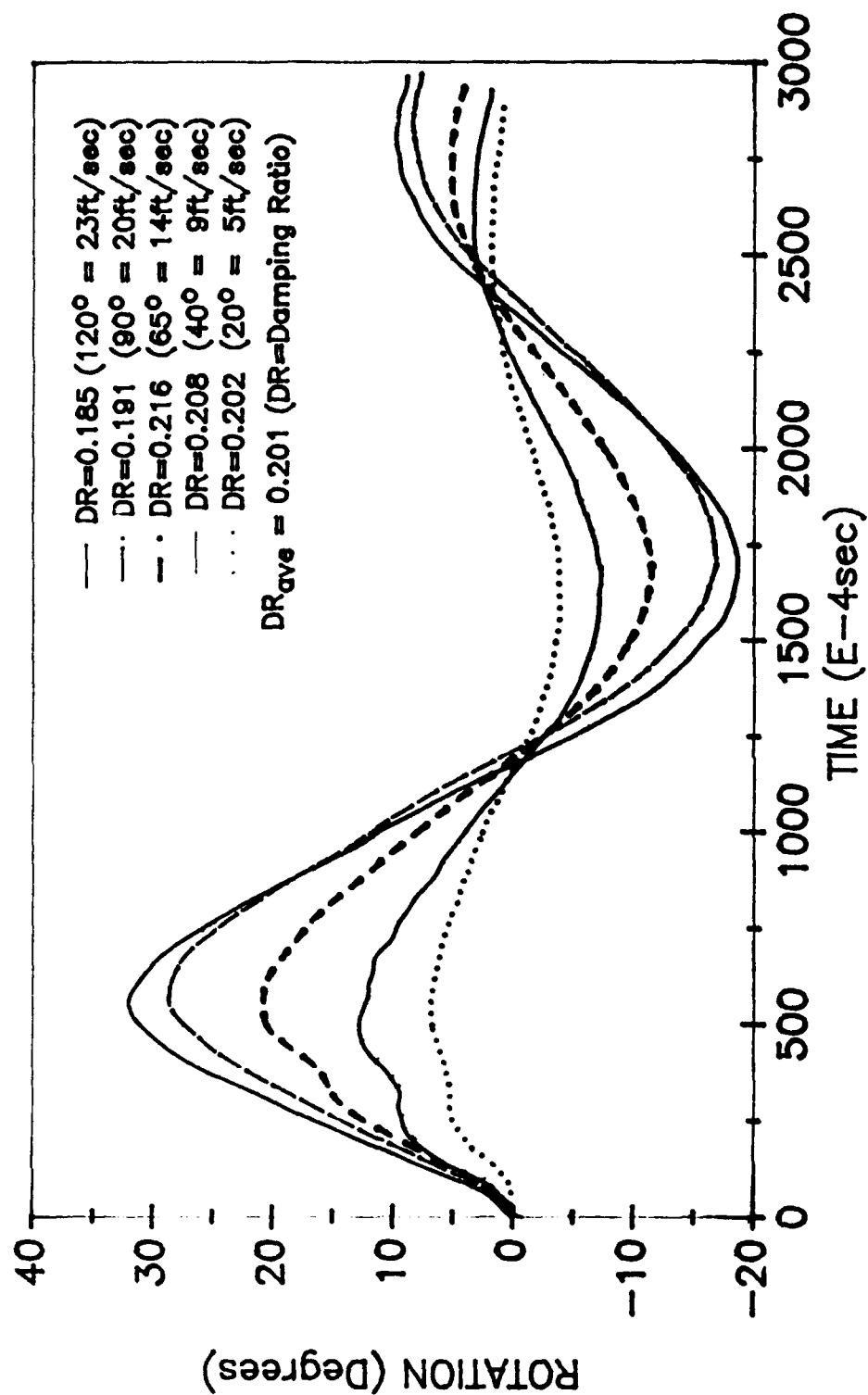


Figure 45 - Hybrid III Rotational Damping All Angles

HYBRID III 120° (23ft/sec)
FLEXION

TOTAL MOMENT VS ROTATION ABOUT NECK BASE

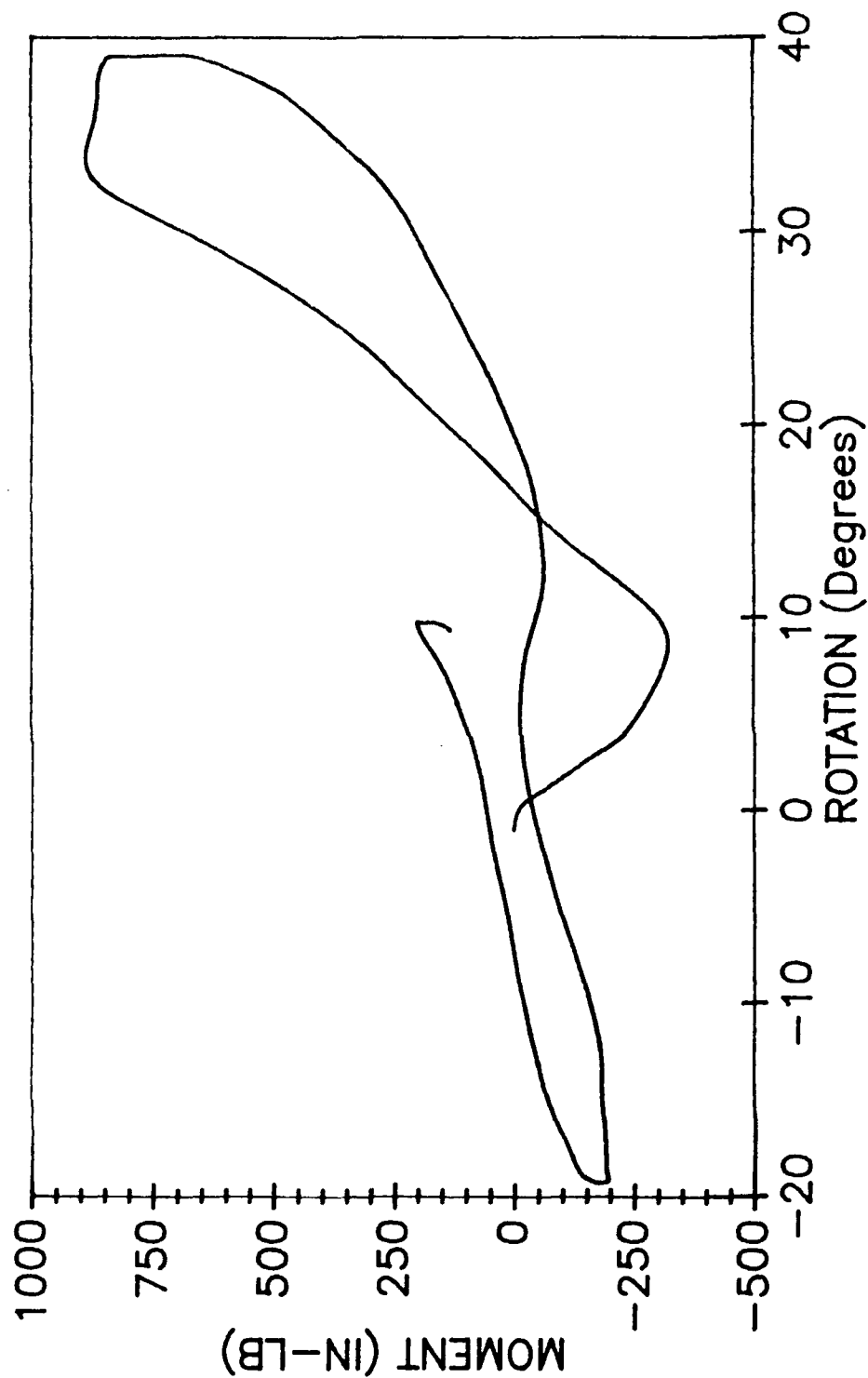


Figure 46 - Hybrid III Total Moment Vs. Neck Rotation

HYBRID III ALL ANGLES FLEXION

TOTAL MOMENT VS ROTATION ABOUT NECK BASE

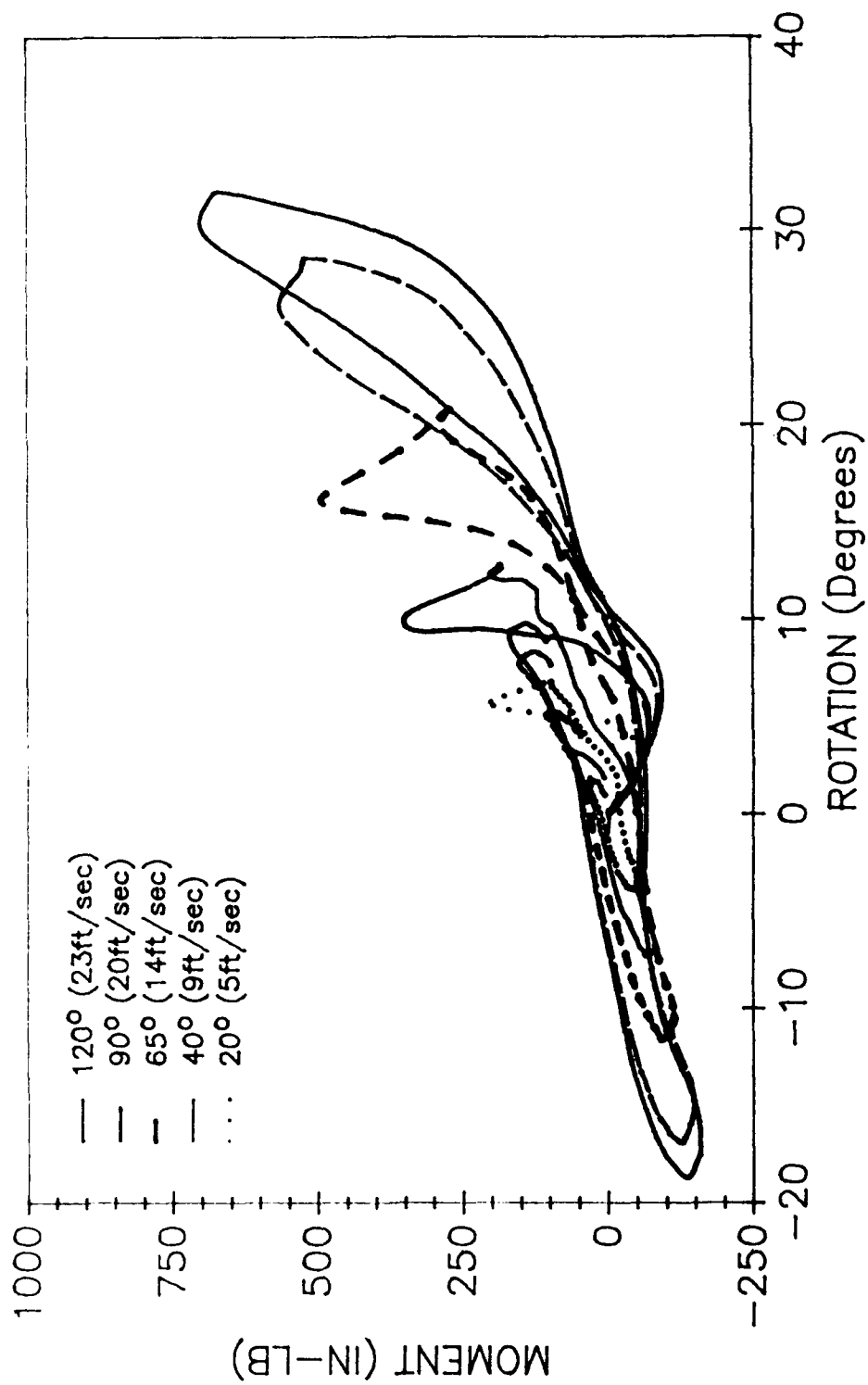


Figure 47 - Hybrid III Total Moment Vs. Neck Rotation All Angles

by a problem with the two potentiometer device sticking, but high speed film of some tests have not been conclusive.

Stiffness and Damping Characteristics

The two Hybrid II and two Hybrid III necks that were tested on the SNT were used on the HNP. A single Hybrid II and Hybrid III head were used with both of their respective necks for inertial property consistency. Flexion, extension, and lateral pendulum tests were conducted as listed in table 10.

Hybrid II Necks

Since neither Hybrid II neck could be certified on the pendulum, only limited results will be included, as these drops should be retested once the problem is isolated and corrected. Since the overall shape of the curves were correct, it was still assumed that most of the data was correct. Figure 48 illustrates the neck rotation for a Hybrid II neck in flexion. Figure 49 illustrates the same neck in extension. Since the neck stiffness for the Hybrid II was the same for any orientation, only the asymmetric inertial properties of the head caused the small change in rotation angle. Overall the Hybrid II necks exhibited very similar damping ratios regardless of impact velocity or orientation.

Therefore, all of the damping ratios for each neck were reduced to a single average. Table 11 lists the damping ratios for each Hybrid II neck and their combined average.

TABLE 11. DAMPING RATIOS FOR HYBRID II NECKS

	S/N 3232 (C/C _c)	S/N 0262P (C/C _c)	Average (C/C _c)
Bending	0.116	0.092	0.104

Chordal displacement is the benchmark of the certification of Hybrid II necks. If the neck data passed through these corridors, then the head c.g. location was correct throughout the test. Figure 50 illustrates the chordal displacement for a flexion test and figure 51 illustrates an extension test. Lateral tests provided similar results. The Denton Inc. head/neck load cell does not interface with a Hybrid II head and neck, so force and moment data about

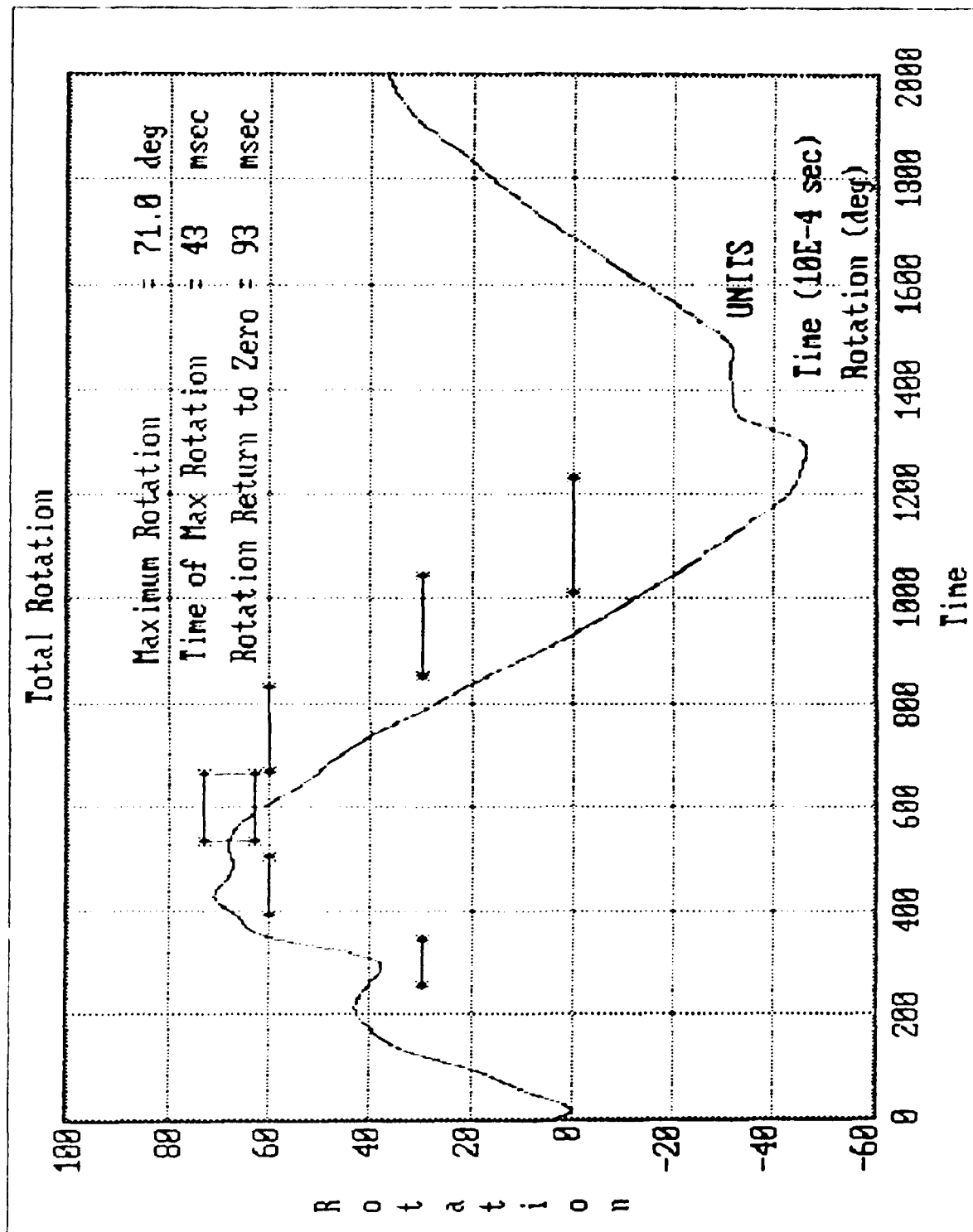


Figure 48. Hybrid II Neck 1 Rotation 90° Flexion

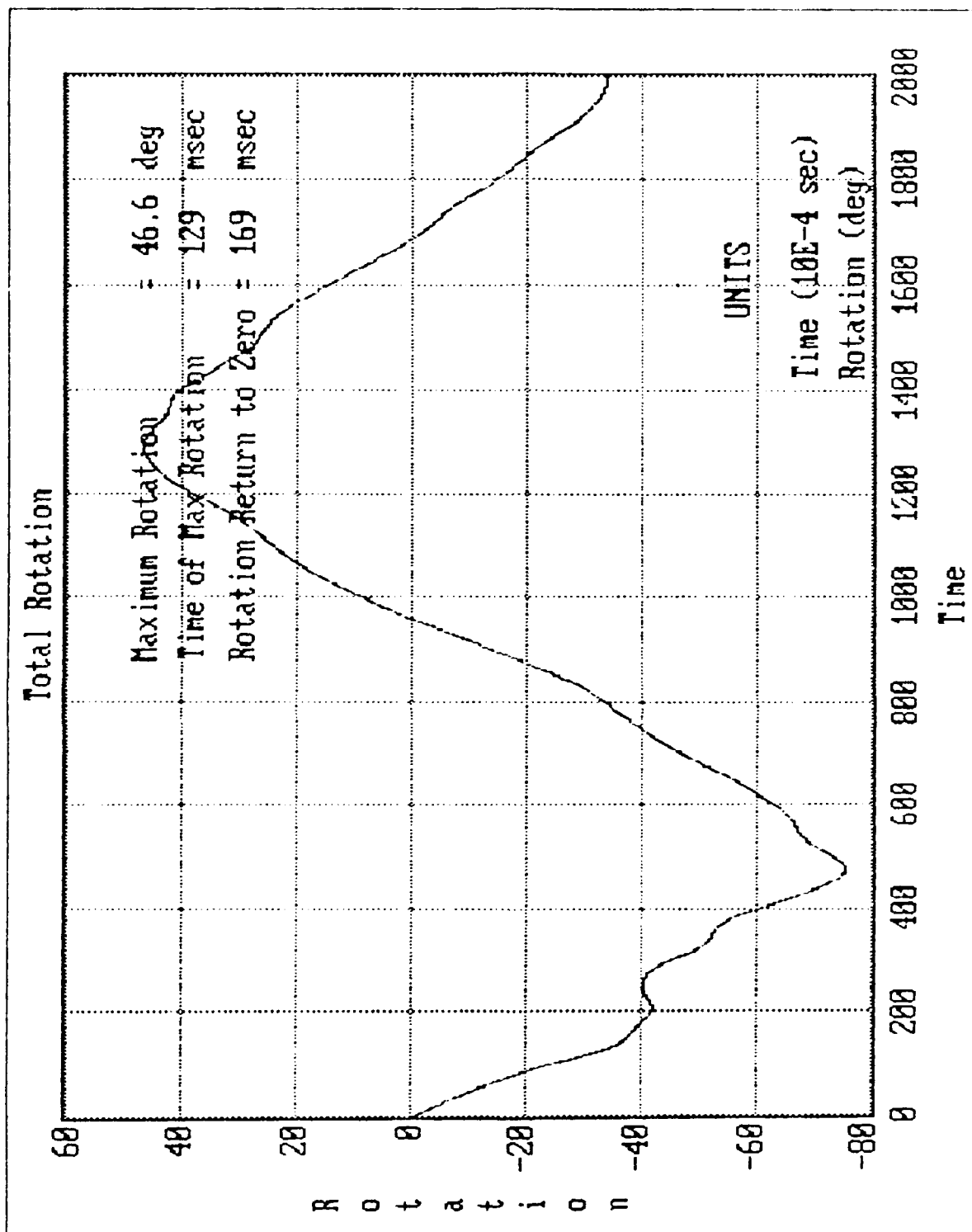


Figure 49. Hybrid II Neck 1 Rotation 90° Extension

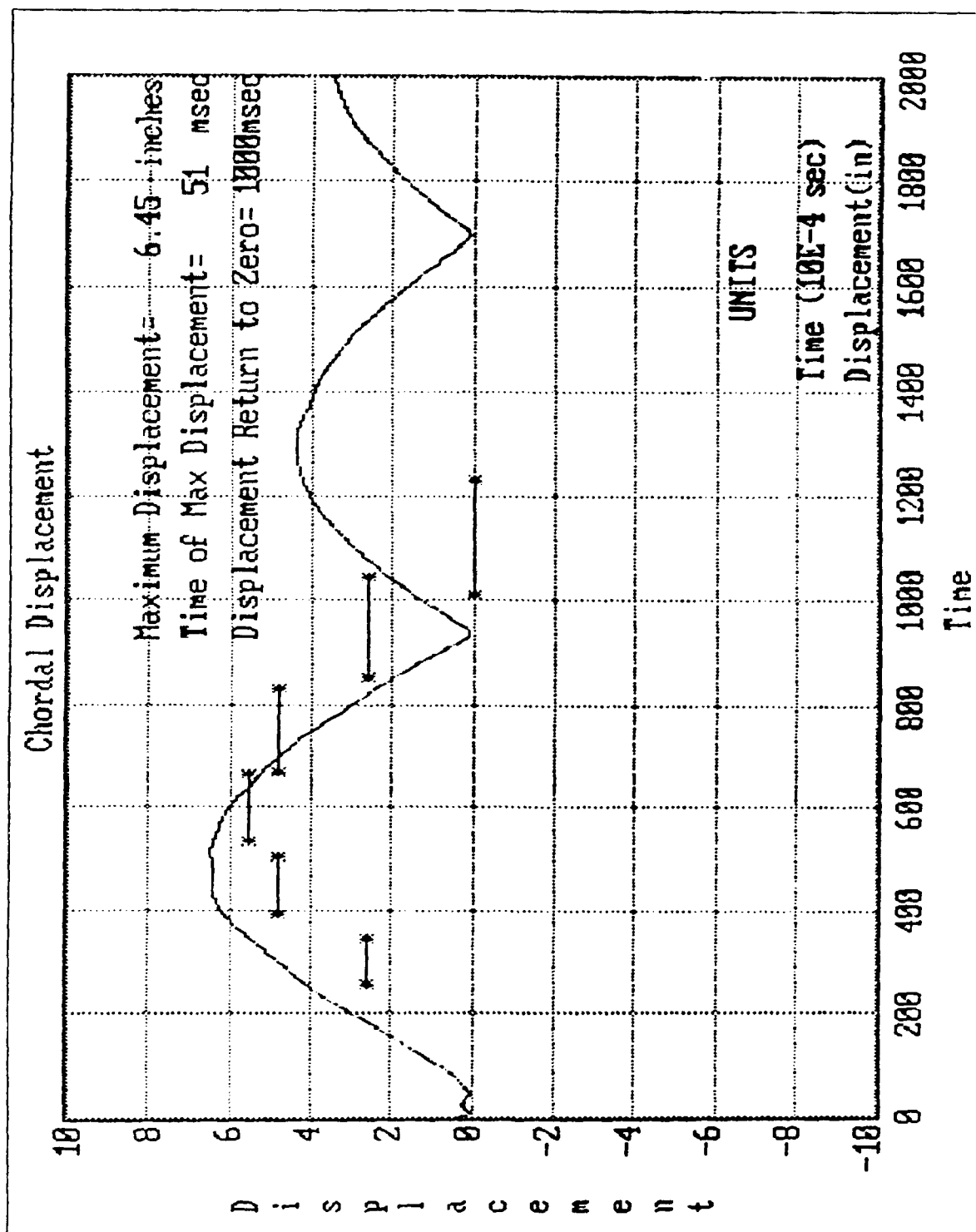


Figure 50. Hybrid II Neck 1 Chordal Displacement 90° Flexion

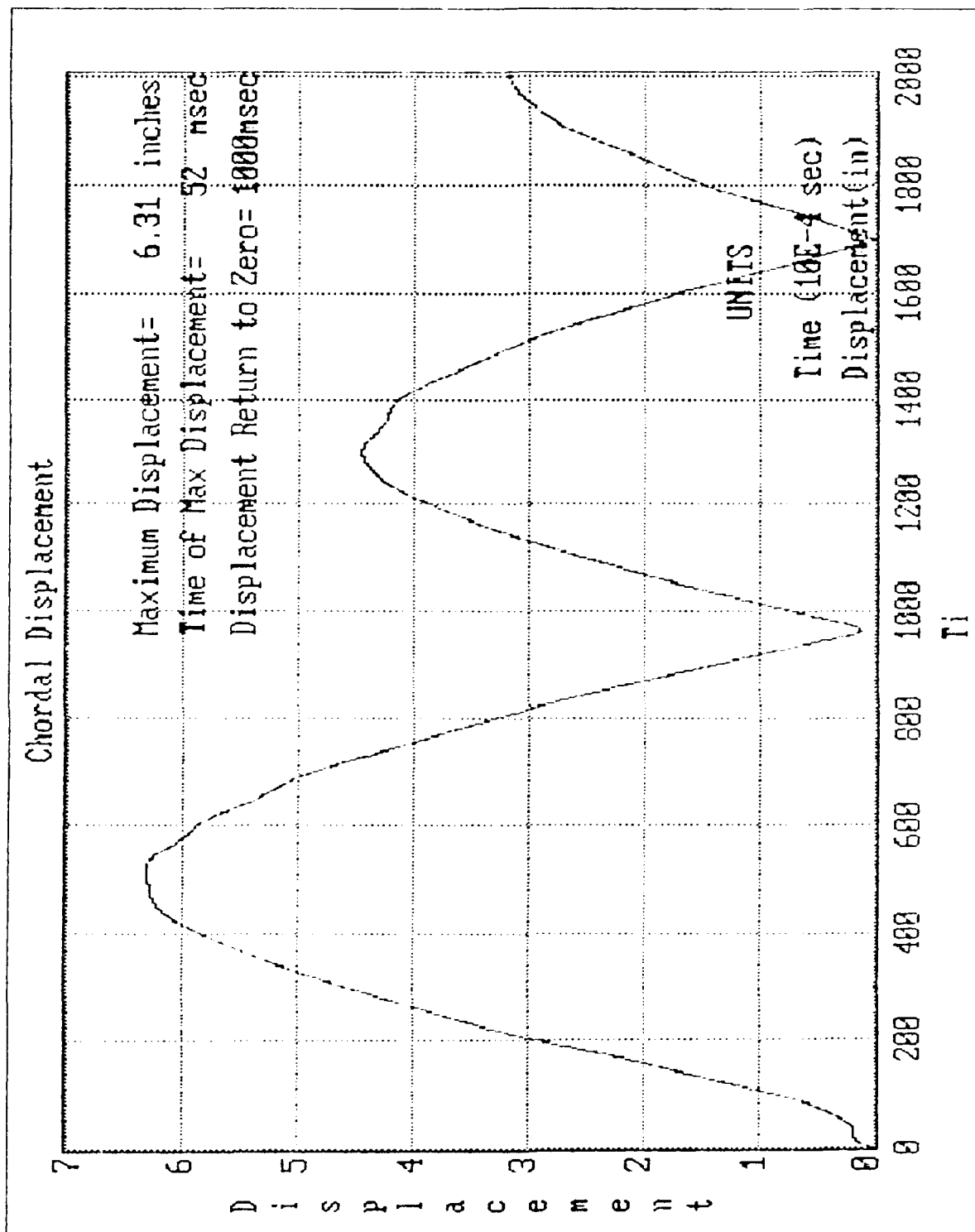


Figure 51. Hybrid II Neck 1 Chordal Displacement 90° Extension

the neck could not be collected.

Hybrid III Necks

A comparison between the two Hybrid III necks in neck rotation is illustrated in figures 52-56. The difference in damping ratios between the two necks was due to the amplitude of the first peak. Both necks had nearly the same amplitude for the second peak, but one neck rotated farther on the first peak than the other. Note that for certification drop angles that both necks met the corridors, so the disparity between the two necks was within the acceptable corridor for certifiable necks. Similar results were found during the extension and lateral tests. Table 12 lists the calculated damping ratios for both necks and their average for flexion, extension, and lateral tests.

TABLE 12. DAMPING RATIOS FOR HYBRID III NECKS

	S/N 569 (C/C _c)	S/N 1201 (C/C _c)	Average (C/C _c)
Flexion	0.212	0.201	0.206
Extension	0.225	0.216	0.221
Lateral	0.221	0.201	0.211

A similar comparison between the necks for moment versus rotation is illustrated in figures 57-61. Again, one neck had the larger neck rotations and consequently larger restoring moments. The general shape was similar and, as just described above for neck rotation, the second rotation (negative angle rotation) of the head and neck matched more closely for each test as well. For a flexion test, the negative rotation was the head and neck moving back into extension. For an extension test, the negative rotation was the neck moving into flexion. Lateral tests rotated in the positive and negative lateral directions. Similar results were obtained from the extension and lateral tests.

A comparison of a Hybrid III neck's static stiffness data overlaid on the same neck's dynamic data is illustrated in figure 62. Note the very different loading path for the flexion test. The unloading paths are similar in shape, but different in magnitude. The second rotations match much more closely. As the energy in the dynamic system diminishes, the stiffness characteristics of the system approach that of the

HYBRID III 120° (23ft/sec)
FLEXION

ROTATION ABOUT NECK BASE

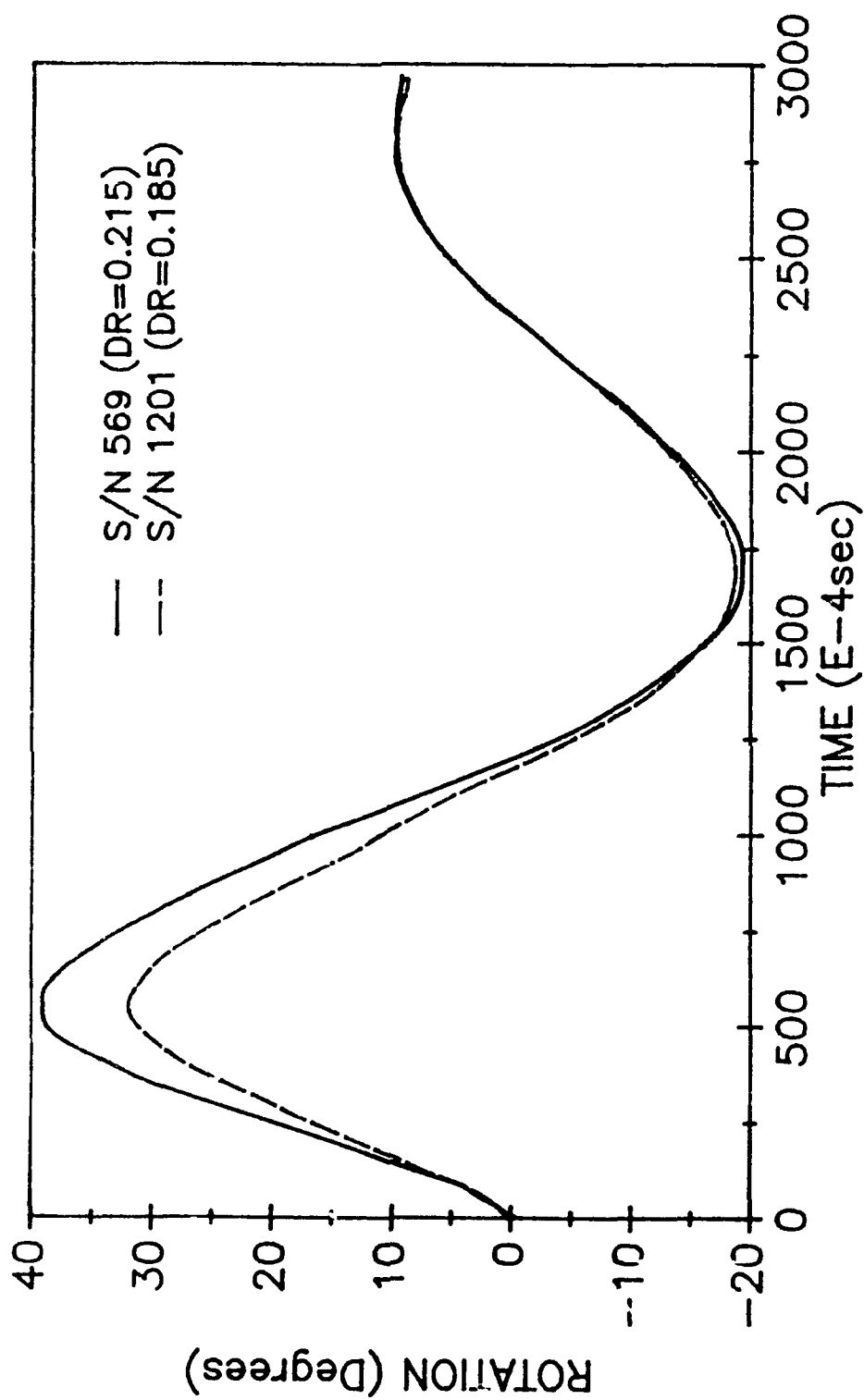


Figure 52 - Hybrid III Neck Rotation Comparison 120°

HYBRID III 90° (20ft/sec)
FLEXION

ROTATION ABOUT NECK BASE

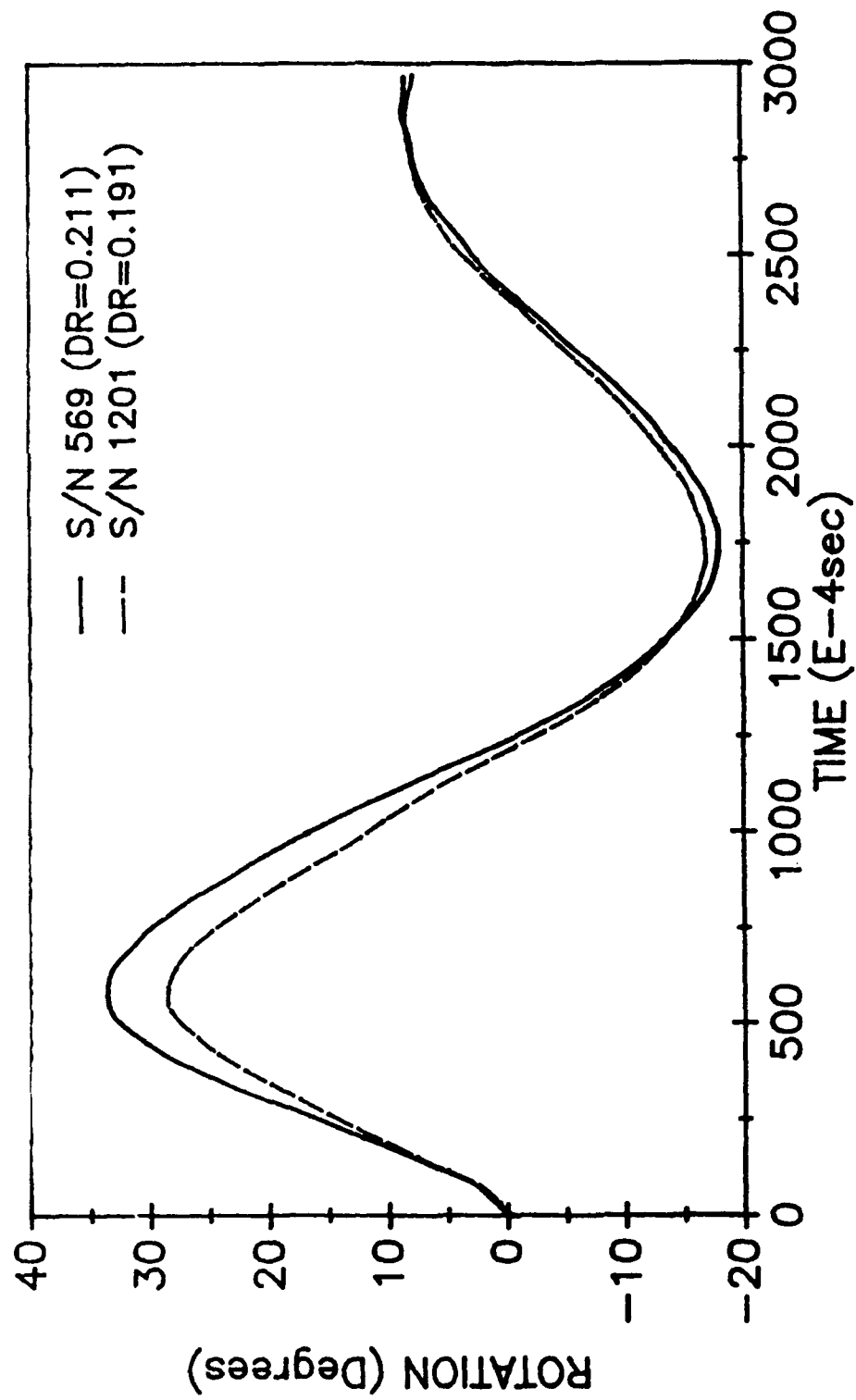


Figure 53 - Hybrid III Neck Rotation Comparison 90°

HYBRID III 65° (14ft/sec)
FLEXION

ROTATION ABOUT NECK BASE

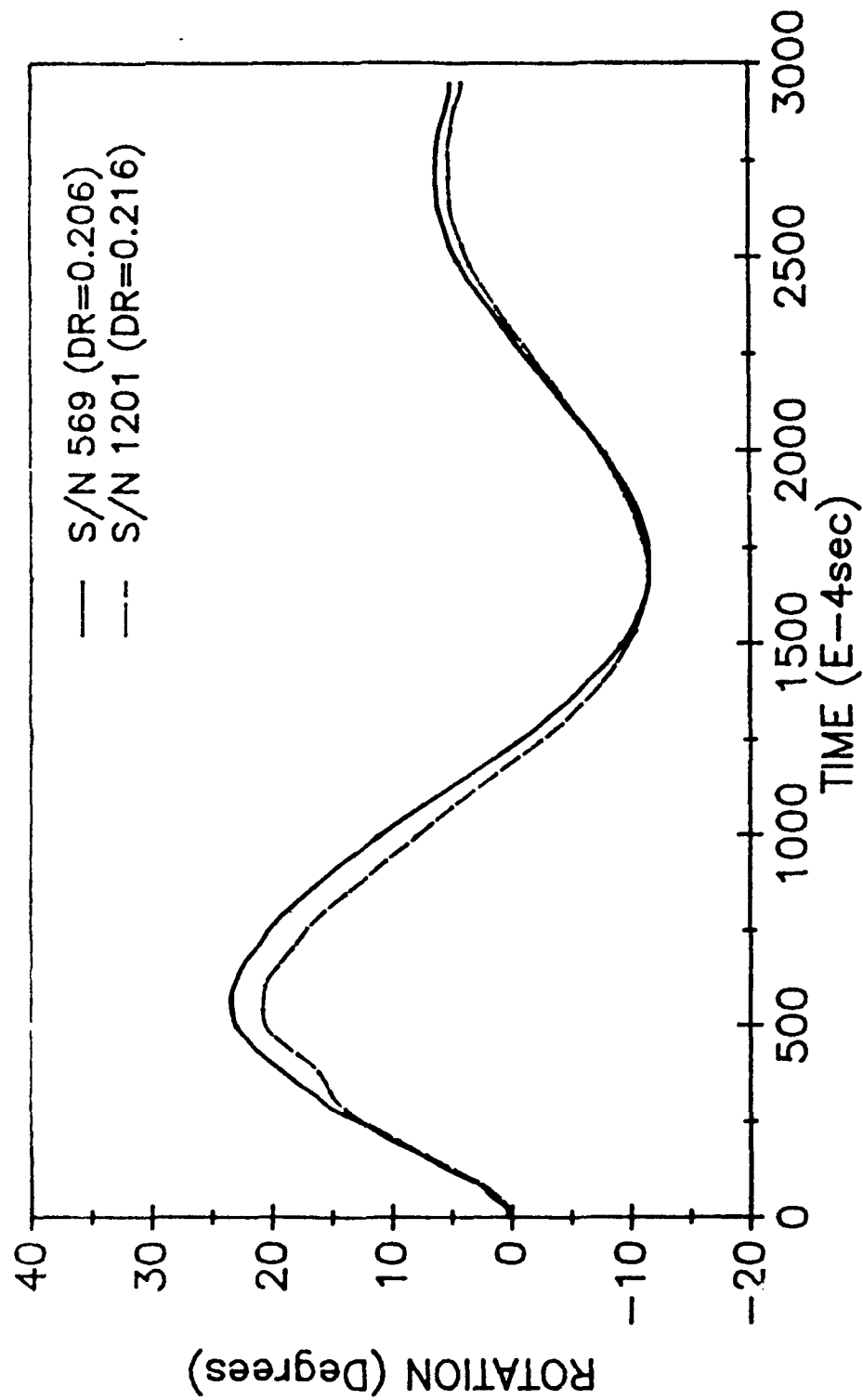


Figure 54 - Hybrid III Neck Rotation Comparison 65°

HYBRID III 40° (9ft/sec)
FLEXION

ROTATION ABOUT NECK BASE

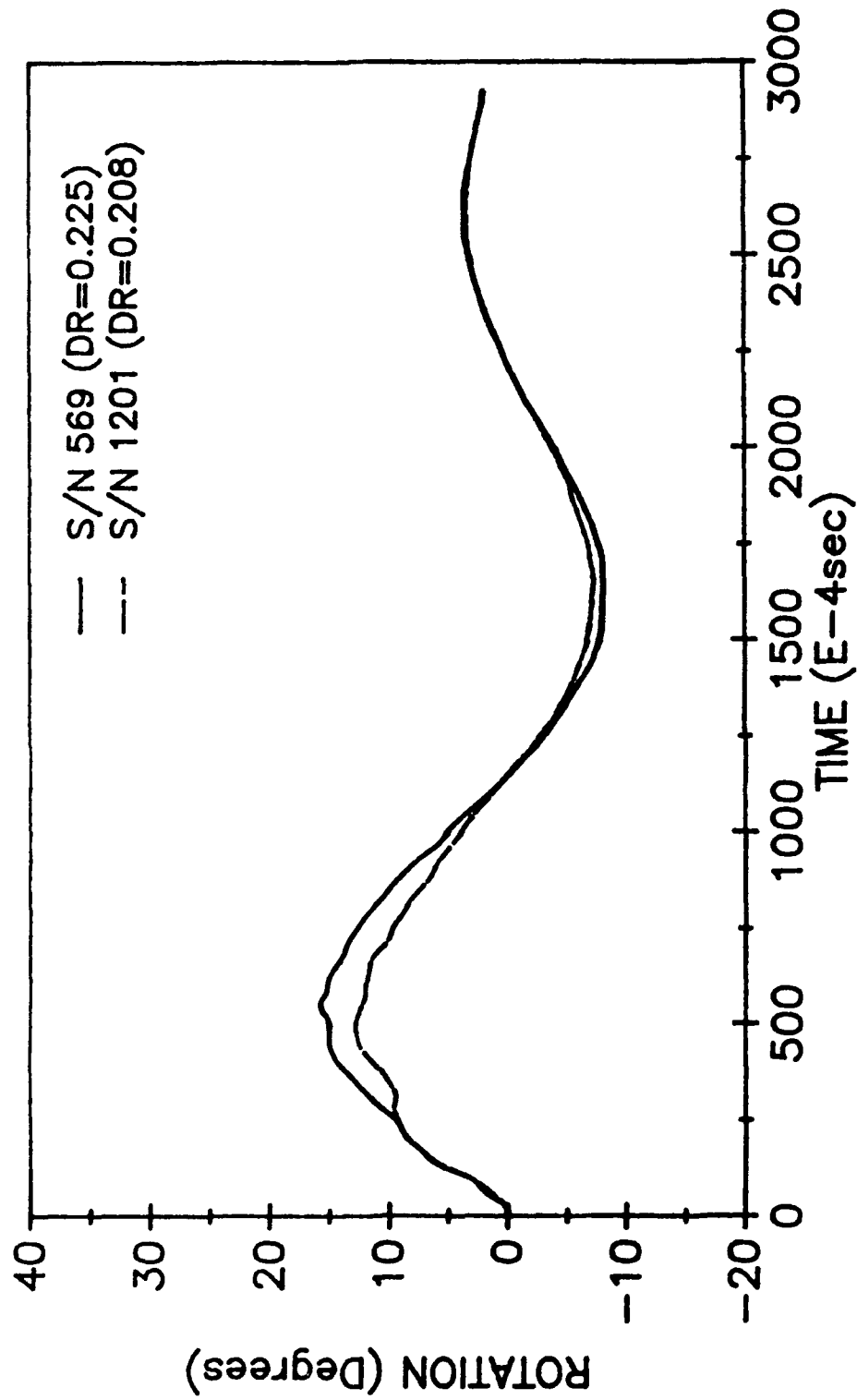


Figure 55 - Hybrid III Neck Rotation Comparison 40°

HYBRID III 20° (5ft/sec)
FLEXION

ROTATION ABOUT NECK BASE

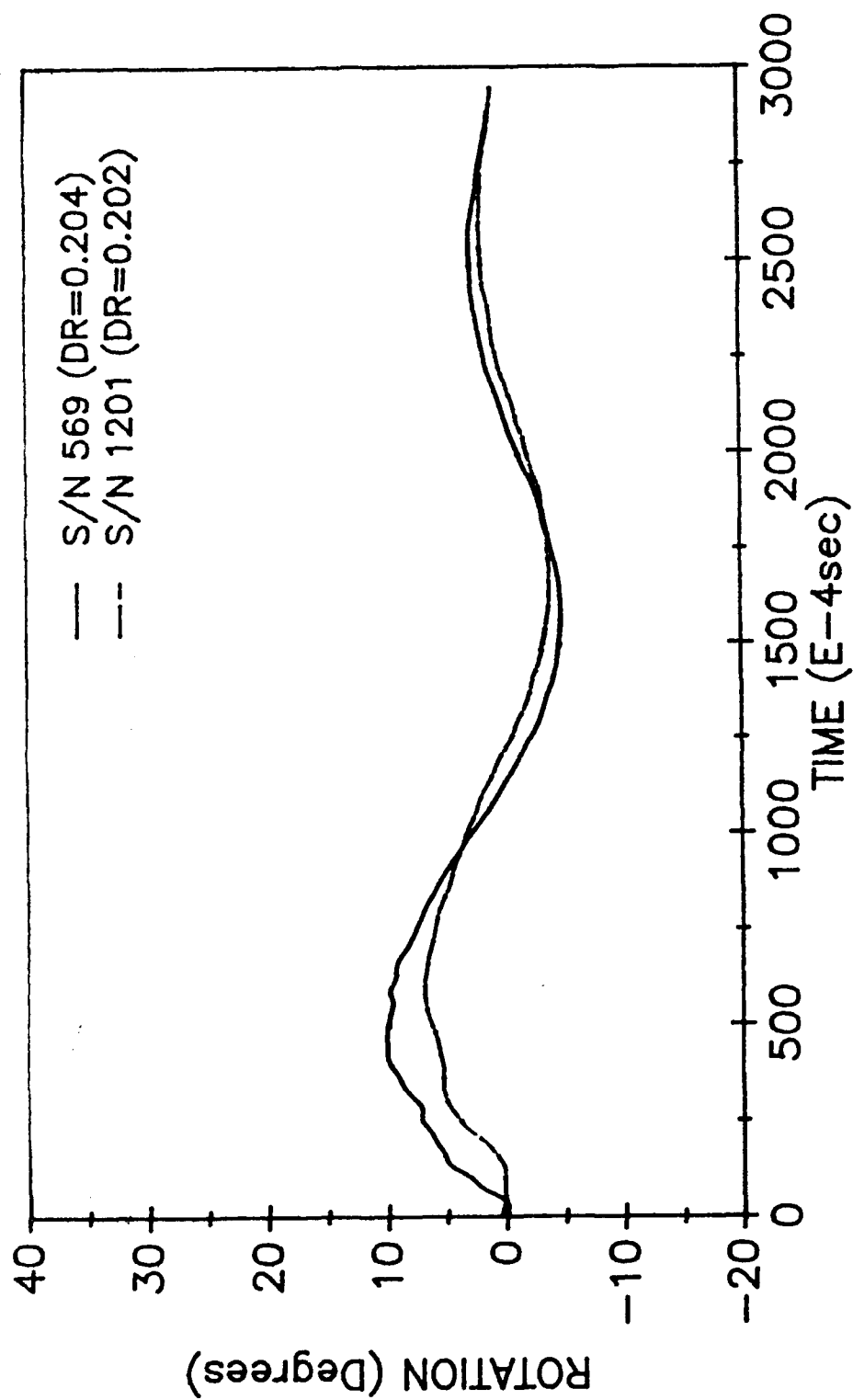


Figure 56 - Hybrid III Neck Rotation Comparison 20°

HYBRID III 120° (23ft/sec)
FLEXION

TOTAL MOMENT VS ROTATION ABOUT NECK BASE

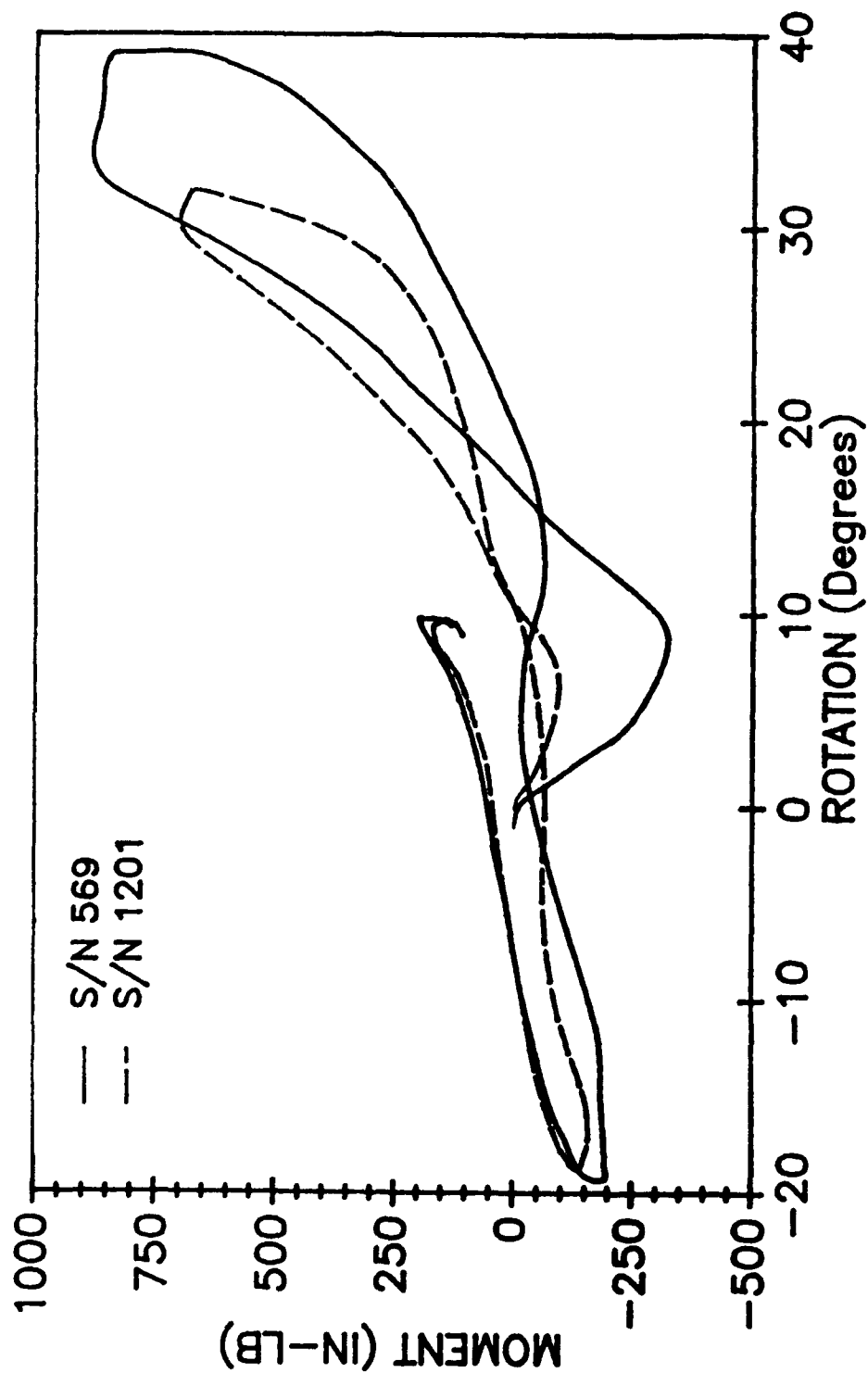


Figure 57 - Hybrid III Neck Moment Vs. Rotation Comparison 120°

HYBRID III 90° (20ft/sec)
FLEXION

TOTAL MOMENT VS ROTATION ABOUT NECK BASE

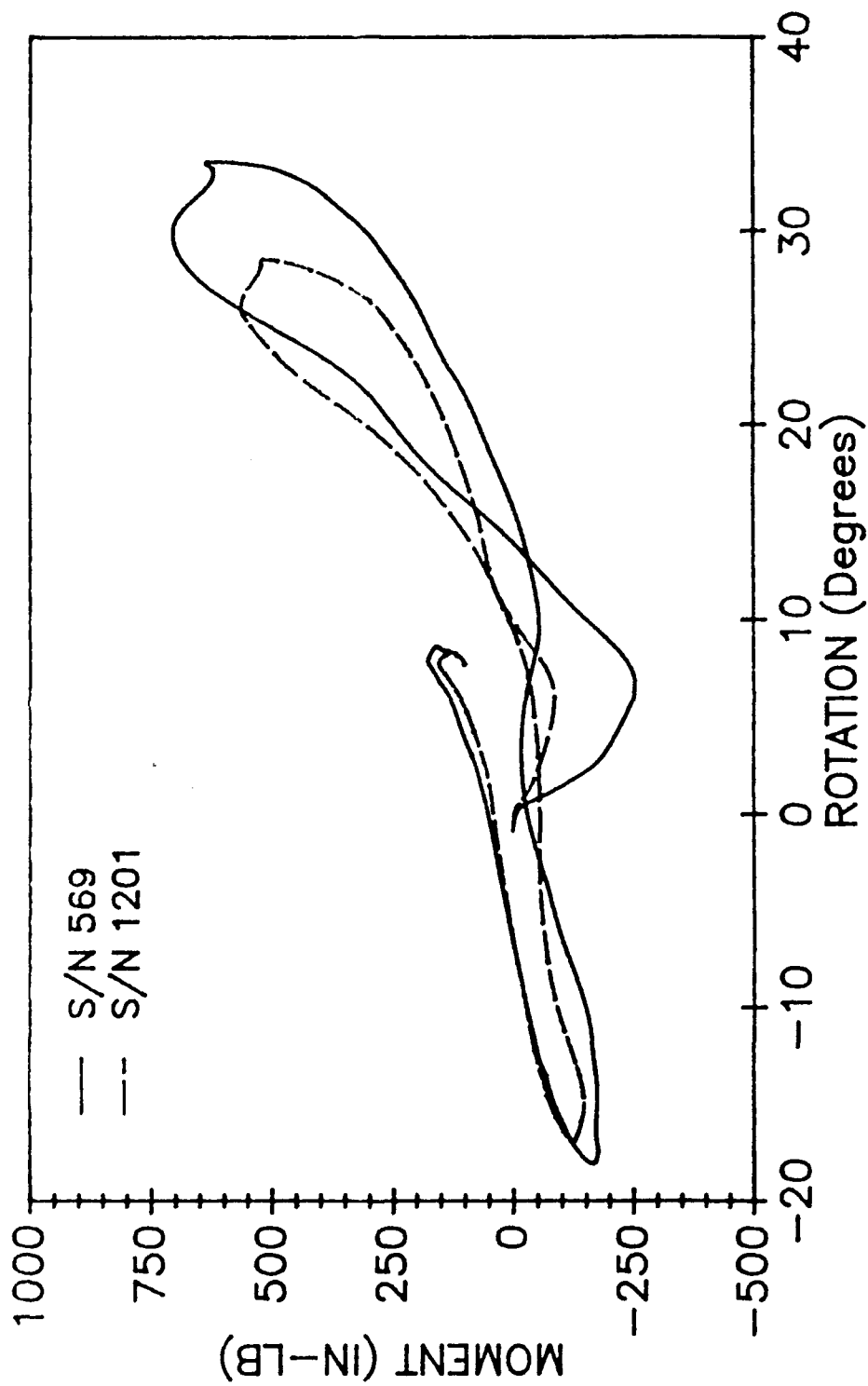


Figure 58 - Hybrid III Neck Moment Vs. Rotation Comparison 90°

HYBRID III 65° (14ft/sec)
FLEXION

TOTAL MOMENT VS ROTATION ABOUT NECK BASE

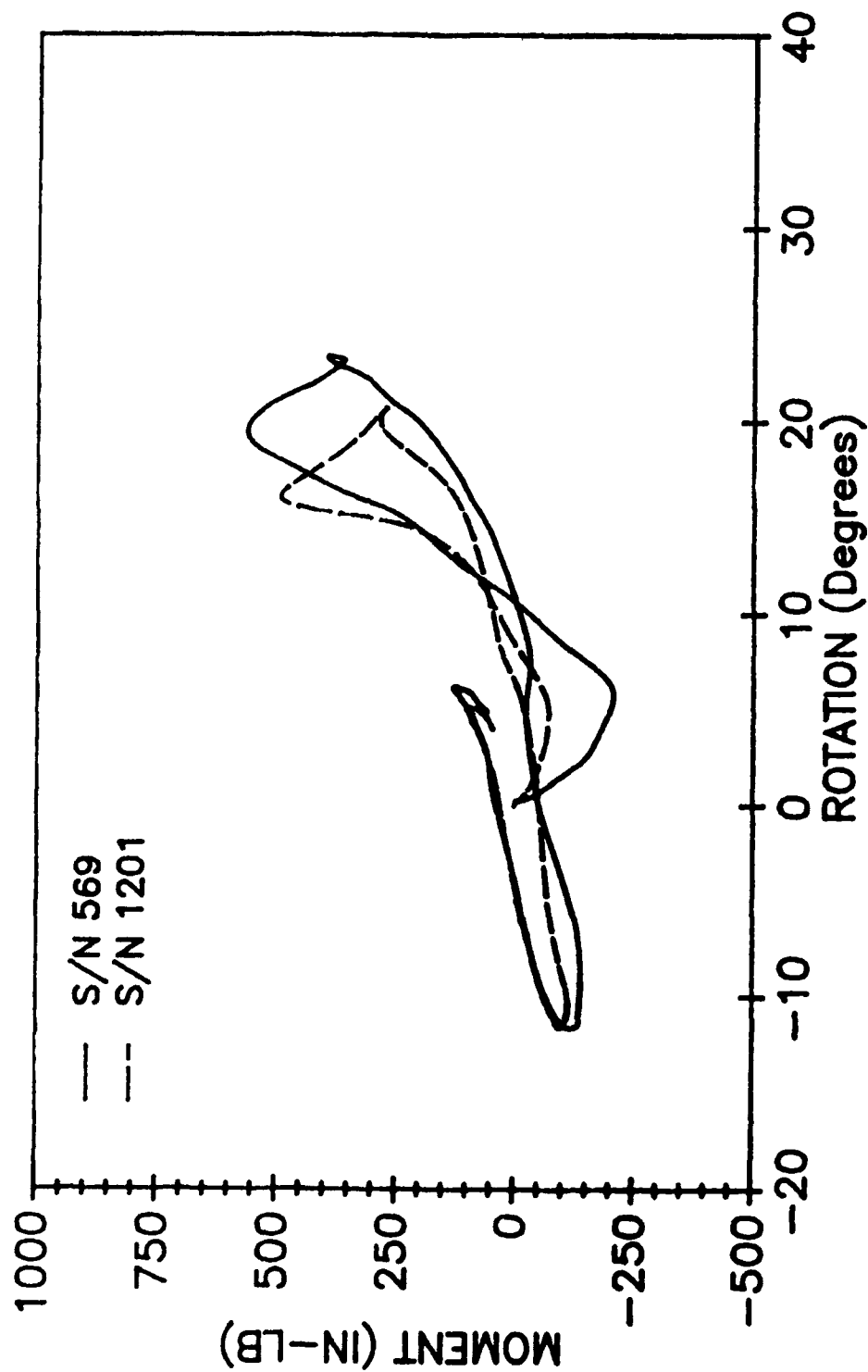


Figure 59 - Hybrid III Neck Moment Vs. Rotation Comparison 65°

HYBRID III 40° (9ft/sec)
FLEXION

TOTAL MOMENT VS ROTATION ABOUT NECK BASE

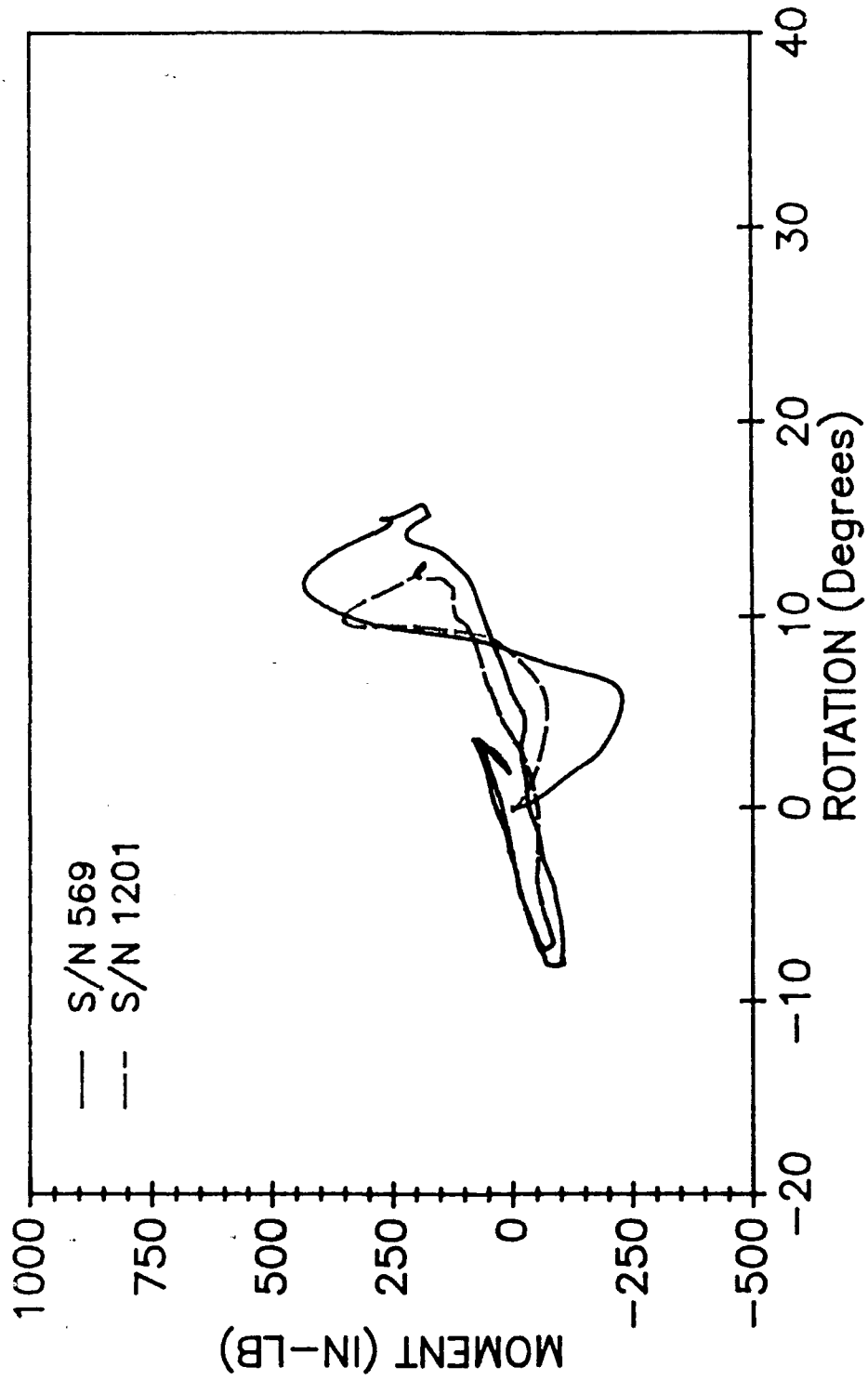


Figure 60 - Hybrid III Neck Moment Vs. Rotation Comparison 40°

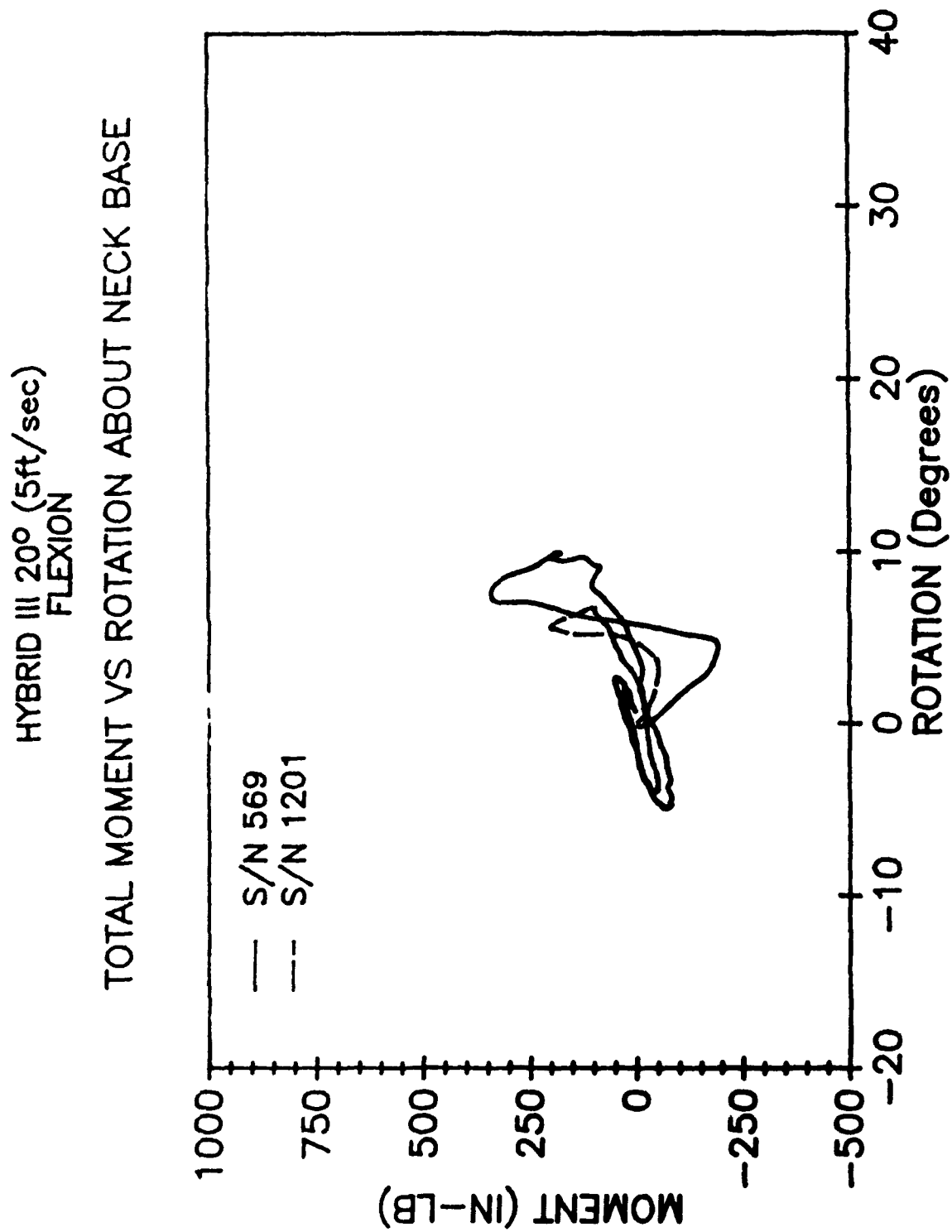


Figure 61 - Hybrid III Neck Moment Vs. Rotation Comparison 20°

HYBRID III DYNAMIC FLEXION TEST
WITH EQUIVALENT STATIC DATA OVERLAY (S/N 569)

TOTAL MOMENT VS ROTATION ABOUT NECK BASE

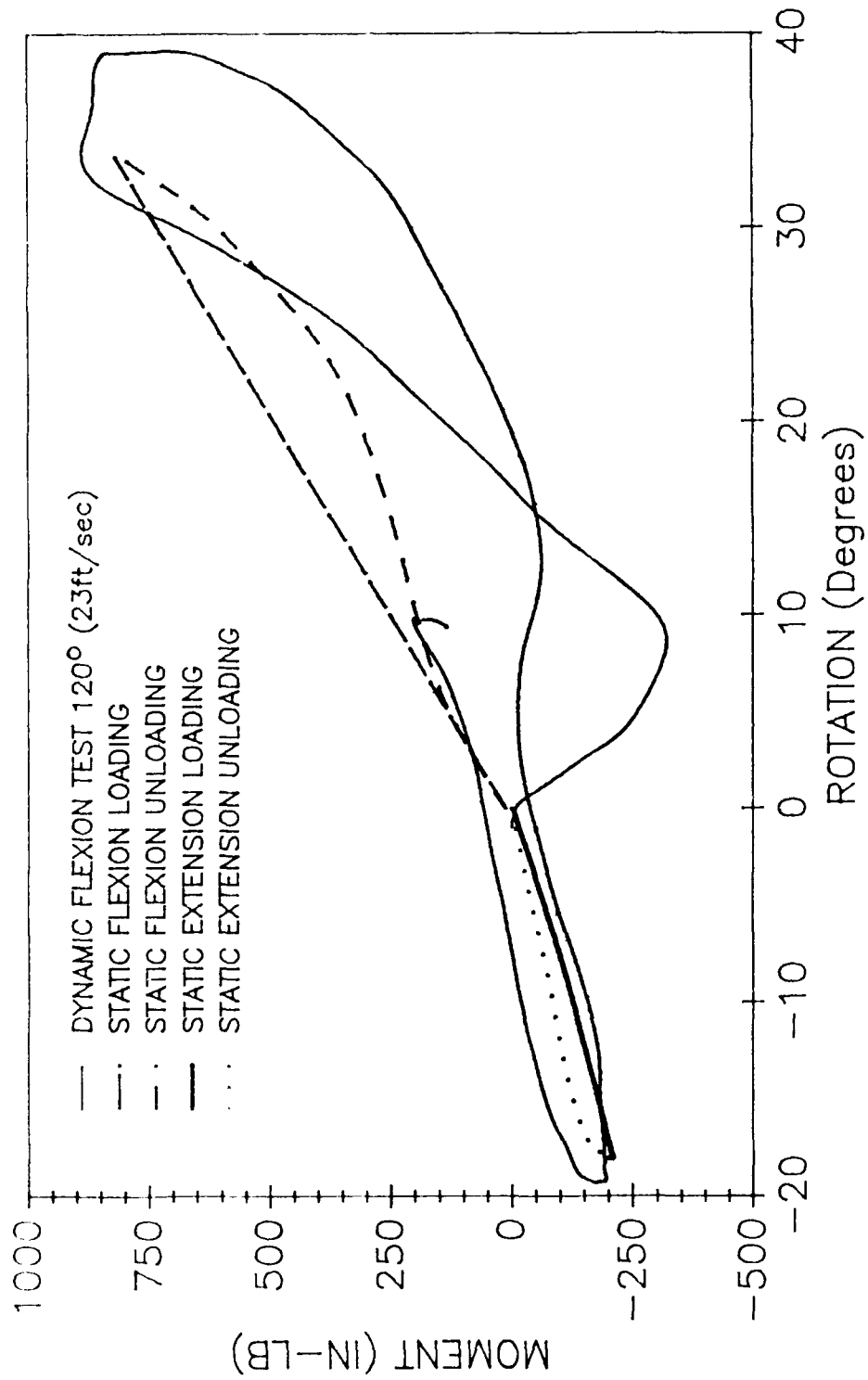


Figure 62 - Hybrid III Neck Moment Vs. Rotation Comparison Overlay

quasi-statically loaded neck. Again, similar results were obtained from the extension and lateral tests.

It is important to note that the SAE 572 Specifications³⁶ do not include certification corridors for lateral impacts. Lateral certification for the Hybrid III necks was inherently accepted from the flexion and extension certifications. As lateral tests were conducted and repeated, the data were compared to assure repeatability.

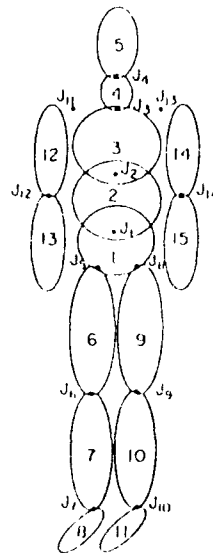
The dynamic tests performed provided a baseline for the computer models about to be discussed. Acceleration profiles and initial velocities from a number of tests were used as input to the computer models. Additionally, high speed cameras were used with several tests to film the event at 500 frames/sec. Photographs made from the films were used to directly compare the test data with the model's graphical output.

ATB MODEL

Model Description

The Articulated Total Body (ATB) Model^{25,26,27} was developed by the Calspan Corporation, when aerodynamic force application and harness belt capability were added to the Crash Victim Simulation (CVS) Program²⁴ for the Air Force. The resulting program became known as the ATB model. Other upgrades have been made to the model since then and the current version of the program is known as ATB-IV. The ATB model has been used most often to predict the motion of humans and manikins in car crashes and rollovers, aircraft crashes, and aircraft ejections.

The ATB model is a rigid body dynamics code that calculates the motion of coupled rigid bodies, which are connected by joints to form an articulated human body structure. Figure 63 illustrates the model of a human with 15 segments and 14 joints.



Joint j connects segment $JNT(j)$ with segment $j+1$

$JNT(j) =$	1	2	3	4	1	6	7	1	9	10	3	12	3	14
$(j) =$	1	2	3	4	5	6	7	8	9	10	11	12	13	14

Figure 63. ATB Model Representation of a Human Body

The specifications of the body include the inertial properties and c.g. of the segments and the location, type, and range of motion resistive properties of the joints. The types of joints include: ball and socket, slip, sliding, fixed, pin, or Euler.

Current Data Set

A current data set for a complete Hybrid III manikin has already been compiled³¹, but the neck characteristics have not proved adequate. The complete data set was listed by Kaleps (et al)³¹. There is currently no data set for a complete Hybrid II manikin.

In the Hybrid III data set the head and neck were modeled as a two joint, two linkage system. One joint represented the head/neck joint and the other the neck/torso joint. One linkage represented the head and the other the neck. The neck stiffnesses and damping coefficients were applied to the joints at each end of the neck. The inertial properties of the head and neck were applied to the c.g. of each segment.

New Data Set

For modeling the head and neck tests performed on the pendulum, three segments and two joints were required. The three segments were the head, neck, and the upper torso. The inertial properties and c.g. location of the upper torso were changed to match those of the pendulum arm. The inertial properties of the head and neck were transferred from the current data set. The only changes to the current data set were the stiffness, damping, and addition of internal hysteresis neck properties.

There were two ways the ATB model accepted stiffness data: equation and tabular. The equation format used the coefficients for the linear, quadratic, and cubic terms of the stiffness equation. The tabular form allowed exact stiffness values at equal bending increments. Since the stiffness of the neck, which was distributed throughout its length, had to be applied as torques at the joints, the joints had to act as two springs in series to provide the correct neck stiffness. Equation (6) defines the requirement.

$$1/K_n = 1/K_{oc} + 1/K_{T1} \quad (6)$$

Equation (7) solves for K_{oc} and K_{T1} .

$$K_{oc} = K_{T1} = 2 * K_n \quad (7)$$

The joint torques to be applied were twice the stiffness measured for the neck. The stiffness of the nodding blocks for the Hybrid III neck also had to be added to the joint at the top of the neck. These values were taken directly from the current data set and added to the new stiffness data for the o.c. joint. Note the nodding blocks were in series with the neck (refer to figure 10) and an equation similar to equation (6) was used to calculate the correct torque for the o.c. joint.

Recall that all of the stiffness data described in the static tests for Hybrid II in any orientation was linear for almost the entire range of rotation. The stiffness data for the Hybrid III in any orientation were linear for at least 40°. Recall from the description of the dynamic tests that the neck rotation was about 50° for Hybrid II tests and not above 40° for any Hybrid III test. Therefore, the linear regression fit for the first 40° rotation was used to derive the tabular stiffness values up to 40°. Above 40° the third order regression coefficients were used. This method provided the best overall fit to the static test data. The ATB model required stiffness data up to 180° to prevent computational errors. If the data set worked correctly, the stiffness values above 50° for Hybrid II and 40° for Hybrid III would not be used.

The ATB model allowed four different stiffness tables to be input: flexion, extension, "+" lateral, and "-" lateral. For the Hybrid II these tables were all identical, but independent flexion, extension, and lateral (+ and - were identical) stiffness tables were input for the Hybrid III. The limitation of the ATB model using this option was that no internal hysteresis could be input. So, the joints were loaded and unloaded using the same stiffness table.

The other option was to use the stiffness equation coefficients. This option allowed the use of a hysteresis coefficient, but the exact unloading profile was assumed and not input. The limitation of this option was that separate flexion, extension, and lateral stiffness coefficients could not be used. One set of coefficients were used for all orientations. This was not a problem for the Hybrid II simulations, as the neck had only one stiffness, but the Hybrid III simulations were limited to only one of the three stiffness curves. Two loading curves were required for flexion and extension tests, because the neck rotated into both during a test.

The stiffnesses calculated for these simulations were on average 30% lower than the stiffnesses in the current data set. As the simulation data will show, the current data set did not allow the head and neck to rotate far enough, but the

lower stiffnesses of the new data set increased the rotation angle.

Damping was input into the model as a damping coefficient found by using equation (8).

$$C_j = \delta 2 (K_j J_j)^{1/2} \quad j=T1 \text{ and o.c.} \quad (8)$$

A different damping coefficient was found for both joints corresponding to the stiffness at that joint and the moment of inertia of the attached segment. The damping ratios calculated from the dynamic data were very close to those found by Kaleps³¹ ($\delta=0.2$ to $\delta=0.22$). But since the stiffnesses for the joints were different (the moments of inertia were the same), the resulting damping coefficients for the new data set were also about 30% lower than the current data set. Previous simulations of the current data set were only plotted to 200msec, so the affect of the damping ratios was not apparent, as the second peak did not occur until 250-300msec after impact.

Modeling Results

Simulations were run with the current data set for the Hybrid III head/neck system. Changes were made to the input deck and the simulations rerun. Simulations were also run using the geometry, inertial properties, stiffness and damping values for the Hybrid II system. The output from the new data set was compared to the current data set and to pendulum test data. Graphic output for the new data was also directly compared to the high speed footage of several pendulum tests.

Hybrid II

A stiffness table was generated for the Hybrid II data set from the average static bending data and input into the ATB model for each of the four orientations: flexion, extension, and "+" and "-" lateral. Figure 64 illustrates the comparison of the model output to the actual test data for the neck rotation. The model did not reach the same amplitude as the test data for the first peak, but the second peak matched well. There is very little phase difference between the two curves.

Head rotation was also compared as figure 65 illustrates. The ATB model predicted head rotations that exceeded the test data. The dynamic response of the head rotation was a function of all Hybrid II HNP tests. It is believed that the noisy response was due to the attachment of the three potentiometer device to the head by use of a long bolt (refer to figure 38). Due to the difficulty in certifying the Hybrid

HYBRID II 90° (20ft/sec)
FLEXION

ROTATION ABOUT NECK BASE

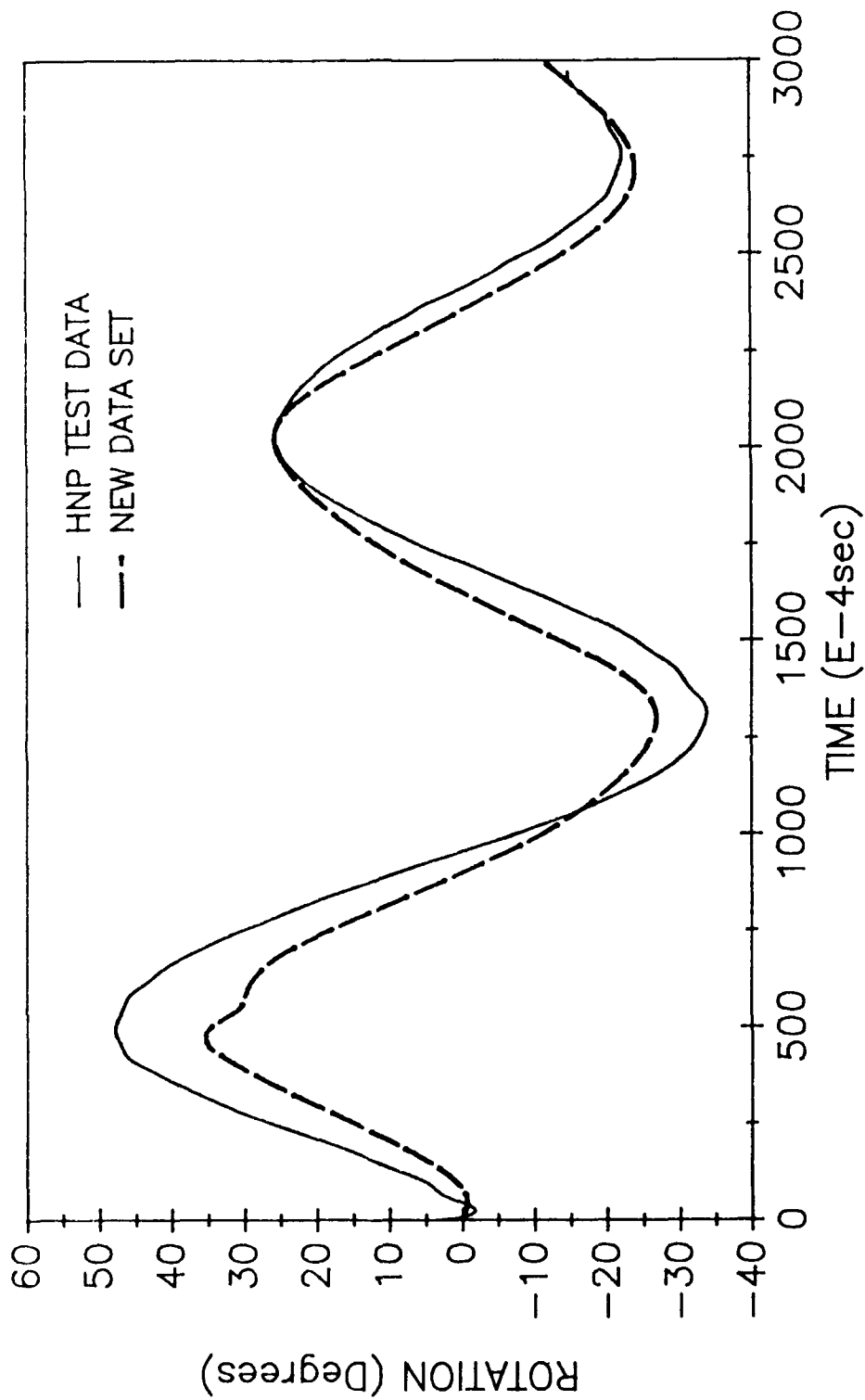


Figure 64 - Hybrid II Flexion Neck Rotation ATB Simulation

HYBRID II 90° (20ft/sec)
FLEXION

ROTATION ABOUT HEAD C.G.

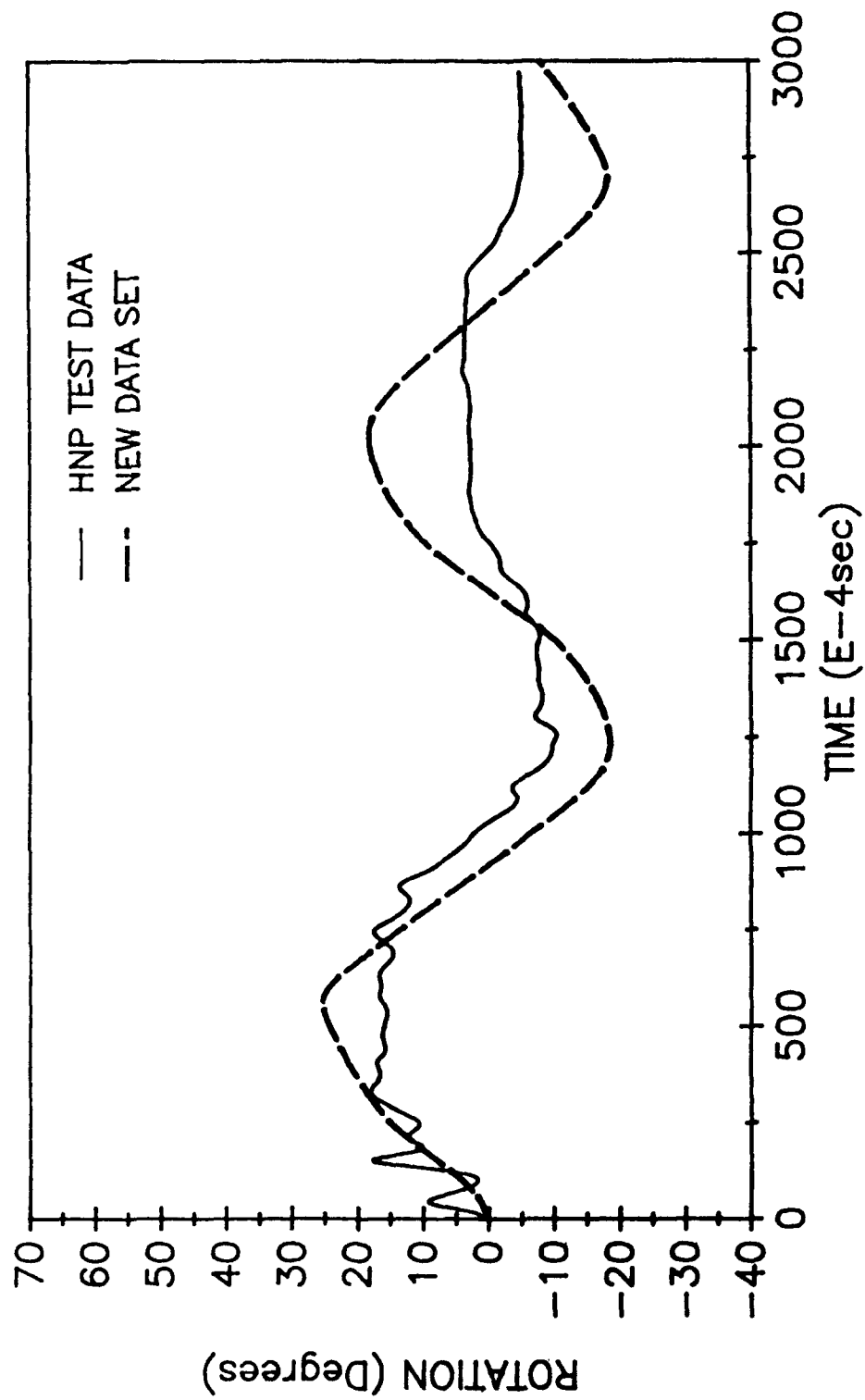


Figure 65 - Hybrid II Flexion Head Rotation ATB Simulation

II necks, it was not known whether the measured dynamic response of the head was completely mechanically related, or if it was also related to the analysis software. The ATB model representation of the Hybrid II head and neck appeared to be good from the available data, but it should be compared directly to a certified neck response.

Hybrid III

Independent stiffness tables were generated for flexion, extension, and lateral bending. The same table was used for "+" and "-" lateral bending. Figure 66 illustrates a comparison of the old and new data sets to the test data for neck rotation. The new data set incorporated the new stiffness tables and damping coefficients. Figure 67 illustrates the same simulation for the O.C. rotation. The new data set matched the test data better. The peak rotation was not quite as high as the test data, but significantly greater than the old data set. The new damping ratios were also better as the second peak dropped nearly as much as the test data. The second peak of the old data set was good, but the first peak was low, so there was insufficient damping.

The phase difference between the curves was also improved, but the new data set was still not in phase with the test data. The lack of a hysteresis option may have caused this time lag. During the actual test, the neck lost about 30% of its stored energy during its unloading rotation. The ATB simulation neck did not lose any stored energy during its unloading rotation. This may have also caused the over-prediction of the model for the extension rotation after the first peak.

Figures 68 and 69 illustrate the ATB model prediction of the extension test. The new data set again improved the response of the model to the test data. The phase difference between the new data set and the test data was smaller for the extension tests, because there was less energy from the impact. The extension simulation was taken from a 90° HNP test, corresponding to a Hybrid III extension certification test. The second peaks of both data sets were greater than the test data because the model did not allow for the hysteresis affect of the neck.

Lateral simulations were also run and compared to test data. Figures 70 and 71 again illustrate the improvement made by the new data set. These plots also showed that the model did not predict the peak initial rotation of the neck, but the new data set was better. The second peaks were better, and the phase difference was greatly improved with the new data set.

Additional simulations were run using the stiffness coefficient option, which enabled the use of a hysteresis coefficient. Figures 72 and 73 illustrate the model's

HYBRID III 120° (23ft/sec)
ATB FLEXION SIMULATION

ROTATION ABOUT NECK BASE

STIFFNESS TABLES, DAMPING

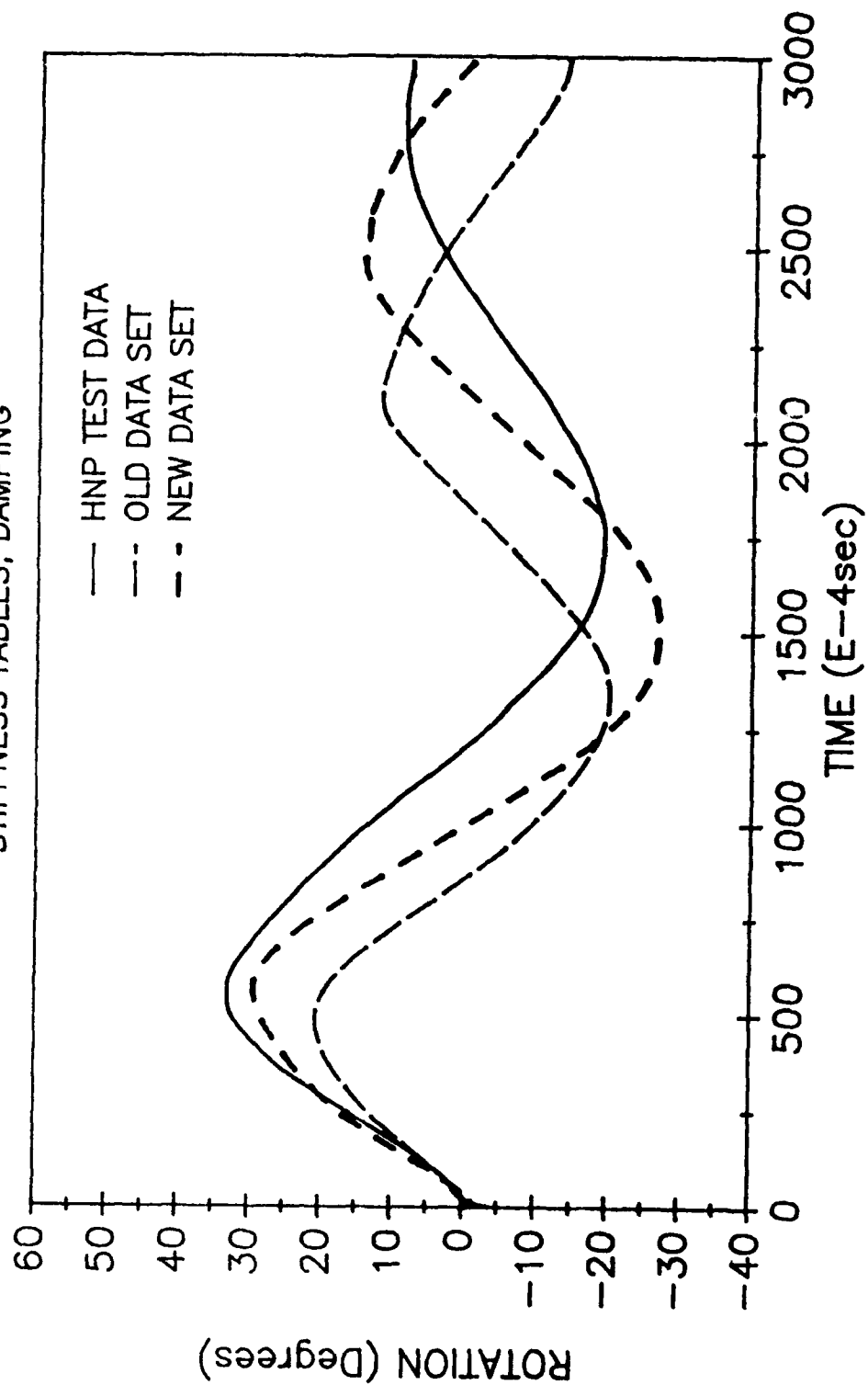


Figure 66 - Hybrid III Flexion Neck Rotation ATB Simulation

HYBRID III 120° (23ft/sec)
ATB FLEXION SIMULATION

ROTATION ABOUT OCCIPITAL CONDYLE

STIFFNESS TABLES, DAMPING

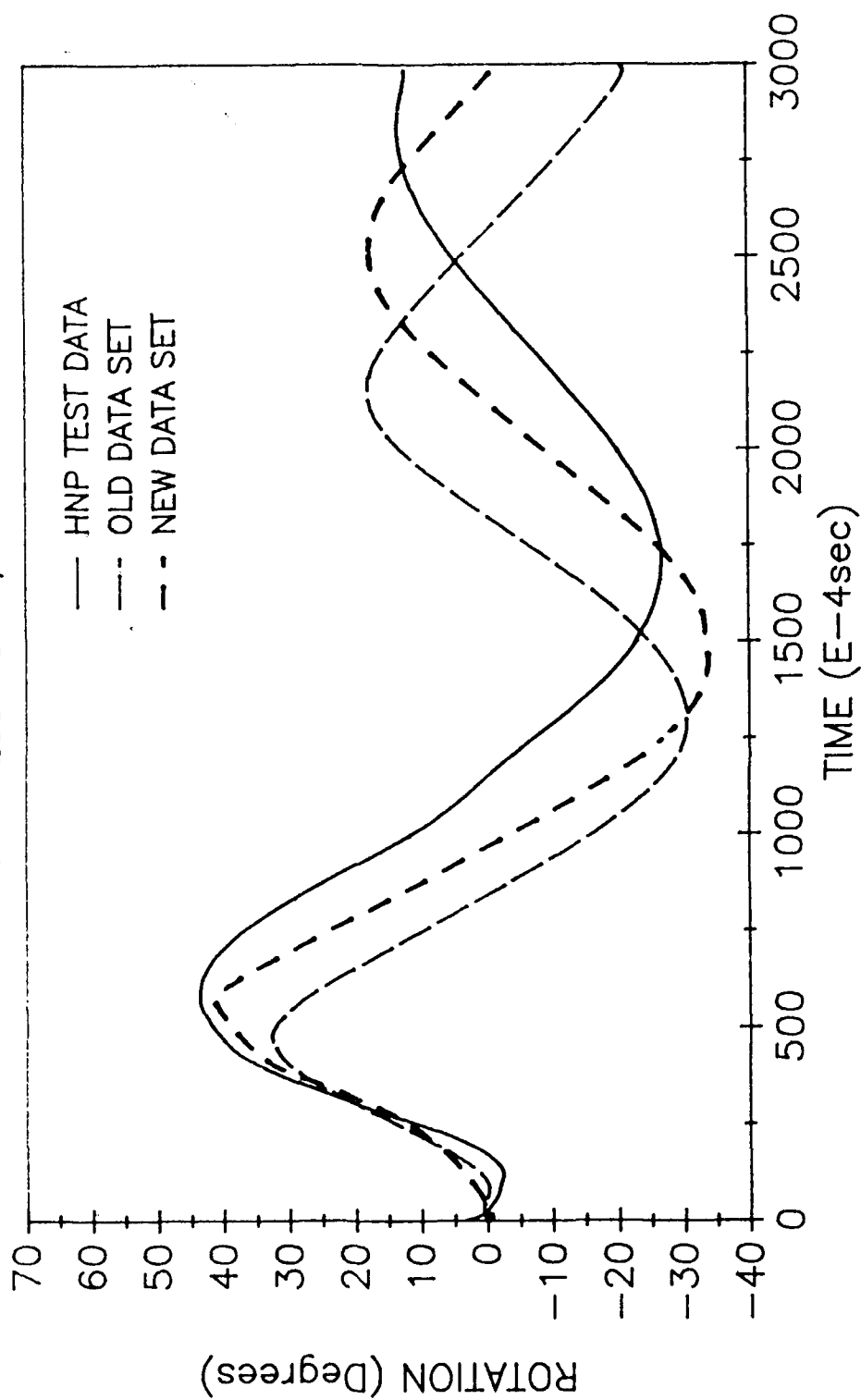


Figure 67 - Hybrid III Flexion O.C. Rotation ATB Simulation

HYBRID III 90° (20ft/sec)
EXTENSION

ROTATION ABOUT NECK BASE

STIFFNESS TABLES, DAMPING

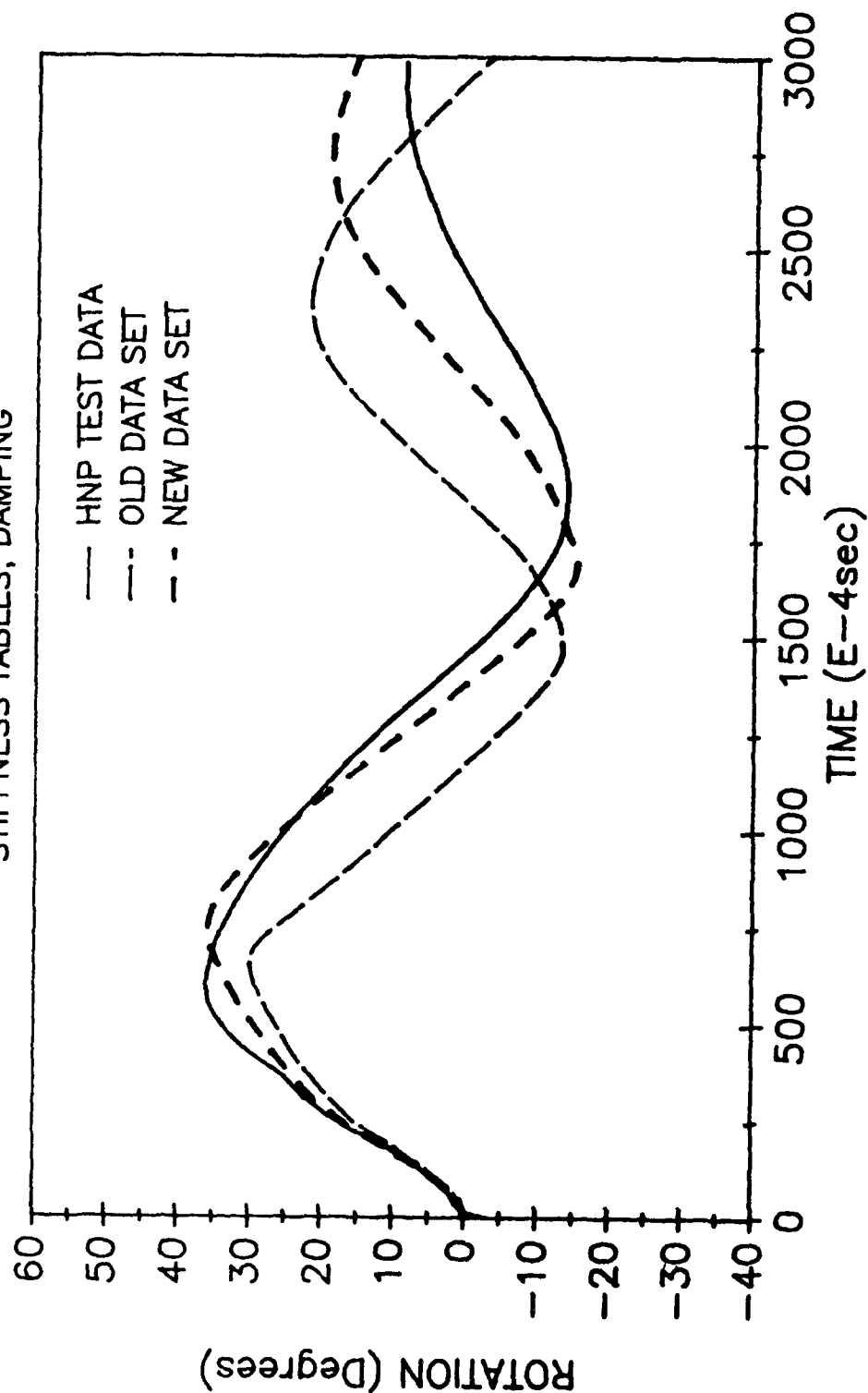


Figure 68 - Hybrid III Extension Neck Rotation ATB Simulation

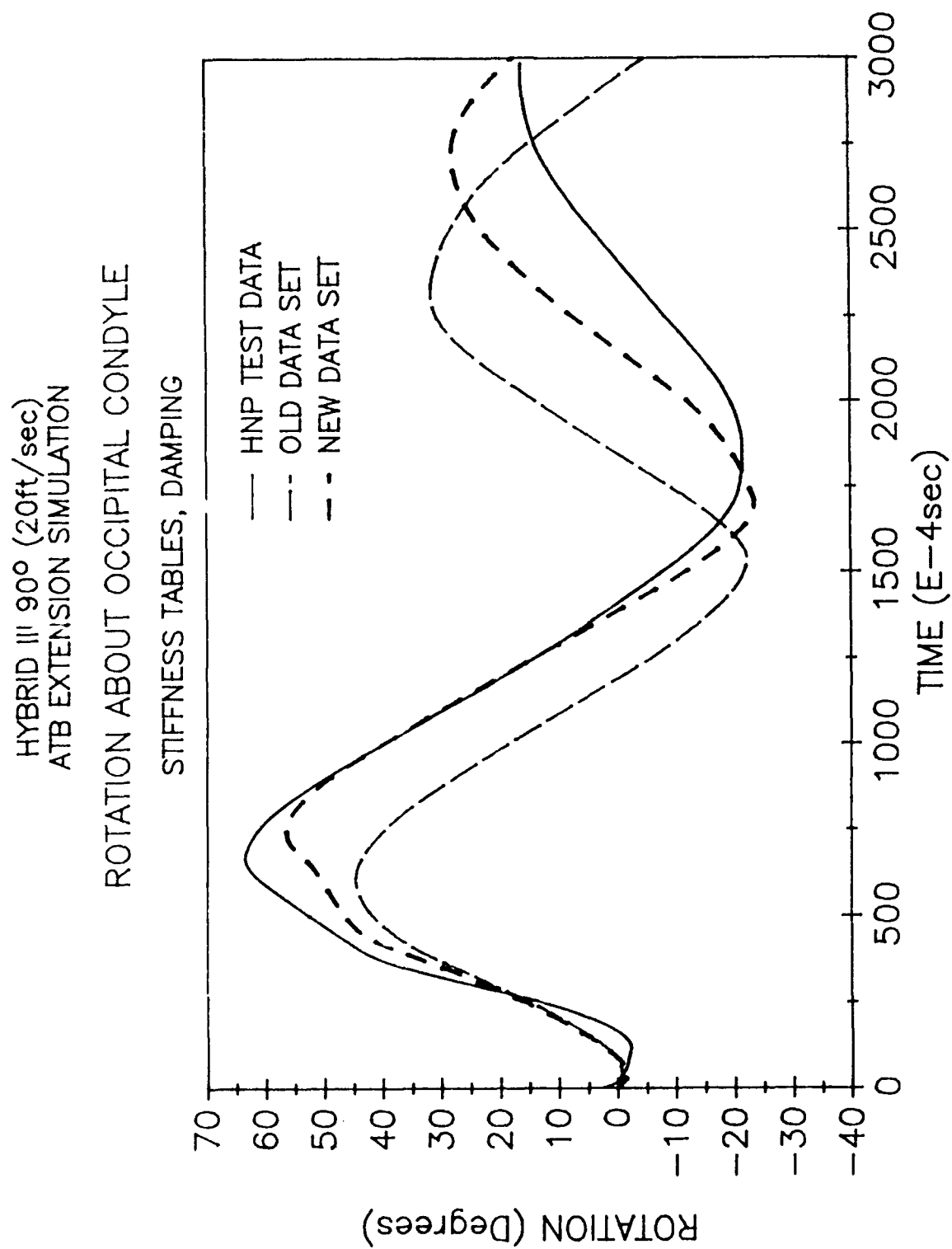


Figure 69 - Hybrid III Extension O.C. Rotation ATB Simulation

HYBRID III 120° (23ft/sec)
LATERAL BENDING

ROTATION ABOUT NECK BASE

STIFFNESS TABLES, DAMPING

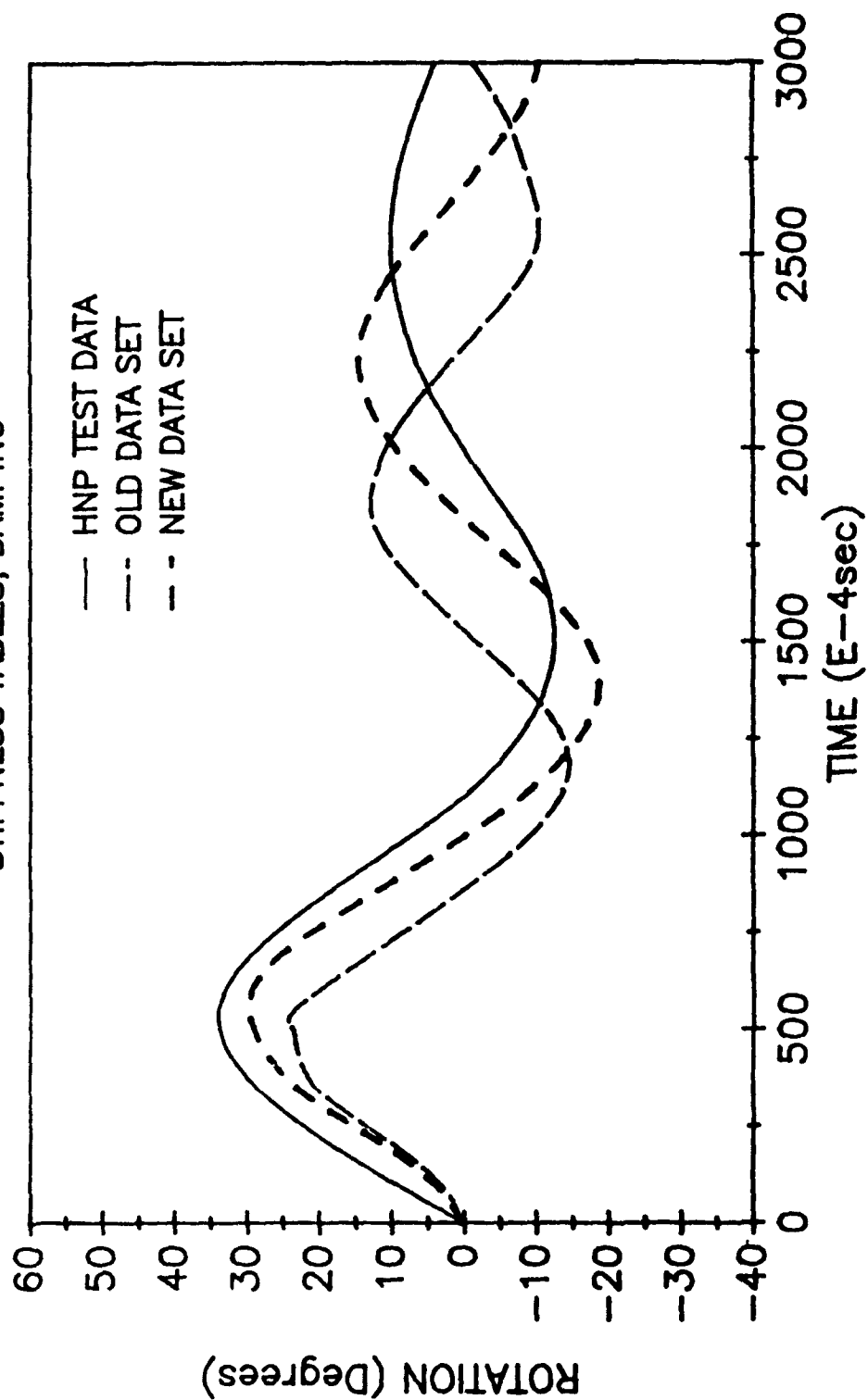


Figure 70 - Hybrid III Lateral Neck Rotation ATB Simulation

HYBRID III 120° (23ft/sec)
LATERAL BENDING

ROTATION ABOUT OCCIPITAL CONDYLE

STIFFNESS TABLES, DAMPING

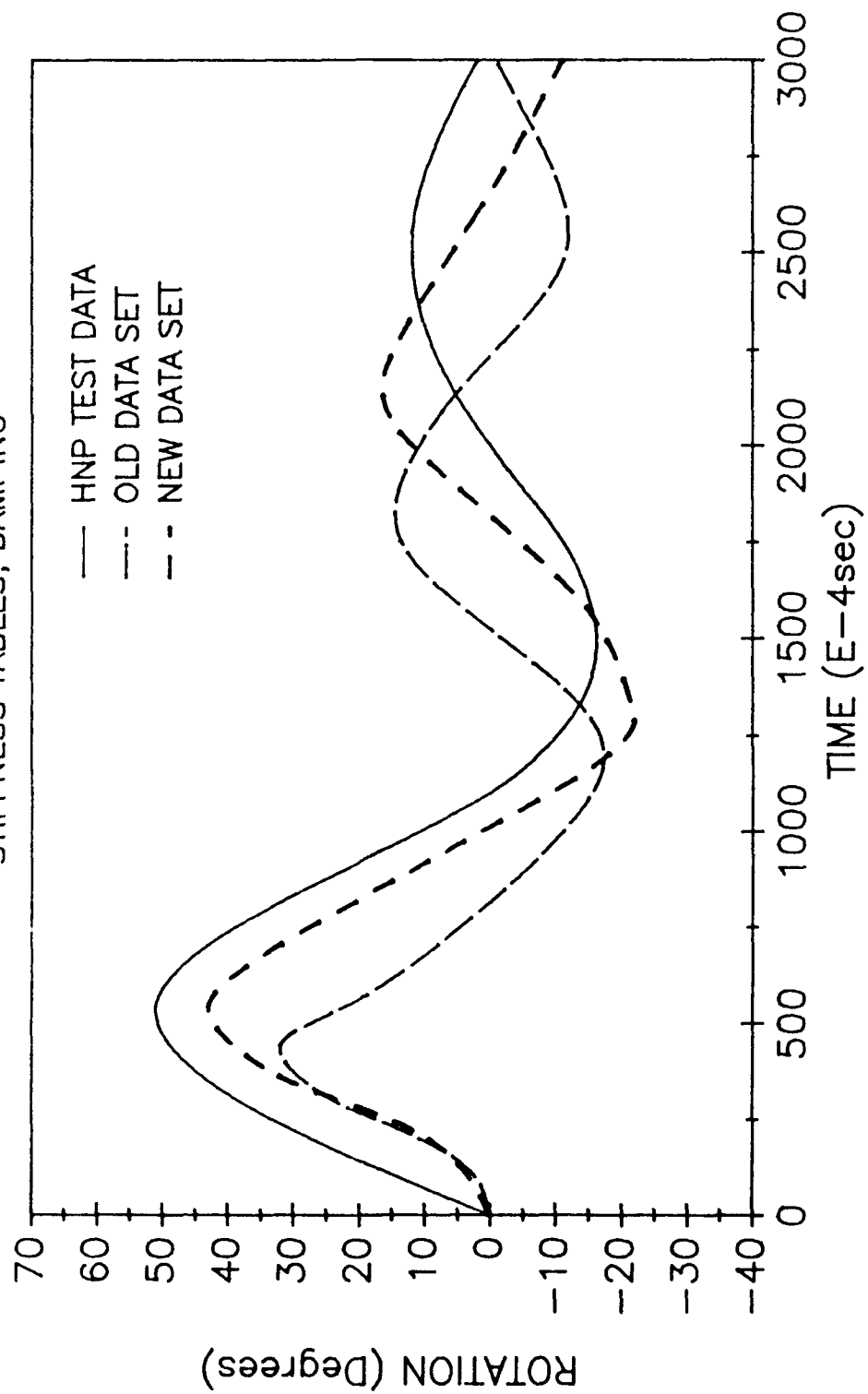


Figure 71 - Hybrid III Lateral O.C. Rotation ATB Simulation

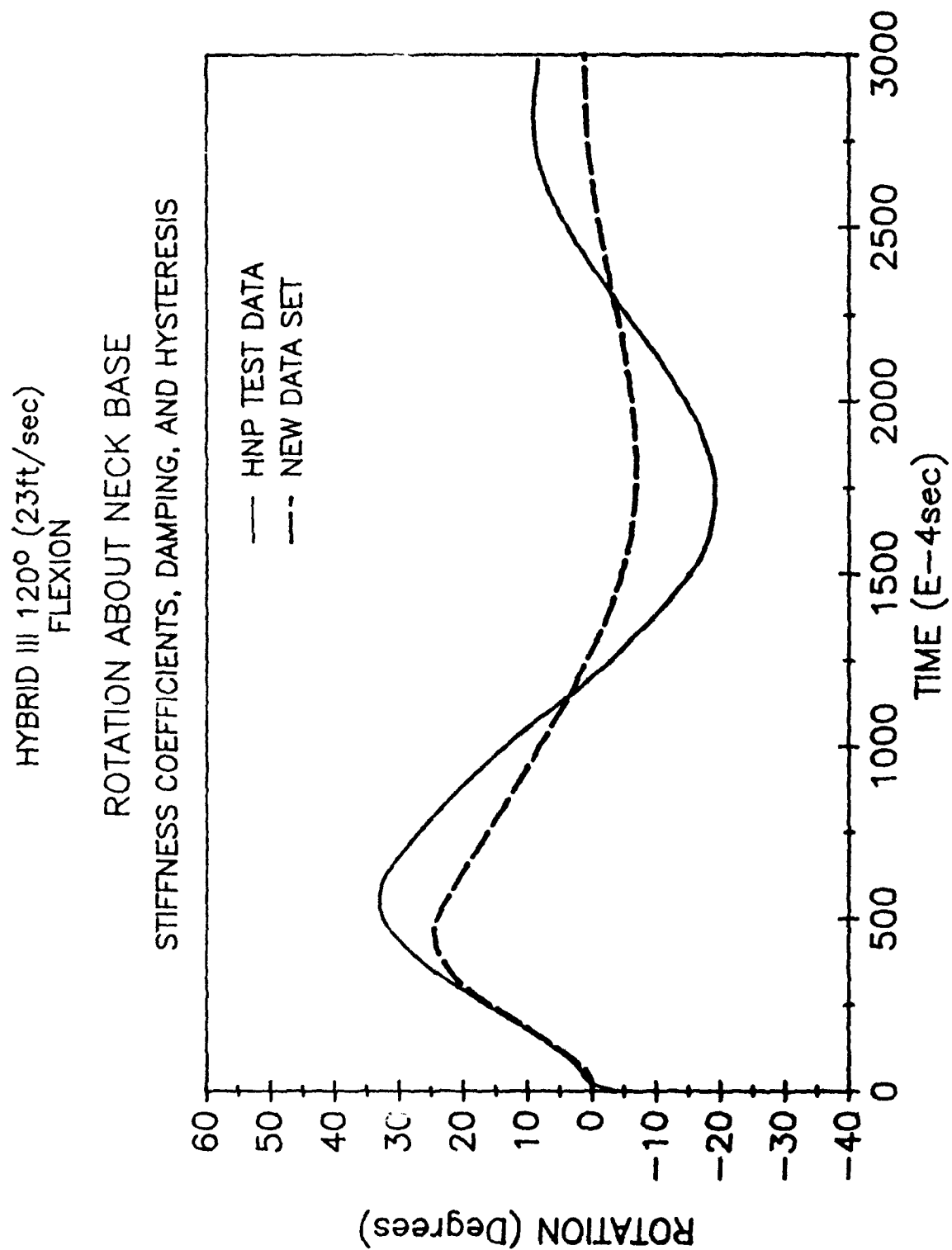


Figure 72 - Hybrid III Neck Stiffness Coefficient Simulation

HYBRID III 120° (23ft/sec)
FLEXION

ROTATION ABOUT OCCIPITAL CONDYLE
STIFFNESS COEFFICIENTS, DAMPING, AND HYSTERESIS

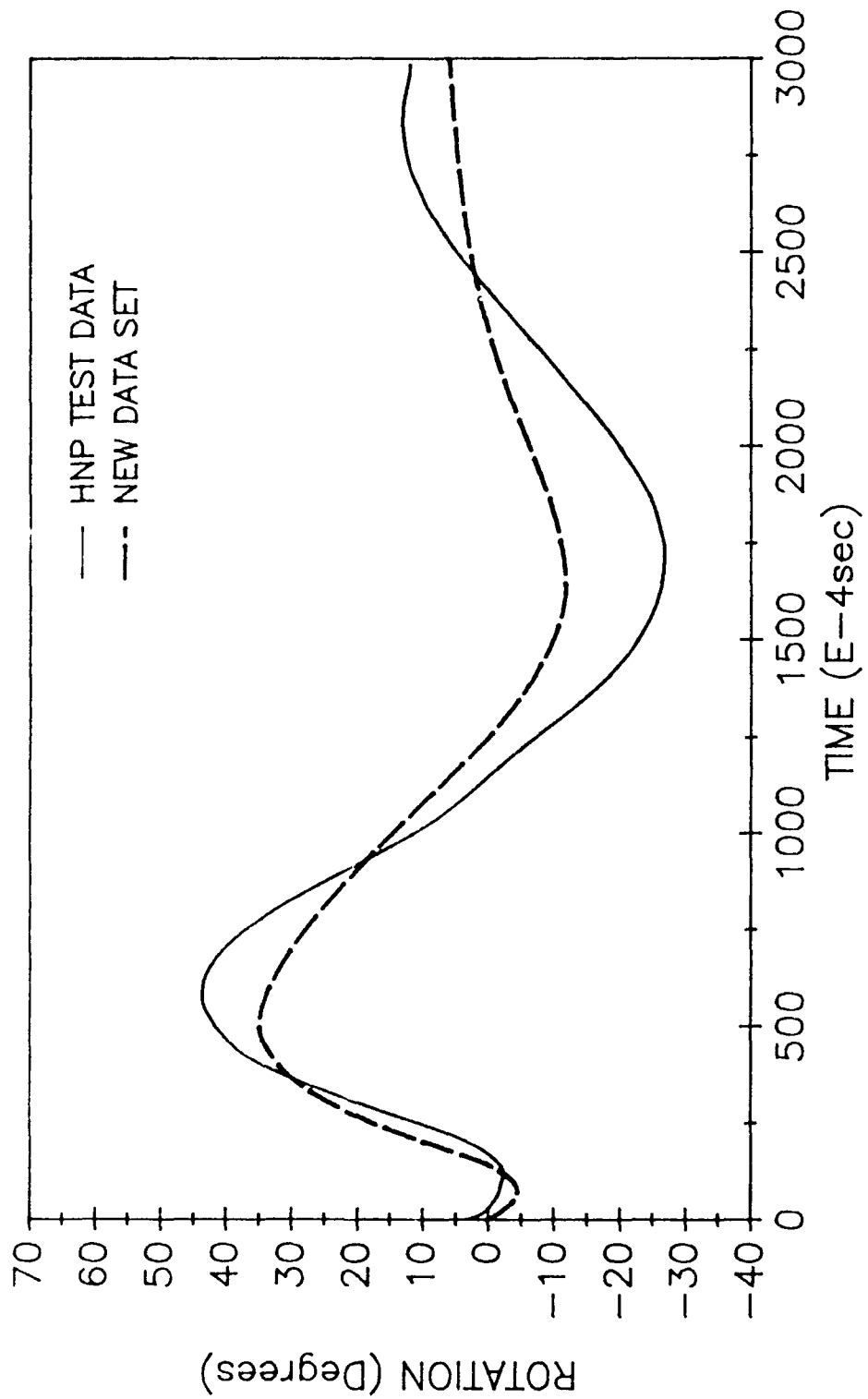


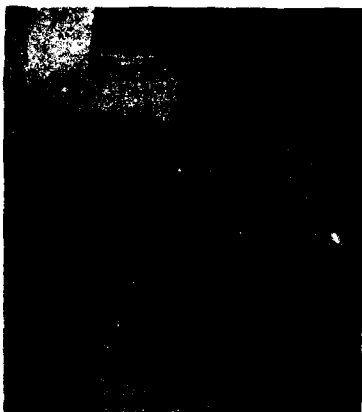
Figure 73 - Hybrid III O.C. Stiffness Coefficient Simulation

prediction with this option. No current data set existed using this option. The response of the model was poor, not because of the hysteresis coefficient, but because of the limitation of the coefficient option. The option used the coefficients for all orientations, therefore, the extension rotation after the first peak was modeled with the same flexion coefficients as the initial rotation. The phase of the two curves appeared to be similar, which may have been attributed to the hysteresis coefficient.

The ATB model's graphical output was compared to photographs taken from high speed films of several tests. Figures 74, 75, and 76 illustrate the new data set, using the tabular stiffnesses, and the test article for flexion, extension, and lateral test simulations. The graphical representation illustrates how closely the new data set predicted the actual test data. Additional refinement of the model could be made if the tabular stiffness option was changed to incorporate a hysteresis coefficient or unloading table.

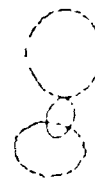
FLEX.569 120' MTL K & C

TIME(MSEC) 0.



FLEX.569 120' MTL K & C

TIME(MSEC) 20.



FLEX.569 120' MTL K & C

TIME(MSEC) 40.



FLEX.569 120' MTL K & C

TIME(MSEC) 60.



FLEX.569 120' MTL K & C

TIME(MSEC) 80.



FLEX.569 120' MTL K & C

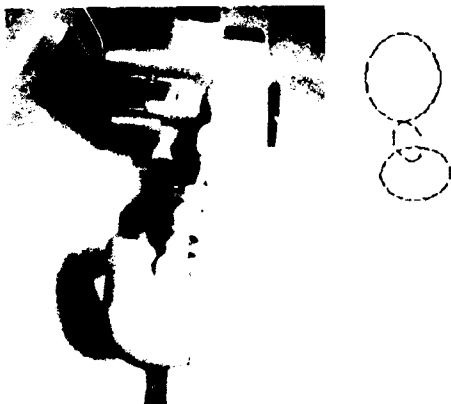
TIME(MSEC) 100.



Figure 74. Graphical Comparison for Flexion Test (1 of 2)

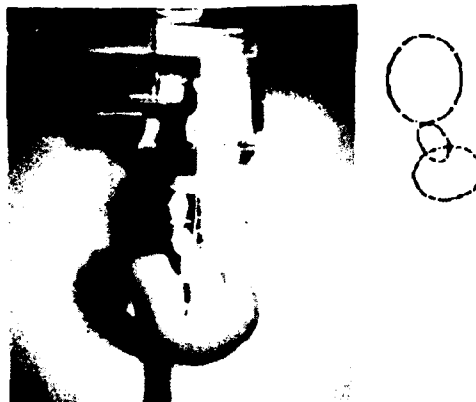
FLEX.569 120' MTL K & C

TIME(MSEC) 120.



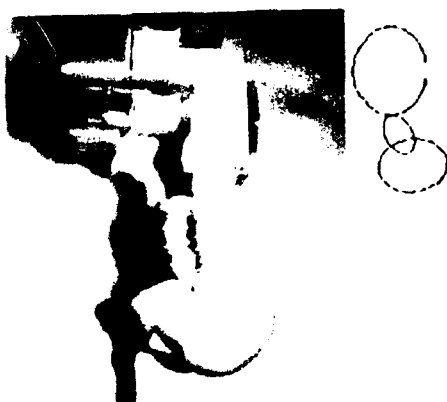
FLEX.569 120' MTL K & C

TIME(MSEC) 140.



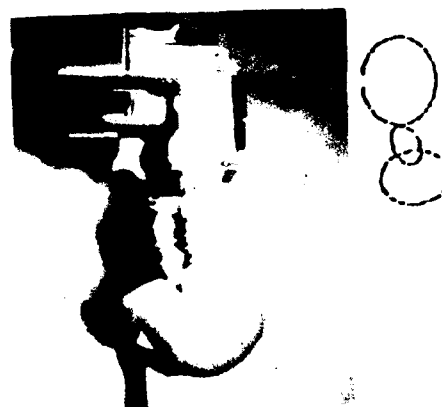
FLEX.569 120' MTL K & C

TIME(MSEC) 160.



FLEX.569 120' MTL K & C

TIME(MSEC) 180.



FLEX.569 120' MTL K & C

TIME(MSEC) 200.

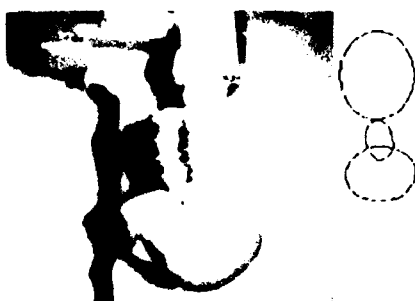
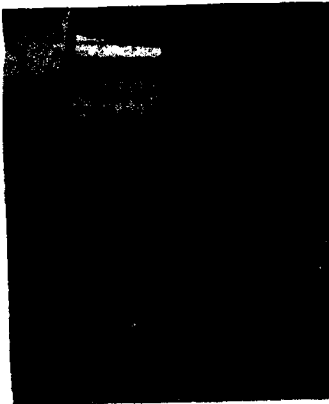


Figure 74. Graphical Comparison for Flexion Test (2 of 2)

EXT.569 90° MTL K & C

TIME(MSEC) 0.



EXT.569 90° MTL K & C

TIME(MSEC) 20.



EXT.569 90° MTL K & C

TIME(MSEC) 40.



EXT.569 90° MTL K & C

TIME(MSEC) 60.



EXT.569 90° MTL K & C

TIME(MSEC) 80.



EXT.569 90° MTL K & C

TIME(MSEC) 100.



Figure 75. Graphical Comparison for Extension Test (1 of 2)

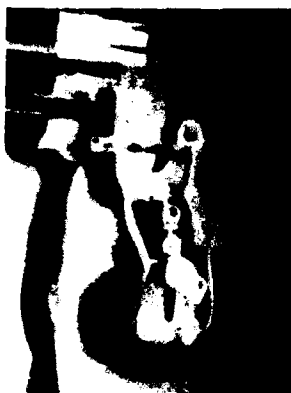
EXT.569 90° MTL X & C

TIME(MSEC) 120.



EXT.569 90° MTL X & C

TIME(MSEC) 140.



EXT.569 90° MTL X & C

TIME(MSEC) 160.



EXT.569 90° MTL X & C

TIME(MSEC) 180.



EXT.569 90° MTL X & C

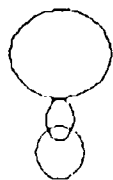
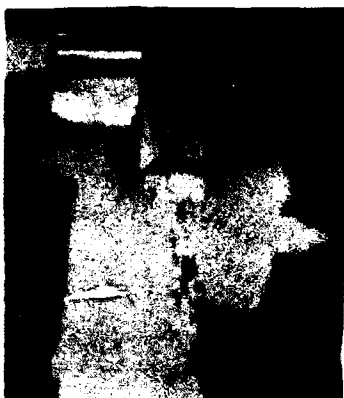
TIME(MSEC) 200.



Figure 75. Graphical Comparison for Extension Test (2 of 2)

LAT.569 120' MTL K & C

TIME(MSEC) 0.



LAT.569 120' MTL K & C

TIME(MSEC) 20.



LAT.569 120' MTL K & C

TIME(MSEC) 40.



LAT.569 120' MTL K & C

TIME(MSEC) 60.



LAT.569 120' MTL K & C

TIME(MSEC) 80.



LAT.569 120' MTL K & C

TIME(MSEC) 100.



Figure 76. Graphical Comparison for Lateral Test (1 of 2)

107.569 120' MTL K & C

TIME(MSEC) 120.



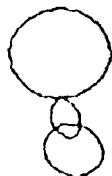
107.569 120' MTL K & C

TIME(MSEC) 140.



107.569 120' MTL K & C

TIME(MSEC) 160.



107.569 120' MTL K & C

TIME(MSEC) 180.



107.569 120' MTL K & C

TIME(MSEC) 200.



Figure 76. Graphical Comparison for Lateral Test (2 of 2)

HSM MODEL

Model Description

The Head Spine Model (HSM)^{29,30} is also known as the Head Cervicle Spine Model. The name reflects the program's complete capability of modeling the head, cervicle, and spine with attached ribs. The HSM has been used to model baboon, chimpanzee, and human cervicle and spine systems.

The HSM is a finite element code that was developed to determine the injury threshold for the cervicle and spine during impact loadings. The code was optimized for ejection sequences, which incur a large vertical loading through the spinal column. The model uses various types of elements with different numbers of nodes. The inherent geometry of the model was also optimized for defining vertebrae and the attachment of muscle and cartilage.

Current Data Set

Data sets have been developed for human, chimpanzee, and baboon cervicle and spine systems. These data sets are quite large and use hundreds of elements. Much simpler data sets have been developed by Doherty (et al)^{32,33} for the Hybrid II and Hybrid III necks using one and four elements. These models were generated to meet the certification corridors described in the SAE Part 572 Specifications³⁶. The stiffnesses and damping coefficients were the model's best predictions of the certification corridors. Doherty also changed the HSM source code to incorporate the asymmetrical bending stiffnesses of the Hybrid III neck.

The results of Doherty's work^{32,33} showed that the four element model of the neck provided only marginally better results than the single element model, but required substantially more computing time. Therefore, in an effort to save computing resources, while still maintaining the integrity of the solution, the one element models of the neck were chosen for analysis.

Baseline data for the existing input decks were generated from material property tables and neck geometry. Pendulum tests were used to collect suitable acceleration pulses and the data compared to the output of the model. Through an iterative process, the best fit stiffnesses and damping coefficients were found. The one element data sets matched the certification corridors well. This study compared the stiffness and damping properties measured from controlled static and dynamic tests to the test data and the optimized model data sets.

New Data Set

Stiffnesses from the static tests were converted to HSM input deck form by converting "in-lb/deg" to "dyne-cm/rad". This conversion allowed the stiffness data to be compatible with the current data set, which was generated using metric units. Unlike the ATB model, the stiffness properties for the HSM model were input for each element, in this case one. No other calculations were required for the stiffnesses.

To enter the damping coefficient into the HSM damping coefficients had to be calculated as shown in equation (9).

$$C = \delta 2(KJ)^{1/2} \quad (9)$$

This damping coefficient then had to be divided by radians before being put into the model. This provided a damping coefficient in terms of the rotation. The other material properties were not changed. The HSM did not have an internal hysteresis option. The viscoelastic element selected provided some hysteresis properties as a function of this element type.

Modeling Results

Simulations were run with the current data sets for both Hybrid II and Hybrid III head/neck systems as baseline data for the model. Changes were made to the input decks and the model rerun so the new data could be compared to the existing data set and to test data collected on the pendulum.

Hybrid II

The stiffness for the Hybrid II necks was slightly smaller than that found in the current data set, while the damping coefficient was slightly larger. Figure 77 illustrates the

HYBRID II 90° (20ft./sec)
FLEXION

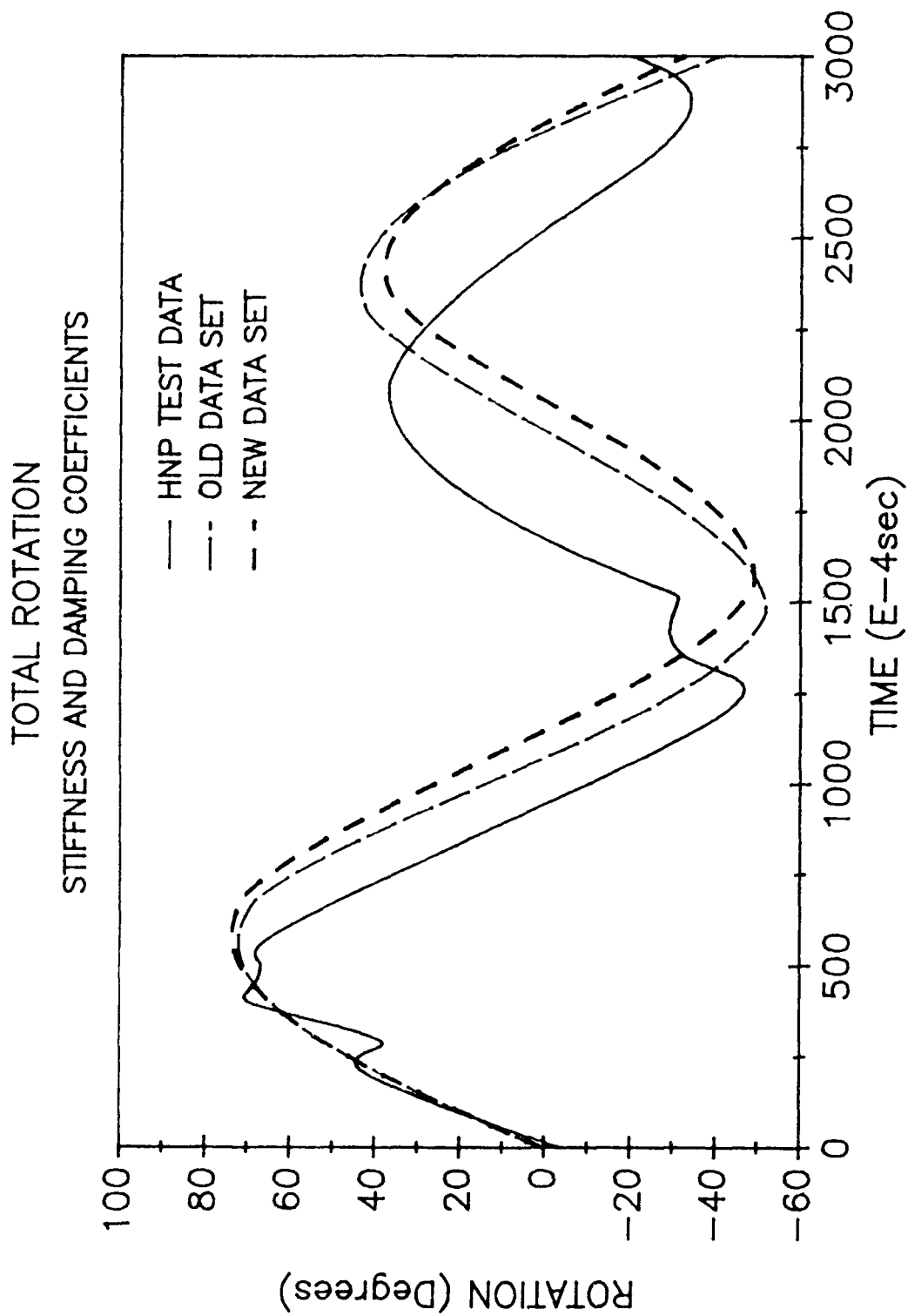


Figure 77 - HSM Hybrid II Flexion Simulation

comparison to the test data. The two HSM data sets matched very closely in amplitude and phase. The new data set allowed a slightly larger initial rotation and matched all of the peaks of the test data better. The two model predictions lagged the rotation of the test data, but the test data did not meet the certification corridors. The predicted curves more closely matched the certification corridors. This result concluded that the stiffness and damping properties measured from the dynamic tests were correct.

Hybrid III

The modeling results of the Hybrid III comparisons were even closer than those shown for the Hybrid II. Figure 78 illustrates the comparison for a flexion certification test. Both data sets matched the test data well, but the new data set provided slightly better peak rotations. The only reason the new data set performed better was that the stiffness and damping coefficients were generated from tests of the same neck in the comparison. Doherty's data set was optimized to meet the center of the certification corridors. The neck in the comparison, although still certified, rotated slightly farther and the peak rotation occurred slightly before the center of the corridor.

A similar comparison was made for the extension data sets. Figure 79 illustrates the comparison for an extension certification test. The results were similar to those shown in figure 78. The new data set stiffness and damping coefficients were similar to the current data set. A slightly larger phase difference occurred between the modeling responses and the test data. The response of the HSM to the test data was good for both data sets.

HYBRID III 120° (23ft/sec)
FLEXION

TOTAL ROTATION

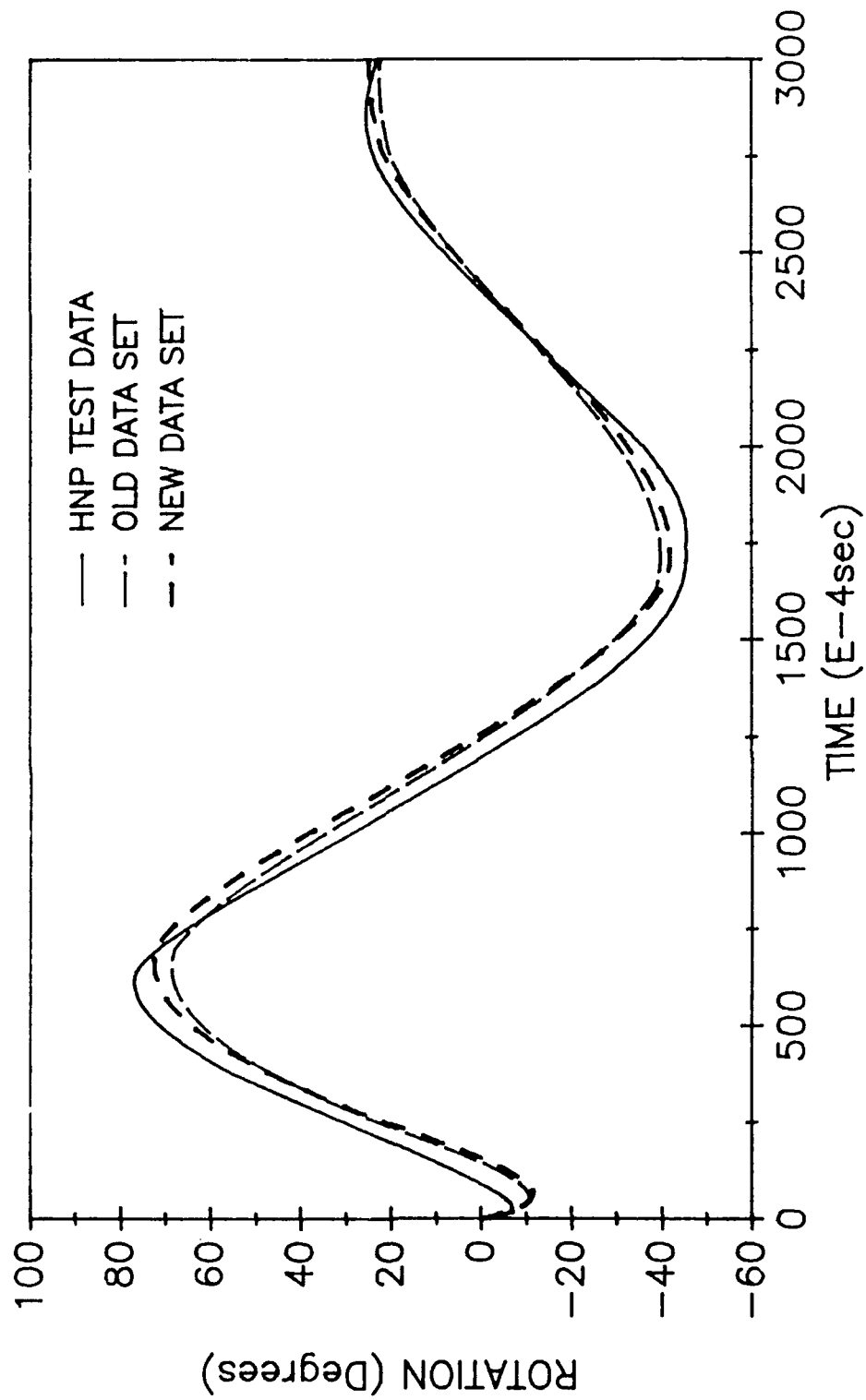


Figure 78 - HSM Hybrid III Flexion Simulation

HYBRID III 90° (20ft/sec)
EXTENSION

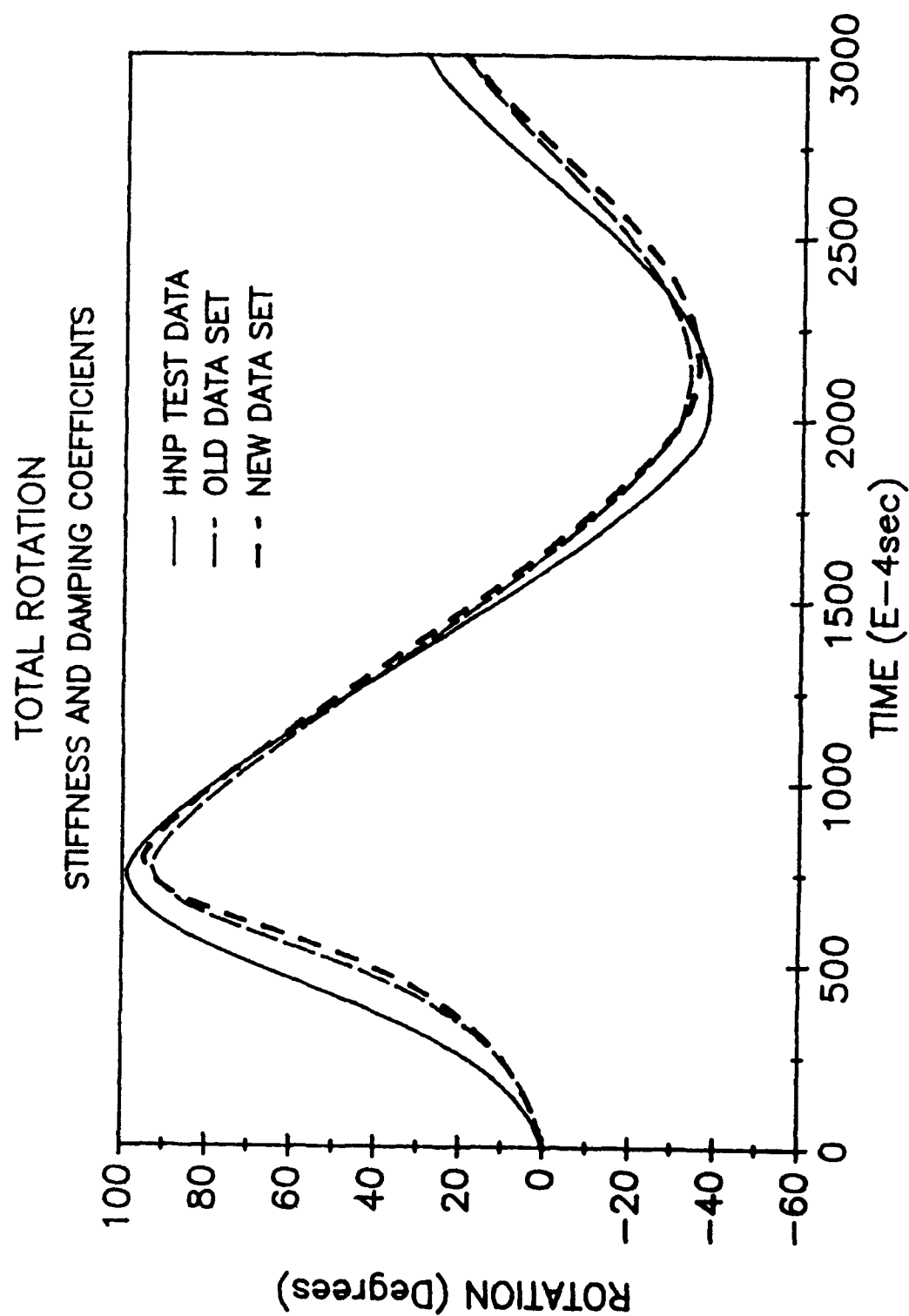


Figure 79 - HSM Hybrid III Extension Simulation

CONCLUSIONS

Static Tests

Due to the symmetric characteristics of the Hybrid II neck, similar bending stiffnesses were found for flexion, extension, and lateral bending. This result was not surprising, but the linearity of the stiffness through an 80° rotation was surprising considering that most viscoelastic materials exhibit a higher stiffness at extreme bending angles.

Higher stiffness values at higher bending angles were apparent from the results of the Hybrid III neck tests. The Hybrid III neck is also made of butyl rubber, so the factors causing the higher than linear stiffness were caused by the geometric design of the neck. This design prevented the neck from over-rotating during flexion and extension testing. Three distinct stiffnesses were found for the Hybrid III necks. The flexion and extension stiffnesses were designed, while the lateral stiffness was a result of the flexion/extension design. As previously mentioned, the results of the lateral impacts are of particular interest as there are currently no lateral certification corridors for the neck.

The internal hysteresis calculations for the Hybrid II and Hybrid III necks were also functions of the butyl rubber material and the geometric design. The Hybrid III design, with the interior steel cable, allowed more energy to be dissipated prior to the return rotation of the neck.

Dynamic Tests

The inability to certify either of the Hybrid II necks questioned the credibility of the Hybrid II dynamic data. The apparent "acceptable" shape of the curves and their recent certification at another facility led to the decision to continue with the tests. Other Hybrid II necks were not immediately available, and the question of certification most significantly falls upon the instrumentation and analysis software, which is currently under scrutiny. The results of the HSM modeling gave credibility to the stiffness and damping

properties calculated from the Hybrid II tests.

The damping ratios calculated for the Hybrid II necks were lower than those for the Hybrid III necks, but the damping ratio calculated for the Hybrid II necks was a function of the material alone. This was not the case with the Hybrid III neck. The Hybrid III neck was designed to take advantage of the interior steel cable and disks to increase the damping ratio exhibited by the neck. The higher damping ratio allowed the Hybrid III neck to better match equivalent human impact data.

Dynamic stiffness was a function of the inertia of the entire system. The system included the pendulum arm, neck, and head. Negative rotational moments and steep loading curves were effects caused by the system inertia. The static/dynamic overlay made this point very clear. The dynamic data, though not resembling the static data, was correct. The task of modeling such a response was difficult. The ATB and HSM were two models that were tried.

ATB Model

The ATB model proved to be a good predictor of the dynamic response of the HNP tests with the new data set. Rigid body dynamic analysis of just the head and neck was considered more difficult due to the limited articulation allowed, when the whole body is considered. The improvements shown by the new data warrant their inclusion into the whole body Hybrid III data set. Peak amplitude differences at the first rotation for flexion and lateral simulations were greater than for the extension simulations due to the lower impact speed for the extension test. The lower impact speed also lowered the inertia of the system at impact.

The affect of the hysteresis coefficient was masked by the flexion stiffness coefficients. This option did not work well and was severely limiting due to its allowance of a single set of stiffness coefficients. The improvement in phase difference with this option led to the conclusion that the hysteresis coefficient should be included with the tabular stiffness option if the source code is modified.

Graphical representation of dynamic tests illustrated the model's predictive capability. The ellipsoids in the figures follow the head and neck rotations of the pendulum tests very closely. Inclusion of the new Hybrid III data set into the whole body Hybrid III data set would significantly improve the head/neck responses for those simulations as well.

HSM Model

The results of the HSM modeling concluded that the current optimized data set did closely match a certified neck pendulum test. The slight improvements to the response were attributed to the mechanical properties being determined from the neck in the comparison. The stiffness and damping coefficients found from the static and dynamic tests in this study were similar to those found in the optimized data set. The similar modeling responses for the Hybrid II neck concluded that the Hybrid II stiffness and damping properties were acceptable even though the Hybrid II necks could not be certified. Although the HSM did not allow a hysteresis coefficient, the inherent characteristics of the viscoelastic element selected provided the appropriate hysteresis affect.

RECOMMENDATIONS

The SNT proved to be a very repeatable and reliable test fixture. It should be used for other material bending tests, as well as, other future neck testing, such as the new Air Force developed neck that was specifically designed for vertical impacts.

The HNP data acquisition system and software were upgraded during this study, but the Hybrid II analysis software should be analyzed thoroughly. With modifications to the two and three potentiometer devices lateral tests were performed for the first time. More lateral tests should be conducted to add to the limited information known about the Hybrid II and Hybrid III necks during lateral impacts. The HNP could also be used to determine the safety of helmet, night vision goggle, and helmet mounted display systems by testing a head and neck with and without head encumbering equipment. Safety corridors could then be established for head rotation, peak moment, and c.g. offset for these helmet systems.

The ATB model provided some very good results with the new data set. Additional simulations should be run to improve the response for inclusion into the whole body Hybrid III data set. Source code modifications to the tabular stiffness option to include a hysteresis coefficient or unloading stiffness curves are recommended to improve the response of the model.

The HSM model provided very good results for a single element model. Additional simulations should be run to refine the parameters and to increase the number of elements. Adding a graphics capability to the HSM or using another finite element code such as DYNA3D to model the head/neck system would allow graphical interpretation of the output. Other finite element programs, though, would require a larger number of elements to model the head/neck system, because the code would not be optimized for the neck and spine geometry or a rapid onset impact.

BIBLIOGRAPHY

1. Payne, P.R., Band, E.G.U. Development of a Dynamic Analog Anthropomorphic Dummy for Aircraft Escape System Testing AMRL-TR-71-10, August 1971.
2. Bartol, A., Hazen, V., Kowalski, J., Murphy, B. and White, R. Jr. Advanced Dynamic Anthropomorphic (ADAM) Final Design Report AAMRL-TR-90-023, March 1990.
3. Rasmussen, R.R., Kaleps, I. The USAF Advanced Dynamic Anthropomorphic Manikin - ADAM AGARD-CP-472, Implications of Advanced Technologies for Air & Spacecraft Escape Munich Germany, 24-28 Apr 1989: 9.1-9.7, February 1990.
4. Miller, J.S. Performance Evaluation of the General Motors Hybrid II Anthropomorphic Test Dummy DOT-HS-800-919, September 1973.
5. Daniel, R.P., Trosien, K.R., Young, B.O. The Impact Behavior of the Hybrid II Dummy Paper No. 751145 Proceedings of the 19th Stapp Car Crash Conference, 1975.
6. General Motors Tech Center, Anthropomorphic Test Dummy - Volumes I-III DOT-HS-801-174, DOT-HS-801-175, and DOT-HS-801-176, October 1974.
7. Hubbard, R.P. Anthropomorphic Basis of the GM ATD 502 Crash Test Dummy SAE-TPS-750429, February 1975.
8. Foster, J.K., Kortge, J.O., Wolanin, M.J. Hybrid III - A Biomechanically-Based Crash Test Dummy Paper No. 770938, Proceedings of the 21st Stapp Car Crash Conference, 1977.
9. Mertz, H.J., Neathery, R.F., and Culver, C.C. Performance Requirements and Characteristics of Mechanical Necks, Human Impact Response, New York, Plenum Press, pp 263-288, 1973.

10. Mertz, H.J., and Patrick, L.M. Investigations of the Kinematics and Kinetics of Whiplash, Proceedings of the 11th Stapp Car Crash Conference, 1967.
11. Wismans, J.H., and Spenny, C.H. Performance Requirements for Mechanical Necks in Lateral Flexion, Proceedings of the 27th Stapp Car Crash Conference, 1983.
12. Wismans, J.H., and Spenny, C.H. Head-Neck Response in Frontal Flexion, Proceedings of the 28th Stapp Car Crash Conference, 1984.
13. Phillips, N.S. An Investigation of Automotive Restraint and Body Positioning Techniques AMRL-TR-71-101, December 1973.
14. Phillips, N.S. Analysis and Measurement of Helmeted Aircrewman Response Resulting from Birdstrike AMRL-TR-79-75, January 1980.
15. Ewing, C.L., Thomas, D.J., Beeler, G.W., Patrick, L.M., and Gillis, D.B. Dynamic Response of the head and Neck of the Living Human to -Gx Impact Acceleration, Proceedings of the 12th Stapp Car Crash Conference, 1968.
16. Ewing, C.L., Thomas, D.J., Patrick, L.M., Beeler, G.W., and Smith, M.J. Living Human Dynamic Response to -Gx Impact Acceleration. II. Accelerations Measured on the Head and Neck, Proceedings of the 13th Stapp Car Crash Conference, 1969.
17. Huston, J.C., and Advani, S.H. Three Dimensional Model of the Human Head and Neck for Automobile Crashes Mathematical Modelling Biodynamics Response to Impact, 1976.
18. Huston, J.C., Passerello, C.E., and Huston, R.L. Numerical Prediction of Head/Neck Response to Shock Impact, Measurement and Prediction of Structural and Biodynamic Crash-Impact Response, 1976.

19. Spenny, C.H., and Wismans, J.H. Kinematic and Dynamic Analysis of Head-Neck Motion, Proceedings of the Symposium of Mechanisms of Head and Spine Trauma, 13th Annual Meeting of the Neuroelectric Society, 1983.
20. Spenny, C.H. Performance Requirements for Mechanical Necks in Flexion, Report for the Department of Aeronautics and Astronautics, Air Force Institute of Technology, WPAFB, Ohio.
21. Melvin, J.W., McElhaney, J.H., and Roberts, V.L. Improved Neck Simulation for Anthropomorphic Dummies, Proceedings of the 16th Stapp Car Crash Conference, 1972.
22. Melvin, J.W., McElhaney, J.H., and Roberts, V.L. Evaluation of Dummy Neck Performance, Human Impact Response, New York, Plenum Press, pp 247-261, 1973.
23. Wismans, J., Maltha, J., van Wilk, J.J. and Janssen, E.G. MADYMO - A crash Victim Simulation Computer Program For Biomechanical Research And Optimization of Designs For Impact Injury Prevention, AGARD Conference Proceedings, Koln, Germany, April 1982.
24. Fleck, J.T., and Butler, F.E. Validation of the Crash Victim Simulator; Volumes 1-4, DOT HS 806 279 - DOT HS 806 282, December 1981 through March 1982.
25. Digges, K.H. Recent Improvements in Occupant Crash Simulation Capabilities of the CVS/ATB Model SAE Paper No. 880655, 1988.
26. Obergefell, L.A., Fleck, J.T., Kaleps, I., and Gardner, T.R. Articulated Total Body Model Enhancements, Volumes 1-3 AAMRL-TR-88-007, AAMRL-TR-88-009, and AAMRL-TR-88-043, January 1988 through February 1988.
27. Obergefell, L.A. and Kaleps, I. Prediction of an Occupant's Motion During Rollover Crashes, Thirtieth Stapp Car Crash Conference Proceedings, SAE Paper No. 861876, October 1986.
28. Grosch, L., Kaiser, H. and Schmid, W. Mathematical Movement and Load Simulation for Persons Involved in Automobile Accident, SAE Paper No. 871109, May 1987.

29. Belytschko, T., Schwer, L. and Schultz, A. A Model for Analytical Investigation of Three-Dimensional Head-Spine Dynamics, NTIS Report No. AD-A025-911, April 1976.
30. Belytschko, T., Privitzer, E. Refinement and Validation of a Three-Dimensional Head-Spine Model AMRL-TR-78-7, August 1978.
31. Kaleps, I., White, R.P. Jr., Beecher, R.M., Whitestone, J., and Obergefell, L.A. Measurement of Hybrid III Dummy Properties and Analytical Simulation Data Base Development AAMRL-TR-88-005, February 1988.
32. Doherty, B.J., Paver, J.G. A Computer Simulation of the Hybrid II Manikin Head-Neck System, Proceedings of the 24th Annual SAFE Symposium, 1986.
33. Doherty, B.J., Paver, J.G. Mathematical Modeling of the Hybrid III Manikin Head-Neck Structure, Proceedings of the 6th International Conference of Mathematical Modeling, 1988.
34. Spittle, E. K. Static Neck Tester System Description In-House Report, May 1991, (Unpublished).
35. Taylor, C. L. Head/Neck Pendulum System Description In-House Report, January 1990, (Unpublished).
36. Department of Transportation, Part 572E Dummy Performance Calibration Test Procedure, Code of Federal Regulations.

LIST OF SYMBOLS

θ_h	- Head Angular Rotation about 'X'
$\dot{\theta}_h$	- Head Angular Velocity about 'X'
$\ddot{\theta}_h$	- Head Angular Acceleration about 'X'
θ_n	- Neck Angular Rotation about 'X'
$\dot{\theta}_n$	- Neck Angular Velocity about 'X'
$\ddot{\theta}_n$	- Neck Angular Acceleration about 'X'
ϕ_h	- Head Angular Rotation about 'Y'
$\dot{\phi}_h$	- Head Angular Velocity about 'Y'
$\ddot{\phi}_h$	- Head Angular Acceleration about 'Y'
ϕ_n	- Neck Angular Rotation about 'Y'
$\dot{\phi}_n$	- Neck Angular Velocity about 'Y'
$\ddot{\phi}_n$	- Neck Angular Acceleration about 'Y'
ψ_h	- Head Angular Rotation about 'Z'
$\dot{\psi}_h$	- Head Angular Velocity about 'Z'
$\ddot{\psi}_h$	- Head Angular Acceleration about 'Z'
ψ_n	- Neck Angular Rotation about 'Z'
$\dot{\psi}_n$	- Neck Angular Velocity about 'Z'
$\ddot{\psi}_n$	- Neck Angular Acceleration about 'Z'
Δ	- Logarithmic Decrement for Damping
δ	- Damping Ratio (C/C_c)
C.G.	- Center of Gravity

C - Damping Coefficient
 C_c - Critical Damping Coefficient
 C_j - Damping Coefficient at joint 'j'
 C_{nx} - Rotational Neck Damping about 'X' Axis
 C_{ny} - Rotational Neck Damping about 'Y' Axis
 C_{nz} - Rotational Neck Damping about 'Z' Axis
 F_x - Force in 'X' Direction
 F_{xoc} - 'X' Direction Force at the Occipital Condyle
 F_{xt} - 'X' Direction Force at T1
 F_y - Force in 'Y' Direction
 F_{yoc} - 'Y' Direction Force at the Occipital Condyle
 F_{yt} - 'Y' Direction Force at T1
 F_z - Force in 'Z' Direction
 F_{zoc} - 'Z' Direction Force at the Occipital Condyle
 F_{zt} - 'Z' Direction Force at T1
 J_h - Head Mass Moment of Inertia
 J_j - Mass Moment for element 'j'
 J_n - Neck Mass Moment of Inertia
 K - Neck Stiffness
 K_j - Stiffness at joint 'j'
 K_n - Neck Stiffness
 K_{nx} - Rotational Neck Stiffness about 'X' Axis
 K_{ny} - Rotational Neck Stiffness about 'Y' Axis
 K_{nz} - Rotational Neck Stiffness about 'Z' Axis
 K_{oc} - Joint Torque at O.C.
 K_{T1} - Joint Torque at T1

M_h - Head Mass
 M_n - Neck Mass
 M_{xoc} - Moment about 'X' axis at occipital condyle
 M_{xt} - Moment about 'X' axis at T1
 M_{yoc} - Moment about 'Y' axis at occipital condyle
 M_{yt} - Moment about 'Y' axis at T1
 M_{zoc} - Moment about 'Z' axis at occipital condyle
 M_{zt} - Moment about 'Z' axis at T1
O.C. - Occipital Condyle (head/neck joint)
T1 - Neck/Torso Joint
 W_h - Head Weight
 W_n - Neck Weight
 X - 'X' Axis Vector
 X_0 - Amplitude of First Rotational Peak
 X_1 - Amplitude of Second Rotational Peak
 \ddot{X}_{cgh} - 'X' Acceleration of the head at the C.G.
 \ddot{X}_{cgn} - 'X' Acceleration of the neck at the C.G.
 X_h - 'X' Distance from the O.C. to the Head C.G.
 X_n - 'X' Distance from T1 to the Neck C.G.
 X_{oc} - 'X' Distance from neck C.G. to O.C.
 Y - 'Y' Axis Vector
 \ddot{Y}_{cgh} - 'Y' Acceleration of the head at the C.G.
 \ddot{Y}_{cgn} - 'Y' Acceleration of the neck at the C.G.
 Y_h - 'Y' Distance from the O.C. to the Head C.G.
 Y_n - 'Y' Distance from T1 to the Neck C.G.
 Y_{oc} - 'Y' Distance from neck C.G. to O.C.

- Z - 'Z' Axis Vector
- \ddot{Z}_{cgh} - 'Z' Acceleration of the head at the C.G.
- \ddot{Z}_{cgn} - 'Z' Acceleration of the neck at the C.G.
- Z_h - 'Z' Distance from the O.C. to the Head C.G.
- Z_n - 'Z' Distance from T1 to the Neck C.G.
- Z_{oc} - 'Z' Distance from neck C.G. to O.C.

APPENDIX A

NEW ATB MODEL INPUT DECK

121

.030999994-.968078140.000000000.000000000.000000000.000000000.000000000
 .032000005-2.36141510.000000000.000000000.000000000.000000000.000000000
 .032999992-3.22252510.000000000.000000000.000000000.000000000.000000000
 .034000006-3.66218420.000000000.000000000.000000000.000000000.000000000
 .035000000-3.45534440.000000000.000000000.000000000.000000000.000000000
 .035999998-2.50542000.000000000.000000000.000000000.000000000.000000000
 .037000000-1.10798500.000000000.000000000.000000000.000000000.000000000
 .037999999.2216700170.000000000.000000000.000000000.000000000.000000000
 .0390000011.054502130.000000000.000000000.000000000.000000000.000000000
 .0399999921.606934910.000000000.000000000.000000000.000000000.000000000
 .0410000091.960832950.000000000.000000000.000000000.000000000.000000000
 .0419999961.849374060.000000000.000000000.000000000.000000000.000000000
 .0430000011.128682970.000000000.000000000.000000000.000000000.000000000
 .044000000-.006098000.000000000.000000000.000000000.000000000.000000000
 .044999998-1.03175290.000000000.000000000.000000000.000000000.000000000
 .045999996-1.45608310.000000000.000000000.000000000.000000000.000000000
 .046999998-1.25389170.000000000.000000000.000000000.000000000.000000000
 .048000000-.875187990.000000000.000000000.000000000.000000000.000000000
 .048999991-.653978050.000000000.000000000.000000000.000000000.000000000
 .049999990-.457603990.000000000.000000000.000000000.000000000.000000000
 .055000000.6866660120.000000000.000000000.000000000.000000000.000000000
 .059999987-.705979050.000000000.000000000.000000000.000000000.000000000
 .064999998-.481662960.000000000.000000000.000000000.000000000.000000000
 .070000000-.171427000.000000000.000000000.000000000.000000000.000000000
 .074999981.7943329810.000000000.000000000.000000000.000000000.000000000
 .079999983.0430029970.000000000.000000000.000000000.000000000.000000000
 .085000001-.402114960.000000000.000000000.000000000.000000000.000000000
 .089999996.5830910210.000000000.000000000.000000000.000000000.000000000
 .094999999.0579890050.000000000.000000000.000000000.000000000.000000000
 .100000001.5465610620.000000000.000000000.000000000.000000000.000000000
 .104999997.5388359430.000000000.000000000.000000000.000000000.000000000
 .1100000071.291586880.000000000.000000000.000000000.000000000.000000000
 .1150000021.702245000.000000000.000000000.000000000.000000000.000000000
 .1199999822.133804560.000000000.000000000.000000000.000000000.000000000
 .1250000002.663601160.000000000.000000000.000000000.000000000.000000000
 .1299999952.440901280.000000000.000000000.000000000.000000000.000000000
 .1350000052.681921960.000000000.000000000.000000000.000000000.000000000
 .1400000012.213988780.000000000.000000000.000000000.000000000.000000000
 .1449999662.345494030.000000000.000000000.000000000.000000000.000000000
 .1500000061.768218040.000000000.000000000.000000000.000000000.000000000
 .1550000011.749288560.000000000.000000000.000000000.000000000.000000000
 .1599999671.348755960.000000000.000000000.000000000.000000000.000000000
 .1650000071.054612990.000000000.000000000.000000000.000000000.000000000
 .170000002.7876409290.000000000.000000000.000000000.000000000.000000000
 .174999997.4515129630.000000000.000000000.000000000.000000000.000000000
 .179999992.1370470230.000000000.000000000.000000000.000000000.000000000
 .185000002-.180177960.000000000.000000000.000000000.000000000.000000000
 .189999998-.450921980.000000000.000000000.000000000.000000000.000000000
 .195000008-.652746980.000000000.000000000.000000000.000000000.000000000
 .200000003-.829559270.000000000.000000000.000000000.000000000.000000000
 .204999998-.964967910.000000000.000000000.000000000.000000000.000000000
 .209999993-1.30634900.000000000.000000000.000000000.000000000.000000000
 .215000018-1.34642210.000000000.000000000.000000000.000000000.000000000
 .220000014-1.49975300.000000000.000000000.000000000.000000000.000000000
 .225000009-1.33927000.000000000.000000000.000000000.000000000.000000000
 .230000004-1.35685130.000000000.000000000.000000000.000000000.000000000
 .234999999-1.15934530.000000000.000000000.000000000.000000000.000000000
 .239999965-1.12167500.000000000.000000000.000000000.000000000.000000000
 .245000005-.785188020.000000000.000000000.000000000.000000000.000000000
 .250000000-.679669800.000000000.000000000.000000000.000000000.000000000


```

.254999995-.363413010.000000000.000000000.000000000.000000000.000000000
.259999990-.228618010.000000000.000000000.000000000.000000000.000000000
.264999956-.052468000.000000000.000000000.000000000.000000000.000000000
.270000011.0049410000.000000000.000000000.000000000.000000000.000000000
.275000006.1924040170.000000000.000000000.000000000.000000000.000000000
.280000001.2735210060.000000000.000000000.000000000.000000000.000000000
.284999996.4505960050.000000000.000000000.000000000.000000000.000000000
.289999932.5525780320.000000000.000000000.000000000.000000000.000000000
.294999927.7430689330.000000000.000000000.000000000.000000000.000000000
.296999931.8003568650.000000000.000000000.000000000.000000000.000000000
DUMMY VEHICLE
.00000.00000.00000.00000.00000.00000.00000      3.00000.05000      OC.2
.05050.05100.05150
      0      0      0      0      0      0      0      0      0      2      0      D.1
      0      0      0
      3      SEGMENT-SEGMENT FCN.      0      0      E.1
0.00000000 -5.00000000 0.00000000 0.00000000 1.00000000
      6
0.00000000 0.00000000 1.00000000 469.999969 2.00000000 889.999878
3.00000000 1220.00024 4.00000000 1470.00000 5.00000000 1580.00000
      7      R FACTOR.      0      0      E.1
0.00000000 0.00000000 0.699999988 0.00000000 0.00000000
      19      CF=.25,CREST=.25      0      0      E.1
0.00000000 0.00000000 0.250000000 0.00000000 0.00000000
999
46      Neck Pivot      6      0      E.7
0.00000000 0.00000000 0.00000000 0.00000000 0.00000000
      19      4
0.00000000 439.000031 876.999939 2051.00049 4823.99902 9384.00195
15864.9990 24399.0000 35118.0000 48156.0000 63645.0000 81718.0156
102505.992 126142.992 152760.984 182493.016 215471.000 251828.000
291696.969
0.00000000 375.000000 750.000000 1361.00000 2524.00000 4534.00000
7686.00000 12277.0020 18600.0000 26951.0039 37626.0000 50919.0000
67126.0000 86541.0156 109461.000 136180.000 166992.984 202196.031
242084.000
0.00000000 197.000000 394.000000 634.000000 1003.00000 1571.99976
2411.99951 3597.00000 5198.00000 7286.00049 9934.99805 13216.0020
17201.0000 21961.0020 27570.0020 34099.0000 41619.0000 50204.0156
59925.0000
0.00000000 375.000000 750.000000 1361.00000 2524.00000 4534.00000
7686.00000 12277.0020 18600.0000 26951.0039 37626.0000 50919.0000
67126.0000 86541.0156 109461.000 136180.000 166992.984 202196.031
242084.000
47      HEAD PIVOT      6      0      E.7
0.00000000 0.00000000 0.00000000 0.00000000 0.00000000
      19      4
0.00000000 345.000000 689.000061 1349.00000 2360.00049 3547.00024
4835.00000 6187.99902 7588.00000 9019.99902 10478.0010 11955.9980
13450.9980 14958.0000 16476.0000 18003.0000 19538.0000 21080.0000
22626.9961
0.00000000 375.000000 750.000000 1361.00000 2524.00000 4534.00000
7686.00000 12277.0020 18600.0000 26951.0039 37626.0000 50919.0000
67126.0000 86541.0156 109461.000 136180.000 166992.984 202196.031
242084.000
0.00000000 175.000000 350.999969 560.000000 859.000000 1278.00012
1828.99988 2510.00000 3312.00024 4220.00098 5220.00098 6299.00098
7444.99951 8647.99805 9897.99805 11189.0010 12515.0000 13871.0049
15251.9990
0.00000000 375.000000 750.000000 1361.00000 2524.00000 4534.00000

```


APPENDIX B

NEW HSM MODEL INPUT DECK

HYBRID II PENDULUM NECK TEST SIMULATION (PART 572)										TABULAR OUTPUT	
3	2	1	1	1	2	500	6	.001			
0	0	1	0	0	0	0	1	0	0	0	1
1											
875.6E6		5.594E9		7.700E8		7.700E8					
				5.		5.		1.06E-3	1.00E-7		
1		0		0		0		1.	1.	1.	1.
2		0		0		12.55					
3		0.55		0		15.245		5.00E3	1.88E5	3.467E5	1.62E5
4		0		100.		0					
1	1	2		3				4	1	3	
1211111											
03010101											
5	5	0									
001102											
003102											
3122											
003302											
3502											
18		0.		0.		0.					
	0.			0.		0.					
.00025		-5.		-8.							
.00175		-26.		-4.							
.005		-26.		0.							
.01200		-22.		0.							
.02000		-22.		0.							
.02933		-22.		2.							
.03350		-5.		4.							
.03475		0.		2.667							
.036		0.		0.							
.063		0.		0.							
.068		0.		0.							
.073		0.		0.							
.08		0.		0.							
.085		0.		0.							
.09		0.		0.							
.10000		0.		0.							
1.		0.		0.							

X-DISPLACEMENT OF NODE 1
 X-DISPLACEMENT OF NODE 3
 X-ACCELERATION OF NODE 3
 Z-DISPLACEMENT OF NODE 3
 ROTATION ABOUT BODY Y-AXIS AT NODE 3